πN, KN and $\overline{K}N$ Scattering: Skyrme Model $vs.$ Experiment[*]

MAREK KARLINER

and

MICHAEL P. MATTIS

Stanford Linear Accelerator Center

Stanford University, Stanford, California, 94305

ABSTRACT

We present a comprehensive partial-wave analysis of the processes $\pi N \to \phi_{\mathrm{PS}} B$, $KN \to \phi_{\mathrm{PS}} B$ and $\overline{K}N \to \phi_{\mathrm{PS}} B$ in the 3-flavor Skyrme model, with ϕ_{PS} an arbitrary pseudoscalar-octet meson and B a $\frac{1}{2}^{+}$ octet or $\frac{3}{2}^{+}$ decuplet baryon. Overall, we find good, poor, and mixed agreement, respectively, between the model and experiment for these three types of processes. We pay particular attention to assessing the independence of our results from the details of the Skyrme Lagrangian. We also examine the effect of including a third light flavor on the linear relations between experimental $\pi N \to \pi N$ and $\pi N \to \pi \Delta$ partial-wave amplitudes that are predicted by 2-flavor soliton models of the nucleon. Although the emphasis throughout is on a detailed qualitative comparison with Nature, we also present Skyrme-model predictions for six processes such as $\pi N \to K\Sigma^{*}$ and $\overline{K}N \to \eta\Sigma$ for which experimental partial-wave analyses are unavailable.

2

I. Summary and Outline

In this paper we present a comprehensive partial-wave analysis of the processes $\pi N \to \phi_{\mathrm{PS}} B$, $KN \to \phi_{\mathrm{PS}} B$, and $\overline{K}N \to \phi_{\mathrm{PS}} B$ in the 3-flavor Skyrme model,[1-6] with ϕ_{PS} denoting an arbitrary pseudoscalar-octet meson and B a $\frac{1}{2}^+$ octet or $\frac{3}{2}^+$ decuplet baryon. As our approach to meson-nucleon scattering in both 2-flavor and 3-flavor soliton models of the baryon has been discussed in detail elsewhere, a fresh introduction hardly seems necessary (see Refs. 7-13 and also Refs. 14-15). Instead, this Section will serve as a summary of our principal results. We should, however, underscore our two principal approximations:

1. Our results are valid only to leading order in $1/N_c$, where N_c is the number of colors of the underlying gauge group;[♮1]

2. Our group-theoretic formalism assumes unbroken $SU(3)_{\mathrm{flavor}}$;[♮2] furthermore, our numerical phase-shift computations are carried out in the limit of massless mesons, *i.e.*, exact chiral symmetry.

In our work on the 2-flavor Skyrme model, we found excellent agreement with experiment for the mass spectrum of nucleon and Δ resonances.[7] (Masses of the nucleon and Δ resonances agreed on the average to within 8% of their experimental values after optimizing the parameters f_π and e that appear in the Skyrme Lagrangian, Eq. (1) below; the results are summarized in Fig. 1b in Section III.) However, given the severity of the second approximation above, we will refrain in the present 3-flavor analysis from making similar quantitative statements about the spectrum of strange baryons in the model. Such statements would be of du-

---

♮1   See Section II of Ref. 8 for a detailed explanation of the large-N_c approximation in the context of meson-baryon scattering.

♮2   The opposite limit, corresponding to $m_K \gg m_\pi$, has been studied by Callan and Klebanov.[16]

bious value until a kaon mass is introduced. Instead, we shall concentrate here on the *qualitative* behavior of the partial-wave amplitudes, and on patterns of size and sign alternation between amplitudes. Unlike mass predictions, such features are *completely independent* of the values of the Skyrme parameters f_π and e: a different choice of parameters would not alter the shapes of the amplitudes, only their parametrization as a function of energy.

We have located experimental data for 165 partial-wave channels[17-42] corresponding to the processes $\pi N \to \pi N$, $\pi N \to \pi \Delta$, $\pi N \to \eta N$, $\pi N \to K\Lambda$, $\pi N \to K\Sigma$, $KN \to KN$, $KN \to K\Delta$, $\overline{K}N \to \overline{K}N$, $\overline{K}N \to \pi\Sigma$, $\overline{K}N \to \pi\Lambda$, $\overline{K}N \to \eta\Lambda$, $\overline{K}N \to \pi\Sigma^*$ and $\overline{K}N \to \overline{K}\Delta$. A detailed pictorial comparison to the Skyrme model is presented in Sections III-V. Several of these processes have been subject to more than one partial-wave analysis; in these cases we usually selected the most recent one to compare to the Skyrme model. This choice was not without repercussions: often there was serious disagreement between independent analyses, and a different selection would have modified the results of our comparison accordingly. We shall bring up differences between various experimental analyses when the Skyrme model sheds light on the issue.

It is conventional to test models of the baryon spectrum by checking the signs of the various amplitudes against experiment. In view of the large number of channels involved in this study, we have summarized the results of this comparison in Tables I-XIII. In these tables, each inelastic amplitude has been assigned a + or − according to whether it first journeys appreciably into the upper or lower half of the unitarity circle, and a zero if this is unclear.[‡3] We have labeled

---

‡3 Our sign definitions differ somewhat from the traditional ones, whereby a + and − refer, not to the amplitude as a whole, but to its value at a resonance; specifically, they indicate

4

the channels in the standard fashion: πN channels are denoted by $L_{2I,2J}$ whereas KN and $\overline{K}N$ channels are labeled by $L_{I,2J}$, where L is the meson's orbital angular momentum, and I and J stand for total isospin and angular momentum. For processes where the final baryon has spin-$\frac{3}{2}$ (Tables II, VII, XII and XIII), the initial and final meson angular momenta L and L' need not be equal, but can differ by two; hence the notation $LL'_{2I,2J}$ or $LL'_{I,2J}$.

In addition to signs, Tables I-XIII present numerical ratings from 1 to 4 which represent our assessment of the degree of *qualitative* agreement between the Skyrme model and experiment, with a "1" being the best and a "4" the worst. The criteria we employed in arriving at such a score are the following: Does the Skyrme amplitude have the same general shape as its experimental counterpart? Does it point in the same general angle in the unitarity circle? Are distinctive features (*e.g.*, cusps, loops, repulsive behavior) mimicked correctly? Are the magnitudes of the curves comparable? Do the graphs share a + or − designation? To score a "1," the answer must be "yes" to all of these questions, with sizes agreeing to within 30%. A "2" guarantees that the + or − assignments will agree, and that the shapes are similar, but the magnitudes can differ substantially (*e.g*, by a factor of 3 or 4); alternatively, the sizes might be in close correspondence while the shapes are rather different. For a "3," the two graphs must lie in either the same or adjacent quadrants (so the signs *can* disagree); there is usually some additional feature of similarity, for example an energy range over which the shapes of the amplitudes are in rough correspondence, but on the whole the agreement

---

whether the resonance occurs at the top (+) or bottom (−) of a circle. For resonant amplitudes, our definition almost always coincides with the traditional definition as applied to the lowest-lying appreciably-coupled resonance in that channel; however, our broader definition allows us to characterize *non*-resonant (*e.g.*, repulsive) amplitudes as well.

looks no better than random. For a "4," the agreement is truly dismal; typically such graphs point in opposite directions. The reader is encouraged to glance at a few plots chosen at random from Sections III-V in order to gain a "feel" for this (admittedly subjective) scoring system.

πN processes. As is apparent from Tables I-V, the results for πN processes are, on the whole, surprisingly good. Elastic πN scattering as calculated in both the 2-flavor and 3-flavor Skyrme models (the two approaches differing even for non-strange processes) was examined previously.[7-15] In general, the 3-flavor model constitutes an improvement over the 2-flavor model. However, in both cases there are serious discrepancies with experiment in the S and P waves, as reflected in the preponderance of 3's and 4's in these channels. The most severe of these is the failure of the model to reproduce the strongly resonant behavior observed in the P_{11} and P_{33} channels, associated with the Roper resonance and with the Δ, respectively. These problems are due to the fact that, in leading order in $1/N_c$, certain states such as the Roper and the Δ are in fact degenerate with the nucleon, and hence could not show up as resonances above threshold. Thus, these are most likely failures, not of the model itself, but rather of our leading-order analysis.

In contrast, for D waves and higher, with the exception of the D_{35}, the agreement is quite impressive. The main source of disagreement in the high waves ($L \geq 4$) is the overly large size of the Skyrme model curves, which is primarily due to the limited number of inelastic channels that we are allowing for ($\phi_{PS}B$ only); this situation is improved when the Skyrme model is enlarged to the 3-flavor case.[13] Significantly, both the 2- and 3-flavor Skyrme models mimic the "big-small-small-big" pattern that characterizes the behavior of the four in-

$$\pi N \;\rightarrow\; \pi N$$

Channel	2-Flav. Skyrme	3-Flav. Skyrme	Channel	2-Flav. Skyrme	3-Flav. Skyrme
S_{11}	3	3	G_{17}	2	2
S_{31}	4	4	G_{19}	2	2
P_{11}	4	4	G_{37}	2	2
P_{13}	3	2	G_{39}	2	2
P_{31}	2	2	H_{19}	2	2
P_{33}	4	4	H_{111}	2	2
D_{13}	1	1	H_{39}	2	2
D_{15}	2	2	H_{311}	2	2
D_{33}	2	2	I_{111}	3	2
D_{35}	3	3	I_{113}	2	2
F_{15}	1	1	I_{311}	3	3
F_{17}	2	2	I_{313}	2	2
F_{35}	1	1	K_{113}	2	2
F_{37}	1	1	K_{115}	2	2
			K_{313}	3	3
			K_{315}	2	2

Table I

(*cf.* Fig. 1)

$$\pi N \;\rightarrow\; \pi \Delta$$

Channel	Exp.	2-Flav. Skyrme		3-Flav. Skyrme	
PP_{11}	+	+	1	+	1
PP_{13}		+		+	
PP_{31}		+		+	
PP_{33}	+	+	2	+	2
DD_{13}	−	−	2	−	1
DD_{15}	+	+	1	+	1
DD_{33}	+	+	3	+	3
DD_{35}		+		+	
FF_{15}	+	+	3	+	2
FF_{17}		+		+	
FF_{35}	+	+	2	+	1
FF_{37}	+	+	1	+	1
SD_{11}	+	+	3	+	3
SD_{31}	−	−	3	−	3
DS_{13}	−	−	2	−	3
DS_{33}	+	+	3	+	3
PF_{13}		+		+	
PF_{33}		−		−	
FP_{15}	−	−	2	−	3
FP_{35}	+	+	2	+	3

Table II

(*cf.* Fig. 2)

$$\pi N \;\rightarrow\; \eta N$$

Channel	Exp.	Skyrme	
S_{11}	+	+	3
P_{11}	−	+	4
P_{13}	−	0	3
D_{13}	−	−	3
D_{15}	−	−	3
F_{15}	+	+	1
F_{17}	+	+	2
G_{17}	+	+	2
G_{19}	0	+	2
H_{19}	+	+	2
H_{111}		+	

Table III

(*cf.* Fig. 3)

$$\pi N \;\rightarrow\; K\Lambda$$

Channel	Exp.	Skyrme	
S_{11}	+	−	4
P_{11}	−	−	2
P_{13}	+	+	3
D_{13}	+	−	4
D_{15}	+	+	2
F_{15}	−	−	2
F_{17}	+	+	3
G_{17}	−	−	4
G_{19}	+	+	2
H_{19}	−	−	2
H_{111}		+	

Table IV

(*cf.* Fig. 4)

$$\pi N \;\rightarrow\; K\Sigma$$

Channel	Exp.	Skyrme	
S_{11}		−	
S_{31}	−	−	2
P_{11}		−	
P_{13}		−	
P_{31}	−	−	3
P_{33}	0	−	2
D_{13}		+	
D_{15}		−	
D_{33}	−	0	4
D_{35}	−	0	4
F_{15}		−	
F_{17}		−	
F_{35}	−	−	2
F_{37}	−	−	1
G_{17}		−	
G_{19}		−	
G_{37}	−	−	2
G_{39}		−	
H_{19}		−	
H_{111}		−	
H_{39}	−	−	2
H_{311}	−	−	2

Table V

(*cf.* Fig. 5)

Tables I-V. πN processes: Skyrme model *vs.* experiment. Inelastic channels are assigned a + or − according to whether the amplitude first journeys significantly into the upper or lower half-plane, and a 0 if this is unclear. The values 1-4 represent the degree of qualitative agreement between the model and experiment, with a "1" being the best and a "4" the worst (see text for details).

7

$KN \rightarrow KN$

Table VI

Channel	Skyrme
S_{01}	4
S_{11}	4
P_{01}	4
P_{03}	2
P_{11}	2
P_{13}	4
D_{03}	2
D_{05}	3
D_{13}	4
D_{15}	4
F_{05}	
F_{07}	
F_{15}	4
F_{17}	
G_{07}	
G_{09}	
G_{17}	4
G_{19}	
H_{19}	4

Table VI

(*cf.* Fig. 6)

$KN \rightarrow K\Delta$

	Solution A	Solution B	Solution C	Skyrme
PP_{11}	−	+	+	+
PP_{13}	+	+	+	+
DD_{13}	−	+	0	+
DD_{15}	+	+	0	+
SD_{11}	+	+	−	−
DS_{13}	+	+	−	+

Table VII

(*cf.* Fig. 7)

$\overline{K}N \rightarrow \overline{K}N$

Channel	Skyrme
S_{01}	4
S_{11}	4
P_{01}	4
P_{03}	4
P_{11}	4
P_{13}	4
D_{03}	1
D_{05}	2
D_{13}	2
D_{15}	1
F_{05}	1
F_{07}	1
F_{15}	2
F_{17}	1
G_{07}	2
G_{09}	3
G_{17}	2
G_{19}	4

Table VIII

(*cf.* Fig. 8)

$\overline{K}N \rightarrow \pi\Lambda$

Channel	Exp. I	Exp. II	Skyrme Sign	Skyrme vs. I	Skyrme vs. II
S_{11}	−	−	+	4	3
P_{11}	−	−	−	3	3
P_{13}	+	+	+	2	4
D_{13}	+	+	−	3	4
D_{15}	−	−	+	4	4
F_{15}	−	−	−	1	1
F_{17}	+	+	+	3	1
G_{17}	−	0	−	1	2
G_{19}		+	+		3

Table X

(*cf.* Fig. 11)

$\overline{K}N \rightarrow \eta\Lambda$

Channel	Exp.	Skyrme
S_{01}		−
P_{01}		−
P_{03}		+
D_{03}		−
D_{05}	−	+
F_{05}	−	−
F_{07}		+
G_{07}	−	−
G_{09}		+

Table XI

(*cf.* Fig. 12)

$\overline{K}N \rightarrow \pi\Sigma$

Channel	Exp.	Skyrme	
S_{01}	+	−	4
S_{11}	+	−	3
P_{01}	−	−	3
P_{03}	+	−	4
P_{11}	−	−	4
P_{13}	−	−	4
D_{03}	+	+	3
D_{05}	−	−	2
D_{13}	+	−	4
D_{15}	+	+	3
F_{05}	−−	−	1
F_{07}	+	−	3
F_{15}	−	−	2
F_{17}	−	−	2
G_{07}	+	−	4
G_{09}	−	−	3
G_{17}	−	−	3
G_{19}		−	

Table IX

(*cf.* Fig. 10)

$\overline{K}N \rightarrow \pi\Sigma^*$

Channel	Exp.	Skyrme		Channel	Exp.	Skyrme	
PP_{01}	+	+	2	SD_{01}	+	+	2
PP_{03}	−	+	4	SD_{11}	−	−	3
PP_{11}		0		DS_{03}		−	
PP_{13}		+		DS_{13}	+	+	3
DD_{03}		−		PF_{03}	−	+	4
DD_{05}	+	+	1	PF_{13}		−	
DD_{13}		+		FP_{05}	−	−	2
DD_{15}	−	+	4	FP_{15}	+	+	3
FF_{05}	+	+	2	DG_{05}	−	+	4
FF_{07}		+		DG_{15}	+	−	4
FF_{15}	+	+	2	GD_{07}		−	
FF_{17}	+	+	1	GD_{17}		+	

Table XII

(*cf.* Fig. 13)

$\overline{K}N \rightarrow \overline{K}\Delta$

Channel	Exp.	Skyrme	
PP_{11}	+	+	4
PP_{13}	−	+	4
DD_{13}	−	+	4
DD_{15}	+	+	4
FF_{15}		+	
FF_{17}	+	+	2
GG_{17}	−	+	4
GG_{19}		+	
SD_{11}	+	+	4
DS_{13}	−	−	2
PF_{13}		+	
FP_{15}	0	−	4
DG_{15}		+	
GD_{17}	+	−	4

Table XIII

(*cf.* Fig. 14)

Tables VI-XIII. KN and $\overline{K}N$ processes: Skyrme model *vs.* experiment. See caption for Tables I-V.

dependent experimental amplitudes $\{L_{1,2L-1}, L_{1,2L+1}, L_{3,2L-1}, L_{3,2L+1}\}$ for each value of pion angular momentum $L > 0$; for example, the F_{15} and F_{37} amplitudes take a much greater excursion through the unitarity circle than do the F_{17} and F_{35} curves.[7,8,13] We shall see this explicitly in Section III.

For the inelastic processes $\pi N \to \pi \Delta$, $\pi N \to \eta N$, $\pi N \to K\Lambda$, and $\pi N \to K\Sigma$, the sign agreement between the Skyrme-model and experimental amplitudes is, respectively, 100%, 80%, 80% and 85%. Such numbers are certainly competitive with traditional algebraic coupling schemes such as $SU(6)_W$ as well as with the nonrelativistic quark model, although unlike the Skyrme model, which is a full-fledged dynamical model, these approaches concern themselves only with the behavior of the amplitudes at resonance energies. As in the elastic case, the lower partial waves in the Skyrme model are often in disagreement with experiment, whereas the F waves—which are the first not to mix with the skyrmion's zero-modes—represent the model at its best. Clearly, a careful treatment of the zero-modes, which would enable us to trust our analysis in the lower partial waves, would be of the utmost importance.

KN processes. The situation is quite the opposite for KN scattering (Tables VI and VII). The agreement for both $KN \to KN$ and $KN \to K\Delta$ is dismal.[♮4] The reason for this is not hard to understand. KN processes occupy a special role from the point of view of the quark model, since resonances in these channels (unlike $\overline{K}N$) cannot correspond to qqq, but rather $qqqq\bar{q}$ states. Not surprisingly, in Nature, the majority of amplitudes show no hint of a resonance, and are in fact repulsive (that is, curve clockwise). The existence of *any* such

---

♮4 In light of the three-fold ambiguity in the experimental solution for $KN \to K\Delta$, we have not presented "scores" in Table VII; however, a comparison of the Skyrme model amplitudes to any one of these solutions would produce mostly 4's.

resonances is still an open question, with the most recent analyses favoring such states in at least two channels. In contrast, there is nothing particularly "exotic" about KN scattering in the skyrmion approach, for reasons we shall discuss below. Consequently, most of the Skyrme-model graphs evince the usual resonant behavior: anticlockwise curves and Breit-Wigner peaks in the speed. In Section IV we shall speculate on whether the (apparent) existence of KN resonances in the real world might be construed as evidence for the soliton nature of the nucleon.

$\overline{K}N$ **processes.** Finally, the Skyrme model gives mixed results in describing $\overline{K}N$ scattering (Tables VIII-XIII). On the level of individual graphs, the model works less well for $\overline{K}N$ than for πN scattering; this is perhaps a consequence of our having set $m_K = 0$, which is much more severe than setting $m_\pi = 0$. Nevertheless, in certain important respects, the agreement is quite pleasing. Most notably, for the processes $\overline{K}N \to \overline{K}N$ and $\overline{K}N \to \pi\Sigma$, the model successfully reproduces a pattern reminiscent of $\pi N \to \pi N$ that characterizes the four independent experimental amplitudes for each value of L: specifically, in the model as in Nature, the P_{01}, D_{03}, F_{05} and G_{07} amplitudes travel significantly further through the unitarity circle than do their counterparts. We shall return to this "big-small-small-small" pattern in Sections V and VI. The sign agreement for $\overline{K}N \to \pi\Sigma$, $\overline{K}N \to \pi\Lambda$, $\overline{K}N \to \eta\Lambda$, $\overline{K}N \to \pi\Sigma^*$ and $\overline{K}N \to \overline{K}\Delta$ is 65%, 64%, 67%, 67% and 55%, respectively. Agreement in the last of these processes is extremely poor.

It should be kept in mind that, for most of the processes summarized in

these tables, the experimental curves do not represent the data directly, but result instead from a multi-parameter fit of the differential cross-section to the squared sum of partial-wave amplitudes. Such a fit involves a complex, model-dependent and frequently ambiguous statistical analysis, or "solution," of multi-body final states. (For example, $\pi\Delta$ must be disentangled from ρN.) In fact, for processes with relatively low statistics, not only can two experiments differ substantially from one another, but two solutions of the *same* data can disagree (*cf.* Table VII and Fig. 7, for example). In light of this, it is noteworthy that the Skyrme model does best for the processes that are relatively well established (*e.g.*, $\pi N \rightarrow \pi N$, $\pi N \rightarrow \pi\Delta$, $\overline{KN} \rightarrow \overline{KN}$), and worst for those that seem the least well understood (*e.g.*, $KN \rightarrow K\Delta$ and $\overline{KN} \rightarrow \overline{K}\Delta$). It would be interesting to see whether, ten years hence, there will be any noticeable improvement in agreement between the model and experiment for these latter processes.

Before proceeding to the specifics of our analysis, we would like, once again, to express our wonderment that so much detailed structure of the meson-nucleon S-matrix—much of it in reasonable accord with Nature—can emerge from a simple meson Lagrangian with no explicit quark or nucleon fields. The moral is that *this structure must be largely determined by the symmetries of the effective Lagrangian alone.* (By this we mean, not just the familiar chiral symmetries, but also the peculiar "K-symmetry" characterizing hedgehog solitons, as reviewed in Appendix B.) It is surprising that effective Lagrangians have so much to say far beyond the "soft-pion" energy regime to which they are normally applied.

The remainder of this paper is organized as follows. In Section II we review the formalism for meson-nucleon scattering in skyrmion models of the nucleon. Sections III, IV and V are devoted to a pictorial comparison between the model

and experiment for πN, KN and $\overline{K}N$ scattering, respectively.

In Section VI, which we consider the theoretical heart of the paper, we explore the degree to which the predictions of the Skyrme model, both successful and unsuccessful, can in fact be considered *model-independent* (*i.e.*, independent of the precise details of the Skyrme Lagrangian, but based only on the familiar "hedgehog" form of the soliton, as reviewed below). In particular, we shall focus on sign predictions for inelastic processes, and on the "big-small-small-big" and "big-small-small-small" patterns mentioned earlier. The question of model-independence is a crucial one; for, if the soliton approach to baryon physics is ever to be honed into an accurate calculational tool, Skyrme's Lagrangian will eventually have to give way to a more realistic model involving many more low-lying mesons. In the course of our investigation, we shall discover what we believe to be the secret behind much of the Skyrme model's success in describing the scattering data. As a consequence, we shall be able to delineate a large *class* of models which, we believe, would enjoy comparable overall success. We hope that this might usefully constrain the model-building efforts currently under way.

In Section VII we leave the Skyrme Lagrangian behind, and concentrate instead on the assumption that the optimal low-energy effective Lagrangian of Nature possesses solitons of the same "hedgehog" structure as in the Skyrme model. It has been shown in the context of 2-flavor skyrmion physics that this assumption implies the existence of energy-independent linear relations between *experimental* $\pi N \to \pi N$ and $\pi N \to \pi \Delta$ partial-wave amplitudes.[8,15] In general, these relations are well satisfied by the experimental data, with certain exceptions in the lower partial waves.[8] Section VII examines to what extent inclusion of a third light flavor modifies these relations; we focus, in particular, on

the peculiar role played by the Wess-Zumino term. We shall find that all but one of these relations emerge virtually unscathed in the 3-flavor formalism. We also discuss some new linear relations designed to test the conclusions of Section VI.

In order to make this paper relatively self-contained, Appendix A depicts some intermediate results of our numerical analysis, Appendix B contains a derivation of the 3-flavor scattering formalism first presented in Ref. 12, and Appendix C gives explicit formulae for the group-theoretic expressions we have used. Finally, Appendix D contains the Skyrme-model graphs for the six $\pi N \to \phi_{PS} B$ and $\overline{K}N \to \phi_{PS}B$ processes for which an experimental partial-wave analysis in the resonance region has yet to be done, namely: $\pi N \to \eta \Delta$, $\pi N \to K \Sigma^*$, $\overline{K}N \to \eta \Sigma$, $\overline{K}N \to \eta \Sigma^*$, $\overline{K}N \to K\Xi$ and $\overline{K}N \to K\Xi^*$. We very much hope that this paper will provide fresh impetus for such work.

II. Basic Notions

In order to pave the way for the detailed comparison that follows between the Skyrme model and experiment, this Section is devoted to a brief review of the meson-nucleon scattering formalism in soliton models. (The casual reader eager for results should skip directly to Section III.) Since we shall be contrasting the 2- and 3-flavor versions of the Skyrme model in Sections III, VI and VII, we shall sketch both formalisms here.

The Skyrme Lagrangian is given by:[1-3]

$$\mathcal{L} = \frac{f_\pi^2}{16} \text{Tr} \, \partial_\mu U \partial^\mu U^\dagger + \frac{1}{32e^2} \text{Tr}[(\partial_\mu U)U^\dagger, (\partial_\nu U)U^\dagger]^2 + \mathcal{L}_{\text{WZ}} \qquad (1)$$

with U an $SU(2)$ or $SU(3)$ matrix in the 2-flavor or 3-flavor model, respectively. Here, the first term is the usual nonlinear sigma model familiar from soft-pion

physics; the second serves to stabilize a finite-size soliton, or "skyrmion," which is our candidate nucleon; and the third, the Wess-Zumino term,[3,43] reflects the presence of anomalies.[‖5] The traditional identification of the Goldstone fields comes from setting

$$
U = \begin{cases} \exp\left(\frac{2i}{f_\pi} \sum_{a=1}^{3} \pi^a \sigma^a\right) & : \quad \text{2-flavor case} \\ \exp\left(\frac{2i}{f_\pi} \sum_{a=1}^{8} \phi^a \lambda^a\right) & : \quad \text{3-flavor case} \end{cases}
$$

in (1).

To study meson-nucleon scattering in this model, one simply breaks up the Goldstone fields π^a or ϕ^a into two pieces: a spatially-varying c-number piece, $i.e.$, the skyrmion, and a fluctuating piece, which we identify with physical mesons. Calculating the meson-nucleon T-matrix[‖6] then reduces to a problem of potential scattering, from which partial-wave phase-shifts can be extracted in the usual manner. In addition, it is necessary to fold in a little group theory, as we now describe.

Consider first the case of 2-flavor scattering, which suffices for the study of the non-strange processes $\pi N \to \pi N$, $\pi N \to \pi \Delta$ and $\pi \Delta \to \pi \Delta$. The quantum numbers needed to describe such processes are the following: the initial and final pion angular momenta L and L'; the initial and final spin (or isospin) representation of the baryon s and s', which equal $\frac{1}{2}$ for nucleons and $\frac{3}{2}$ for Δ's; and the total pion-baryon isospin and angular momentum $\mathbf{I}$ and $\mathbf{J}$. The T-matrix

---

‖5 The Wess-Zumino term is not present in the 2-flavor model unless it is gauged.[3]

‖6 In order to facilitate comparison to experiment, we will present all our results in terms of T-matrix elements. The T-matrix is related to the S-matrix via $\mathbf{T} = (\mathbf{S} - \mathbf{1})/2i$, where $\mathbf{1}$ is the identity operator on the Hilbert space (which vanishes for inelastic scattering).

describing such processes in the Skyrme model can then be shown to be:[8,15]

$$\mathbf{T}(\{LsIJ\} \rightarrow \{L's'IJ\})$$

$$= (-1)^{s'-s}\sqrt{(2s+1)(2s'+1)}\sum_K (2K+1) \left\{ \begin{array}{c} KIJ \\ s'L'1 \end{array} \right\} \left\{ \begin{array}{c} KIJ \\ sL1 \end{array} \right\} \mathcal{T}_{KL'L} \,. \qquad (2)$$

The expressions in curly brackets are $6j$-symbols, and the sum over K extends over all integer values consistent with $|L-1| \leq K \leq L+1$ and $|L'-1| \leq K \leq L'+1$. The quantities $\mathcal{T}_{KL'L}$, which are functions of pion energy ω, are the "reduced amplitudes" of the model, obtainable numerically from a phase-shift analysis about the classical soliton solution of the Lagrangian. (In contrast, we shall refer to the bold-face $\mathbf{T}$'s as "physical amplitudes.") Although these reduced amplitudes have been presented previously,[7,14] we display them in Appendix A in a form more suited to our purposes.

Although, in Eq. (2), K plays the part of a dummy index, it actually has an interesting physical interpretation. Specifically, K can be viewed as the vector sum of the pion's angular momentum and isospin in the unphysical frame in which the pion scatters, not from a nucleon, but rather from an unrotated soliton of the "hedgehog" form. (A hedgehog soliton is one in which the c-number piece of the pion field, an isovector, is proportional to $\hat{r}$; $cf.$ Eq. (15) in Appendix B below.) This frame is "unphysical" in that a nucleon properly corresponds to a *rotating* hedgehog soliton in the skyrmion approach.[49] More details on the meaning of K can be found in Refs. 7-15, as well as in Appendix B below.

The 3-flavor analog of Eq. (2) is of the same general structure albeit a little more complicated. The 3-flavor scattering processes that we are focusing on are

special cases of the general quasielastic process

$$\phi_{\rm PS} B \to \phi'_{\rm PS} B',$$

where $\phi_{\rm PS}$ and $\phi'_{\rm PS}$ are pseudoscalar-octet mesons and B and B' are $\frac{1}{2}^+$ octet or $\frac{3}{2}^+$ decuplet baryons. The meson-baryon system in either the entering or exiting channel for such a process can be fully characterized by the following set of quantum numbers: the orbital angular momentum L of the meson; the spin s and flavor representation R of the baryon [*i.e.*, $(s,R) = (\frac{1}{2},\mathbf{8})$ or $(\frac{3}{2},\mathbf{10})$]; the total meson-baryon angular momentum $\mathbf{J}$; and the total $SU(3)_{\rm flavor}$ quantum numbers $\{R_{\rm tot}, \gamma, I_{\rm tot}, I_{z\rm tot}, Y_{\rm tot}\}$.[♮7] As in the 2-flavor case, the physical T-matrix can be expressed as a superposition of reduced amplitudes:[12,13]

$$\mathbf{T}(\{LsRR_{\rm tot}\gamma I_{\rm tot}I_{z\rm tot}Y_{\rm tot}\mathbf{J}\} \to \{L's'R'R_{\rm tot}\gamma' I_{\rm tot}I_{z\rm tot}Y_{\rm tot}\mathbf{J}\}) \quad =$$

$$(-1)^{s'-s}\frac{\sqrt{\dim R \cdot \dim R'}}{\dim R_{\rm tot}} \sum_{\{IY\}} \sum_i \sum_K (2i+1)(2K+1) \left\{ \begin{matrix} KiJ \\ s'L'I \end{matrix} \right\} \left\{ \begin{matrix} KiJ \\ sLI \end{matrix} \right\} \qquad (3)$$

$$\times \left(\begin{matrix} R_{\rm tot}\gamma' \\ i,1+Y \end{matrix} \middle| \begin{matrix} R' & \mathbf{8} \\ s'1 & IY \end{matrix} \right) \left(\begin{matrix} R & \mathbf{8} \\ s1 & IY \end{matrix} \middle| \begin{matrix} R_{\rm tot}\gamma \\ i,1+Y \end{matrix} \right) \tau_{KL'L}^{\{IY\}} .$$

This expression, whose derivation is reviewed in Appendix B, requires some explication. The quantities in parentheses are $SU(3)$ isoscalar factors, tabulated by DeSwart.[44] The pair $\{IY\}$ is summed over $\{1,0\}, \{0,0\}$, and $\{\frac{1}{2},\pm 1\}$. The index K assumes integral values when $\{IY\} = \{1,0\}$ or $\{0,0\}$ and odd-half-integral values when $\{IY\} = \{\frac{1}{2},\pm 1\}$, while the index i assumes odd-half-integral

---

♮7 Here γ is a largely redundant index whose only real purpose is to distinguish between degenerate representations that can occur in the product of two $SU(3)$ representations, as for example the $\mathbf{8}_{\rm sym}$ and $\mathbf{8}_{\rm antisym}$ in $\mathbf{8} \times \mathbf{8}$.[44] As can be seen in Eq. (3), it is *not* in general conserved, even for exact $SU(3)_{\rm flavor}$. To understand this, one need only consider the nonvanishing $\mathbf{8}_{\rm antisym} \leftrightarrow \mathbf{8}_{\rm sym}$ coupling $\mathrm{Tr}(\{\overline{B}, \Phi\}[B, \Phi])$ between the baryon octet B and the meson octet Φ.

and integral values, respectively, in these cases. In addition, these sums are constrained by the various triangle inequalities implicit in the two $6j$ symbols, as a consequence of which we find the following contributing reduced amplitudes for physical processes:[8]

$\phi_{\rm PS} B \to \phi'_{\rm PS} B'$ with $L' = L$:

$\{\mathcal{T}^{\{1,0\}}_{L\pm 1,LL},\ \mathcal{T}^{\{1,0\}}_{LLL},\ \mathcal{T}^{\{0,0\}}_{LLL},\ \mathcal{T}^{\{\frac{1}{2},1\}}_{L\pm\frac{1}{2},LL},\ \mathcal{T}^{\{\frac{1}{2},-1\}}_{L\pm\frac{1}{2},LL}\}$ all contribute;

$\phi_{\rm PS} B \to \phi'_{\rm PS} B'$ with $L' = L \pm 2$:

only $\mathcal{T}^{\{1,0\}}_{KL'L}$, $K = (L + L')/2$, contributes. Furthermore, by time-reversal invariance,[7-8] it follows that $\mathcal{T}^{\{1,0\}}_{KL'L} = \mathcal{T}^{\{1,0\}}_{KLL'}$.

Useful closed-form expressions for the group-theoretic coefficients in Eq. (3) that multiply these reduced amplitudes are given in Appendix C.[9]

It turns out that the reduced amplitudes $\mathcal{T}^{\{\frac{1}{2},1\}}_{KLL}$ and $\mathcal{T}^{\{\frac{1}{2},-1\}}_{KLL}$ are numerically quite close to one another for all energies.[10] It is therefore convenient to introduce the linear combinations

$$\mathcal{T}^{\pm}_{KLL} = \frac{1}{2}\left(\mathcal{T}^{\{\frac{1}{2},1\}}_{KLL} \pm \mathcal{T}^{\{\frac{1}{2},-1\}}_{KLL}\right), \quad K = L - \frac{1}{2} \ \ \text{or} \ \ L + \frac{1}{2};$$

these are depicted in Appendix A. It happens that, in the Skyrme model, these are the only new quantities that one needs in order to pass from the 2-flavor to

---

[8] Parity precludes the case $L' = L \pm 1$.
[9] The analogous 2-flavor quantities are tabulated in Appendix B of Ref. 8.
[10] In fact, they would be precisely equivalent to one another in the absence of the Wess-Zumino term;[13] that they are so close means that the Wess-Zumino term has a small effect on the meson-nucleon phase-shifts in the Skyrme model.

the 3-flavor formalism. Specifically, the amplitudes $T_{LLL}^{\{0,0\}}$ turn out to be trivial:

$$T_{LLL}^{\{0,0\}}(\omega) \equiv 0,$$

while the quantities $T_{KL'L}^{\{1,0\}}(\omega)$ are identical to the 2-flavor reduced amplitudes $T_{KL'L}(\omega)$ that appear in Eq. (2).

From the discussion in this Section we can make the following observations:

1. Since all physical amplitudes for processes with $L' = L \pm 2$ are proportional to the single reduced amplitude $T_{KL'L}^{\{1,0\}} = T_{KLL'}^{\{1,0\}}$ with $K = (L + L')/2$, it follows that *all such amplitudes for each value of K are necessarily proportional to one another.* The group-theoretic coefficients of (2) and (3) furnish the relative magnitudes and signs of these amplitudes for the 2- and 3-flavor model, respectively.

2. Processes with $L = L'$ are more complicated from a group-theoretic standpoint, since they are expressed as a superposition of eight reduced amplitudes. However, from the graphs in Appendix A, we see that, with a few exceptions in the lower partial waves, *the three reduced amplitudes* $\{T_{L-1,LL}^{\{1,0\}}, T_{LLL}^{\{1,0\}}, T_{L-\frac{1}{2},LL}^{+}\}$ *vary much more dramatically as functions of energy than do the other five amplitudes* $\{T_{L+1,LL}^{\{1,0\}}, T_{LLL}^{\{0,0\}}, T_{L+\frac{1}{2},LL}^{+}, T_{L-\frac{1}{2},LL}^{-}, T_{L+\frac{1}{2},LL}^{-}\}$*, and consequently provide the dominant contributions to the physical Skyrme-model amplitudes.*

3. Lastly, we ought to point out that *Eqs. (2) and (3) are valid for any soliton model of the baryon, not just Skyrme's, in which the soliton is a "hedgehog" configuration.* The only model-dependent input is the precise values of the reduced amplitudes.

We will make frequent use of these observations throughout the remainder

of the paper. We turn now to a channel-by-channel comparison of the Skyrme model T-matrix with experiment.

III. πN Scattering

We begin with the elastic case $\pi N \to \pi N$. This process has been studied before in the context of both the 2-flavor[7-12,14-15] and 3-flavor[12-13] Skyrme models; in particular, the reader is referred to Ref. 7 for a discussion of the spectrum of baryon resonances in the 2-flavor model. Elastic πN scattering is extremely well understood experimentally, as evidenced by the close agreement between the three principal partial-wave analyses (Refs. 17-19). As such, it represents a crucial test for the Skyrme model.

Figure 1a displays the 30 experimental $\pi N \to \pi N$ partial-wave amplitudes for $0 \leq L \leq 5$ (Ref. 18) and $6 \leq L \leq 7$ (Ref. 17) juxtaposed with both the 2- and 3-flavor Skyrme-model graphs.[‖11] For completeness, we have also summarized the results of our mass spectrum calculation[7,13] in Fig. 1b. We consider the overall degree of agreement impressive. Obviously, for G waves and higher, the Skyrme model graphs are much too large;[‖12] this is primarily due to the fact that, in our formalism, we are not allowing for the large variety of inelastic processes that dominate these channels in Nature. In this regard, the 3-flavor Skyrme model, which allows for final states involving strangeness such as $K\Sigma$, constitutes a clear improvement over the 2-flavor model. Inclusion of a

---

‖11 In Ref. 7, in contrast, we compared the Skyrme-model curves solely to Ref. 17. Overall, the Skyrme model agrees somewhat better with Ref. 18 than with Ref. 17. The most recent experimental analysis (Ref. 19) only goes up to $E_{\text{CM}} = 1726$ MeV and $L = 3$.

‖12 Note the magnification by a factor of 4 in the experimental graphs with $L \geq 4$.
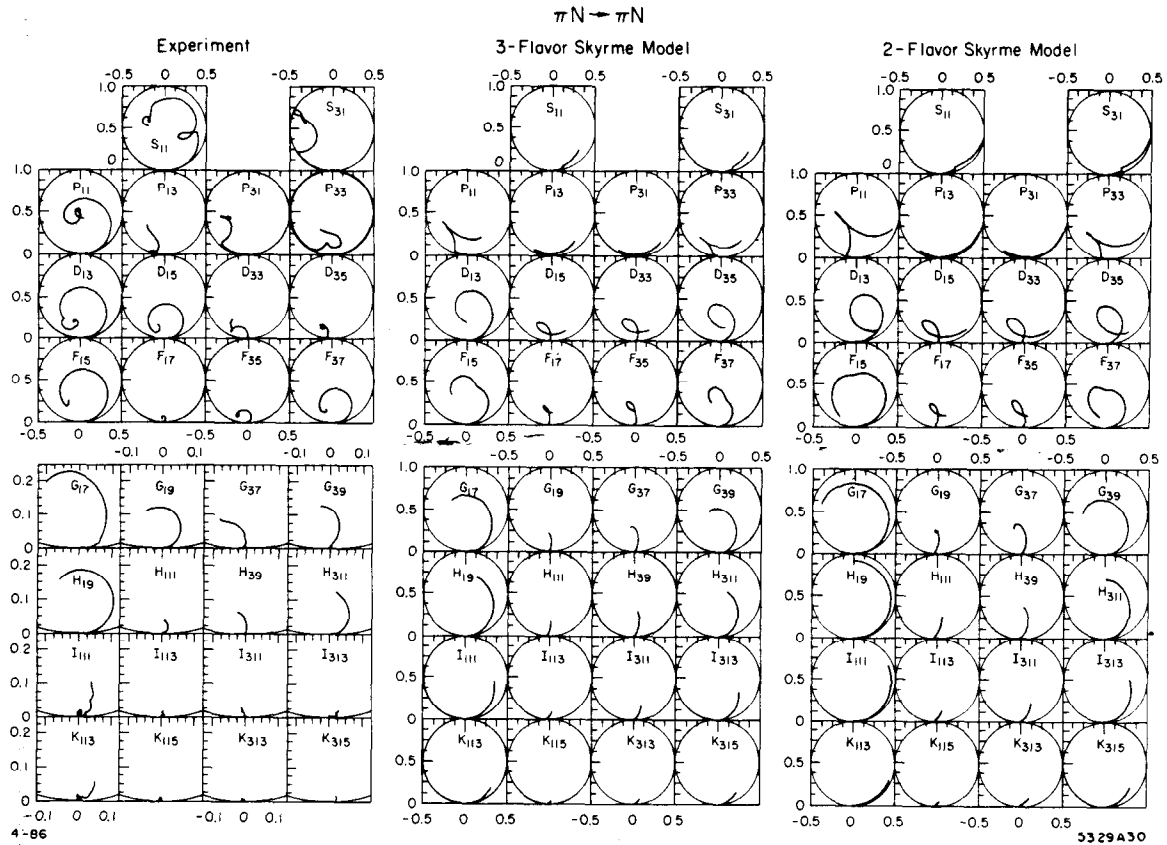
FIG. 1a. $\pi N \to \pi N$: comparison between the 2- and the 3-flavor Skyrme models and the experimental solutions of: (i) Ref. 18 for $L \le 5$ (1.08 GeV $\le E_{CM} \le$ 2.40 GeV); (ii) Ref. 17 for $6 \le L \le 7$ (1.08 GeV $\le E_{CM} \le$ 2.50 GeV). The plots show Im(T) $vs.$ Re(T) for each channel. Channels are labeled by $L_{2I,2J}$, where L is the pion angular momentum, I is the total isospin and J the total angular momentum. Note the change of scale for the experimental graphs with $L \ge 4$.

mass (GeV)

3.5

3.0

2.5

2.0

1.5

1.0

0.5

$N(1550)\ S_{11}$
$N(1850)\ S_{11}$
$N(939)\ P_{11}$
$N(1440)\ P_{11}$
$N(1700?)P_{11}$
$N(1700)\ P_{13}$
$N(1525)\ D_{13}$
$N(1675)\ D_{13}$
$N(1675)\ D_{15}$
$N(1680)\ F_{15}$
$N(1882)\ F_{15}$
$N(1970)\ F_{17}$
$N(2200)\ G_{17}$
$N(2250)\ G_{19}$
$N(2230)\ H_{19}$
$N(2577)\ I_{1,11}$
$N(2612)\ K_{1,13}$
$\Delta(1620)\ S_{31}$
$\Delta(1890)\ S_{31}$
$\Delta(1910)\ P_{31}$
$\Delta(1232)\ P_{33}$
$\Delta(1600)\ P_{33}$
$\Delta(1920)\ P_{33}$
$\Delta(1710)\ D_{33}$
$\Delta(1940)\ D_{35}$
$\Delta(1910)\ F_{35}$
$\Delta(2200)\ F_{35}$
$\Delta(1950)\ F_{37}$
$\Delta(2350)\ F_{37}$
$\Delta(2200)\ G_{37}$
$\Delta(2300)\ G_{39}$
$\Delta(2400)\ H_{39}$
$\Delta(2400)\ H_{3,11}$
$\Delta(2794)\ I_{3,13}$
$\Delta(2990)\ K_{3,15}$
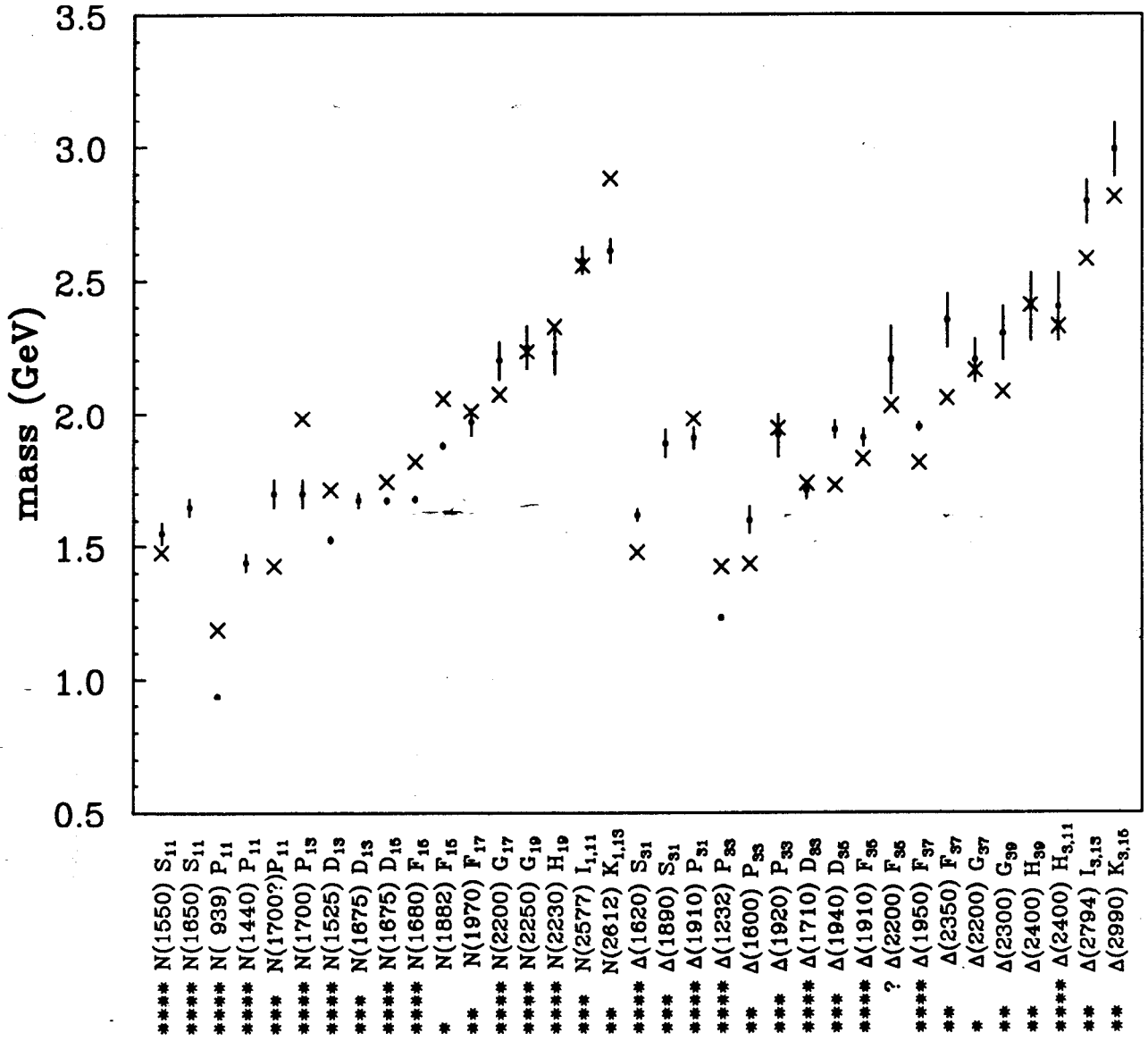
FIG. 1b. Spectrum of N and Δ resonances: Skyrme model vs. experiment. The experimental masses (indicated by dots) and uncertainties are taken from Ref. 18, except for the $N(1882)\ F_{15}$ and the four I- and K-wave states, which are taken from Ref. 17. The Skyrme-model predictions of Refs. 7 and 13 are indicated by crosses. In general, the 2- and 3-flavor predictions are identical; the exceptions are the $N(1882)\ F_{15}$ and the $\Delta(2350)\ F_{37}$, which only exist in the 3-flavor Skyrme model.[13] Resonances have been assigned stars in accord with the Particle Data Group, ranging from four stars for the best established down to one star for the least well established states. The most recent analysis[19] finds no evidence for the $N(1700)\ P_{11}$, but instead finds a state near 1500 MeV. Also shown are the four observed 3- or 4-star resonances which have no Skyrme-model counterparts in our analysis, namely the $N(1650)\ S_{11}$, the $N(1440)\ P_{11}$, the $N(1675)\ D_{13}$, and the $\Delta(1890)\ S_{31}$. The Skyrme-model values for m_N and m_Δ are obtained from Eq. (9) of Ref. 49, using our "best fit" parameters $\{e = 4.79,\ f_\pi = 150\,\text{MeV}\}$.

third flavor can also be seen to improve the agreement in the P_{13}, P_{31} and D_{13} channels.

The case of the F waves is more subtle. Although the 3-flavor curves do not appear at first glance to be in quite so close correspondence with Nature as their 2-flavor counterparts, they actually constitute an improvement: a "speed analysis"[13] reveals the emergence of a second resonance in both the F_{15} and the F_{37} 3-flavor amplitudes, in agreement with Nature (see Ref. 13 for details).

Most of the severe disagreement between the model and experiment is concentrated in the lower partial waves, especially the S_{31}, P_{11}, P_{33} and D_{35} channels. As discussed in detail in Refs. 7 and 8, this is probably a failure, not of the Skyrme model *per se*, but rather of our leading order analysis in $1/N_c$.[14] It is illuminating to summarize the situation for these four "problem" channels:

(*i*) The Δ (*i.e.*, the $P_{33}(1232)$) is degenerate with the nucleon in the large-N_c limit; they are split in mass only by terms that scale like $1/N_c$.[49] Consequently, the Δ does not—indeed, cannot—show up as a resonance in a leading-order 2- or 3-flavor analysis such as ours.[15] It is interesting that, *beyond* the energy range associated with the Δ, the experimental and Skyrme-model amplitudes appear to be in quite reasonable agreement (note the cusp-like behavior in each case).

(*ii*) Similar disagreement plagues the P_{11} channel, where the Skyrme-model amplitude stands in stark contrast to the classic resonant behavior that appears

---

[13] This entails looking for Breit-Wigner peaks in the function $|dT/dE|$ plotted against energy.

[14] Specifically, the S, P and D waves can be shown to couple to the rotational and translational zero-modes of the skyrmion, and therefore turn out to be extremely sensitive to next-order $1/N_c$ corrections.[7-8]

[15] Skyrme himself recognized the lack of a P-wave resonance in his model:[2] "The P-wave meson-particle interaction [is] repulsive on the average. There is no indication of the strong attraction observed in the pion-nucleon resonant state, but this would hardly be expected in a static classical treatment where the rotational splitting of the particle states has been ignored."

in Nature, associated with the Roper resonance at 1440 MeV. In light of the qualitative similarity between the P_{11} and P_{33} amplitudes in both the Skyrme model and experiment, we proposed somewhat optimistically in Ref. 7 that the same $1/N_c$ corrections that are expected to produce a low-lying Skyrme-model resonance in the P_{33} channel (i.e., the Δ) are likely to produce a low-lying resonance in the P_{11} channel too (i.e., the Roper).

At the time, this scenario left us somewhat in a quandary, for the following reason. A speed analysis reveals that the Skyrme-model P_{11} amplitude in both the 2-flavor and 3-flavor case contains a weak resonance before the cusp, at approximately 1430 MeV.[16] On aesthetic grounds, it would certainly be hard to justify identifying this tenuous state with the robust Roper resonance seen in Nature; indeed, as just mentioned, we preferred to equate the Roper with a Skyrme-model state that we hoped would emerge in the next order in $1/N_c$. This left us no choice but to associate the Skyrme-model state at 1430 MeV with the next-excited state observed in this channel, which is traditionally assigned a mass near 1700 MeV. The large discrepancy between these two values stood out as one of the most disappointing results in an otherwise successful Skyrme-model spectroscopy (see Fig. 1b). However, the experimental situation for this channel has since changed. Surprisingly, the most recent πN experimental partial-wave analysis[19] finds *no evidence* for a P_{11} excitation at 1700, but instead finds a second state nearly degenerate with the Roper—in much closer agreement with the Skyrme model.[17] It is interesting that, from the point of view of skyrmion physics, these two nearly-degenerate states arise in very different ways: the Roper

---

[16] Note that the amplitude does in fact curve counterclockwise in this region.

[17] The analysis of Ref. 19, which probes an energy range $E_{CM} \leq 1726$ MeV, is not sensitive enough in the upper region to exclude definitively the $P_{11}(1700)$.

(like the Δ) is split from the nucleon only by an energy of $\mathcal{O}(1/N_c)$, while its partner has an excitation energy of $\mathcal{O}(1)$. The observed near-degeneracy is an accidental consequence of the fact that, in the real world, N_c is not a very large number.

(iii) Another area of severe disagreement between the Skyrme model and experiment is in the S_{31} channel, which is repulsive near threshold in Nature but attractive in the Skyrme model. Again, this discrepancy is an artifact of our leading-order $1/N_c$ analysis. Specifically, the repulsive threshold behavior of the S_{31} amplitude, predicted by the Weinberg-Tomozawa two-soft-pion theorem,[46] emerges in the Skyrme model only at order $1/N_c$.[8,47–48]

(iv) Finally, the poor agreement between the model and experiment in the D_{35} channel deserves some comment. It is clear from Fig. 1 that, in the Skyrme model, the D_{35} amplitude is nearly as big as the D_{13}, while in Nature it is by far the smallest of the four D-wave amplitudes. Furthermore, the resonance masses of the four D-wave states are nearly degenerate with one another in both the 2- and 3-flavor Skyrme models,[7,13] while in Nature the D_{35} state at 1940 MeV is 200-300 MeV higher in mass than its three partners.[‖18] It is interesting to speculate as to the reason for these discrepancies between the model and experiment.

It happens that the $D_{35}(1940)$ is of particular interest from the quark point of view, since, in the language of $SU(6)$, it is the only state present in the $L_{\mathrm{quark}} = 1$ 56 that is not contained in the $L_{\mathrm{quark}} = 1$ 70; as such, it serves as a "marker" for this multiplet.[‖19] Now, in Nature, the $L_{\mathrm{quark}} = 1$ 56 is substantially higher

---

‖18 It is noteworthy that the D_{35} amplitude is clearly resonant (hence qualitatively closer to the Skyrme model) in the experimental analysis of Ref. 18, as opposed to that of Ref. 17.

‖19 We thank Bob Jaffe for an illuminating discussion on this point.

in mass than the $L_{quark} = 1$ **70**. However, there is a well-known problem that plagues naive bag-model spectrum calculations:[45] namely, the physical quark excitations corresponding to this multiplet turn out to mix with the (unphysical) translational zero-modes of the center of mass of the system, which also generate an $L_{quark} = 1$ **56**. The result of this mixing is to lower the predicted mass of the multiplet to a phenomenologically-unacceptable level.

It is likely that a similar phenomenon is taking place in our Skyrme-model calculations. One would therefore expect that a proper "factoring-out" of the skyrmion's translational zero-modes would raise the mass of the Skyrme-model prediction for the mass of the D_{35}, improving the agreement with experiment. Hopefully, the overall *size* of the Skyrme-model curve in this channel would be diminished as well. (Of course, the other S- and D-wave states would also be expected to be modified, to the extent that they, too, contain admixtures of the $L_{quark} = 1$ **56**.)

Fortunately, the other $\pi N \to \pi N$ partial waves pose no such problems. It is particularly striking that both the 2- and 3-flavor Skyrme models reproduce the "big-small-small-big" pattern found in Nature, whereby, for instance, the F_{15} and F_{37} amplitudes take much larger excursions through the unitarity circle than do the F_{17} and F_{35} curves;[‖20] furthermore, in the model as in Nature, the first amplitude is almost always bigger than the last: $F_{15} > F_{37}$, *etc.* We shall return to this phenomenon in Section VI, where we shall argue that both the Skyrme model and the optimal 2- and 3-flavor effective Lagrangians of Nature (which we do not know) lie in a large *class* of models which can be expected to display a

---

‖20 The pattern emerges even more sharply if the experimental curves are cut off at the natural resonance scale for each value of L.[8]

big-small-small-big pattern.

A technical aside is in order concerning our parametrization of energies. Each of the Skyrme-model graphs depicted in Fig. 1 extends from threshold to an excitation energy of $2ef_\pi$, where e and f_π are the two independent parameters that enter into the Skyrme Lagrangian, Eq. (1). It is not clear to us how best to convert this energy into GeV's, especially in light of our having set $m_\pi = m_K = 0$ in our phase-shift calculations. However, for purposes of comparison with experiment, an excitation energy of $2ef_\pi$ can be thought of as corresponding roughly to a total center-of-mass energy of 2.5 GeV.[7] We emphasize once again that the *shapes* of the Skyrme-model curves are *completely independent* of the values of e and f_π, apart from the issue of determining precisely where the tails of the curves should be cut off. For simplicity, we shall cut off *all* Skyrme-model graphs presented in this paper at $2ef_\pi$ (although the experimental cutoffs vary).

Let us turn to the process $\pi N \to \pi \Delta$. Of all the inelastic processes that we shall survey, this one is by far the best understood. As a measure of this, the recent partial-wave analysis of Manley *et al.*,[20] which is based on a quarter-million $\pi\pi N$ events, is in good overall agreement with the three principal analyses that preceded it.[21-23]

Figure 2 displays the experimental $\pi N \to \pi \Delta$ solution drawn from Ref. 20 compared with the 2- and 3-flavor Skyrme-model predictions. As in the elastic case, the agreement is surprisingly good. In fact, there is 100% agreement between both the 2- and 3-flavor models and experiment in the signs of the $\pi N \to \pi \Delta$ amplitudes.[21] We find the correctly-rendered minus-sign in the DD_{13}

---

‡21   The reader is referred to Ref. 20 for a survey of sign predictions made by competing theories.
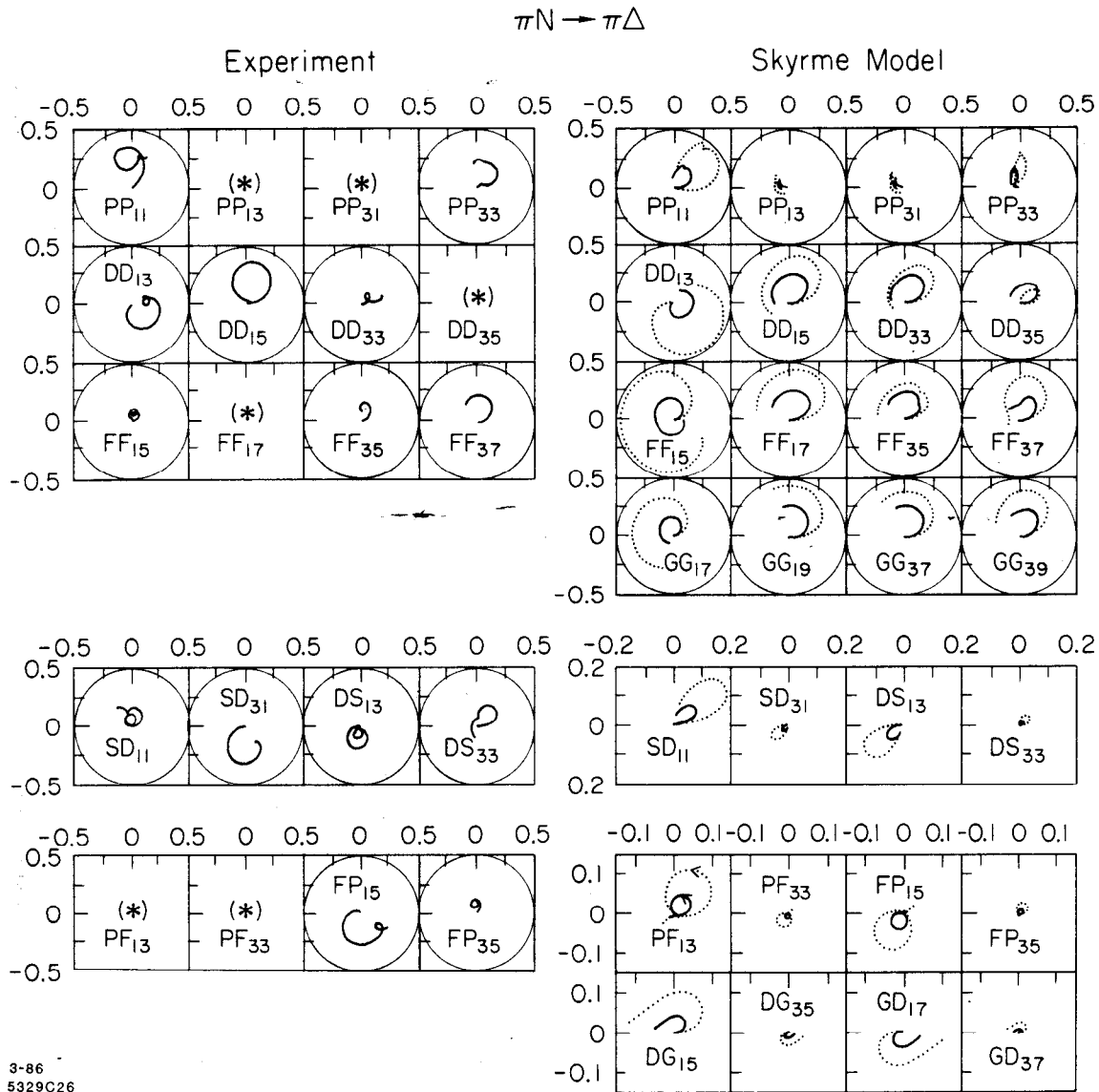
FIG. 2. $\pi N \to \pi \Delta$: comparison between the 2- and the 3-flavor Skyrme models and the experimental solution of Ref. 20 (1.34 GeV $\leq E_{\text{CM}} \leq$ 1.91 GeV). Channels are labeled by $LL'_{2I,2J}$, with L and L' the incoming and outgoing pion angular momenta, respectively. 3-flavor Skyrme model results are depicted by solid lines, 2-flavor results by dotted lines. An asterisk here (and henceforth) denotes amplitudes which were found to be small and/or poorly determined by the available data, and were therefore not included in the experimental solution. Note change of scale for Skyrme-model plots with $L' = L \pm 2$.

channel especially gratifying, in view of the fact that all other PP, DD and FF graphs lie in the upper-half plane. It is also noteworthy that, in both the model and experiment, the FF_{15} amplitudes circle around much more than the FF_{35} and FF_{37} curves.

For channels where $L = L'$, it is clear that the 3-flavor model improves significantly on the 2-flavor model as regards the magnitudes of the curves. However, the reverse is true when $L' = L \pm 2$: in these channels, the 3-flavor curves are uniformly smaller by a factor of $5\sqrt{10}/36 \approx .4$ than their 2-flavor counterparts, which were already smaller than experiment. We shall see when we discuss the processes $KN \to K\Delta$, $\overline{K}N \to \pi\Sigma^*$ and $\overline{K}N \to \overline{K}\Delta$ that the Skyrme model systematically underestimates the sizes of the amplitudes with $L' = L \pm 2$ compared to those with $L' = L$.

In the remainder of this Section, and in Sections IV and V to follow, we shall examine processes that involve strange particles. As a result, whenever we refer to the Skyrme model, we shall mean the 3-flavor version necessarily.

Figures 3 and 4 display the Skyrme model juxtaposed with experimental solutions for the processes $\pi N \to \eta N$ [24] and $\pi N \to K\Lambda$.[26] In general, the Skyrme-model graphs are too small for the former, but too big for the latter. For $\pi N \to \eta N$, the agreement is poor for the lower partial waves ($L \leq 2$) but quite respectable for the higher waves ($L \geq 3$). Probably, this is largely due to the fact that the S-, P- and D waves in the model are highly sensitive to $1/N_c$ corrections, as mentioned earlier. However, the issue is clouded by the fact that the two most recent experimental analyses for this process are themselves in severe disagreement with one another for these waves.[24-25]

The overall degree of agreement is somewhat better for $\pi N \to K\Lambda$. Here,
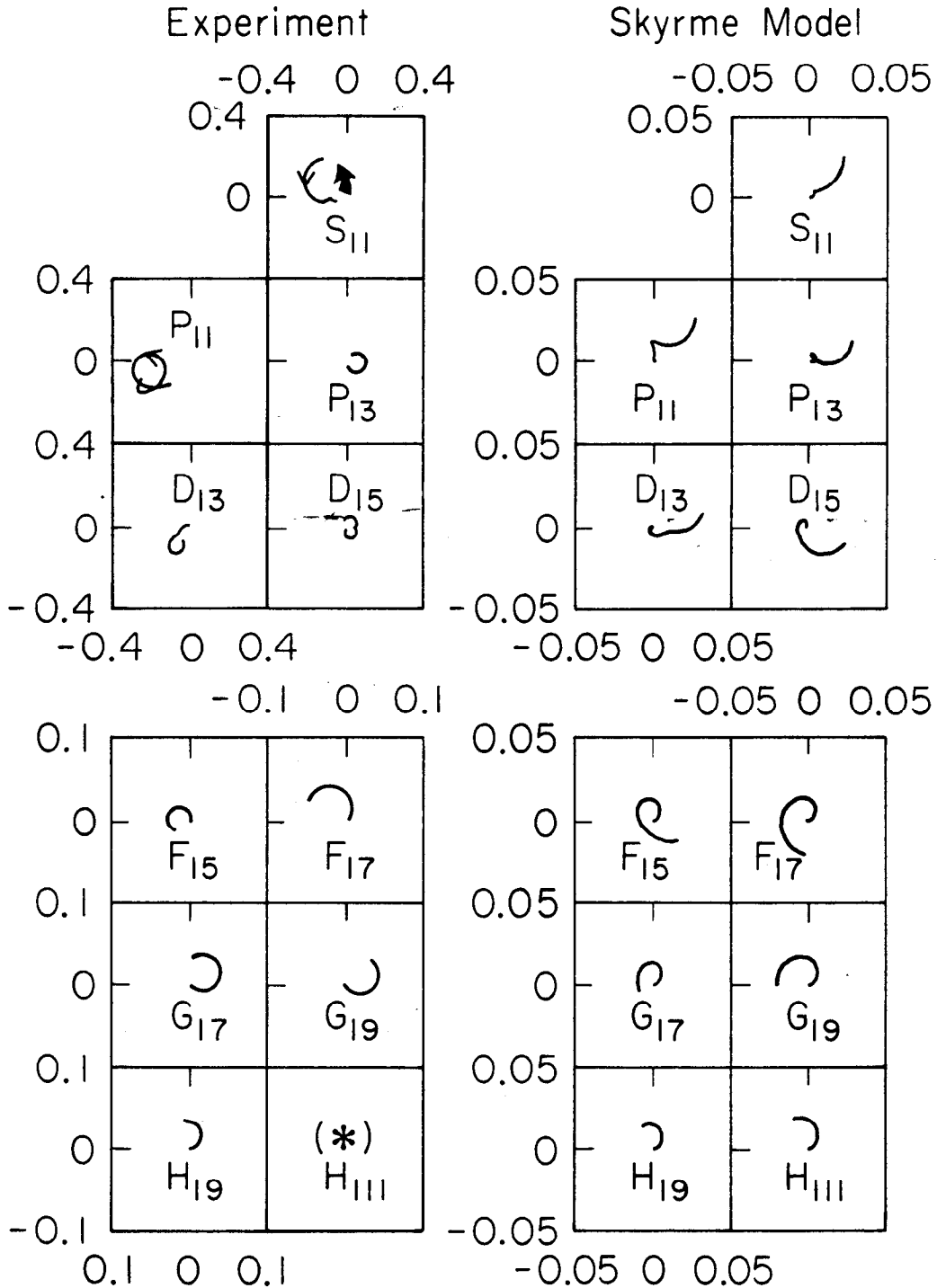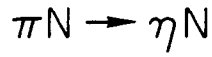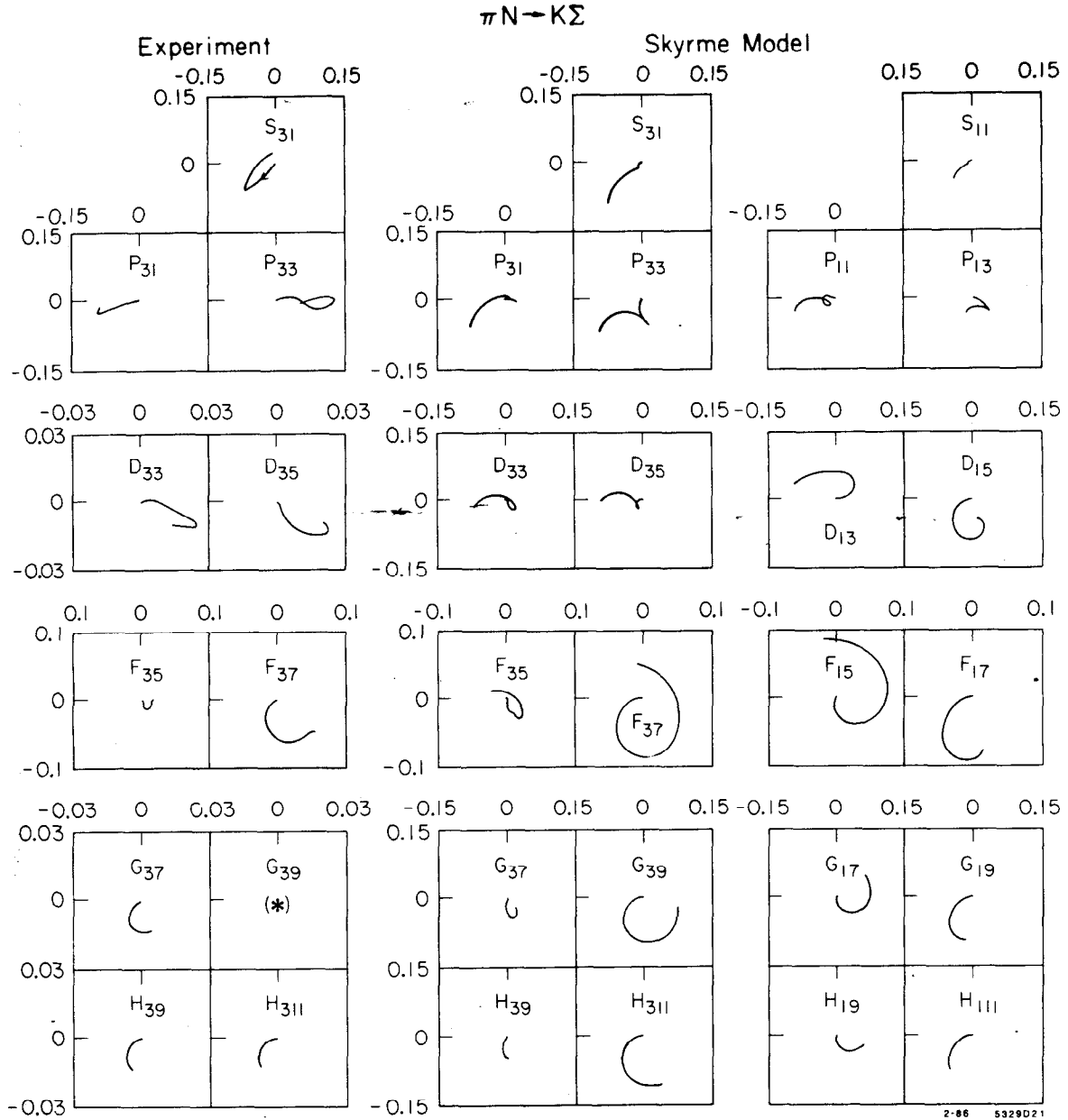
FIG. 3. $\pi N \to \eta N$: comparison between the Skyrme model and the experimental solution of Ref. 24 (1.51 GeV $\leq E_{\text{CM}} \leq$ 2.27 GeV). Channels are labeled by $L_{2I,2J}$. For a fairer comparison, we have added a detached arrow in the experimental S_{11} channel to indicate the expected behavior of the amplitude if one were to extrapolate below the ηN threshold to the πN threshold (recall that these are degenerate in our unbroken-$SU(3)$ treatment of the Skyrme model). Note that experimental and Skyrme-model plots are shown on different scales.

πN→KΛ
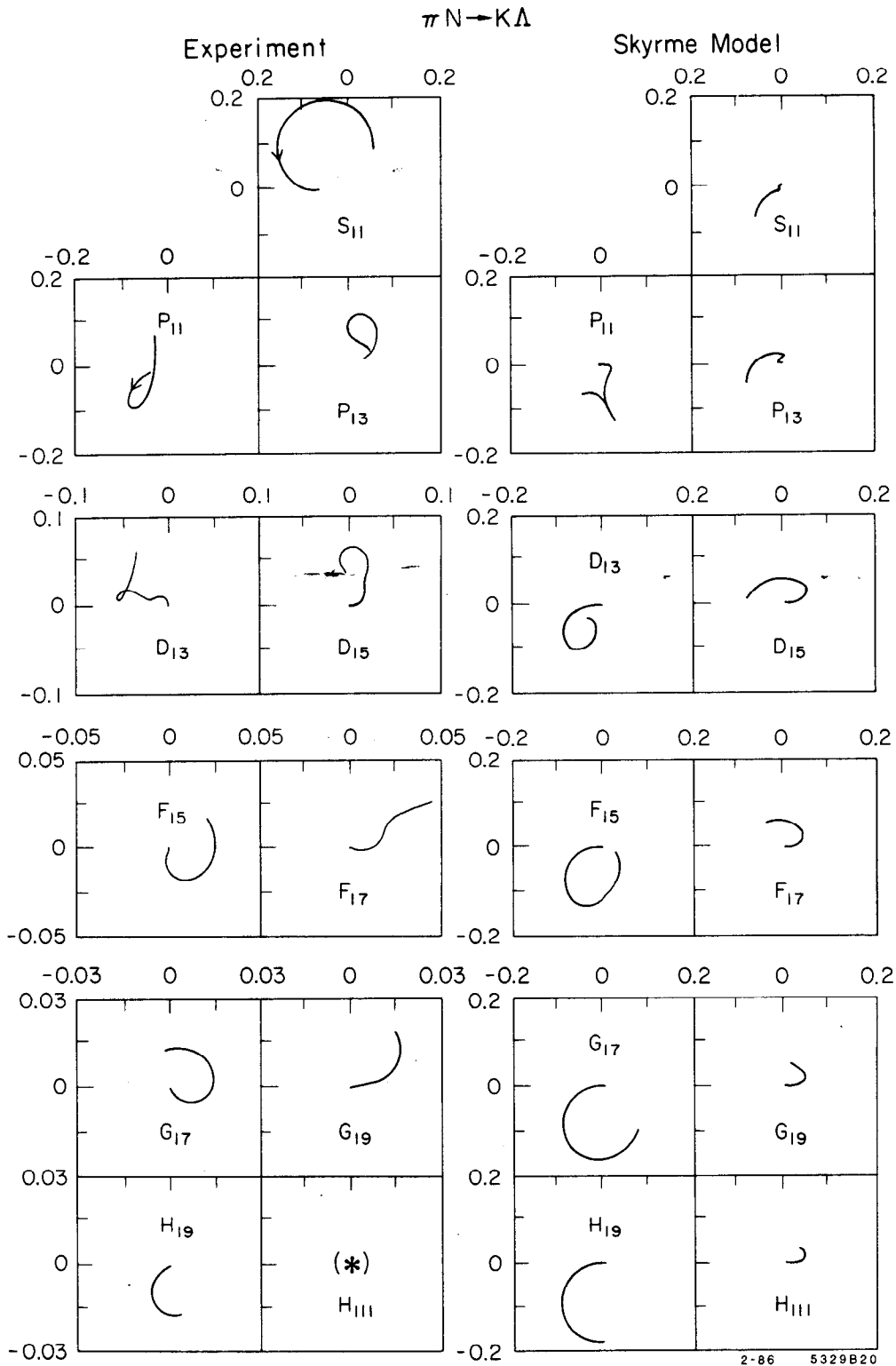
FIG. 4. $\pi N \to K\Lambda$: comparison between the Skyrme model and the experimental solution of Ref. 26 (1.63 GeV $\leq E_{\mathrm{CM}} \leq$ 2.30 GeV). Channels are labeled by $L_{2I,2J}$. Note that experimental and Skyrme-model plots are shown on different scales.

FIG. 5. $\pi N \rightarrow K\Sigma$: comparison between the Skyrme model and the experimental solution of Ref. 27 (1.68 GeV $\leq E_{\mathrm{CM}} \leq$ 2.35 GeV). Channels are labeled by $L_{2I,2J}$. The experimental analysis of Ref. 27 involves only $I = 3/2$ channels, whereas the Skyrme-model results are shown for both $I = 3/2$ and $I = 1/2$. Note that experimental and Skyrme-model plots for G waves are shown on different scales.

31

the most noticeable feature of the model is the sign alternation characterizing the plots; this pattern appears to be present in Nature as well, albeit in a more ambiguous manner.

Figure 5 depicts the process $\pi N \to K\Sigma$.[27] Despite the scale difference between the Skyrme model and experiment in the D, G and H waves, the agreement generally is quite good. It is interesting to compare the experimental graphs of Ref. 27, which are the ones displayed in Fig. 5, with the results of previous partial-wave analyses.[28-30] These earlier analyses, based on an order of magnitude fewer events, required several additional strongly-coupled resonances in the lower partial waves. Furthermore, the four solutions presented in Ref. 29 and the two solutions given in Ref. 30 are all characterized by positive F_{35} and F_{37} amplitudes, and they predict that the F_{35} amplitude should be *larger* than the F_{37}. On all of these counts, the Skyrme-model results argue strongly in favor of Ref. 27.

Unfortunately, the analysis of Ref. 27 is restricted to isospin-$\frac{3}{2}$ channels. In the isospin-$\frac{1}{2}$ sector, there is no visible agreement among the previous studies, although on the whole the Skyrme-model graphs seem closest to those of Ref. 30.

The comparison with the Skyrme model sheds light on an interesting observation made by the authors of Ref. 27. They regard the fact that their partial-wave amplitudes lie almost entirely in the lower-half plane as compelling evidence against the existence of "exotic" 27-plet resonances in these channels.[‖22] This claim is based on the observation that, in the isospin-$\frac{3}{2}$ channels, the **27**

‖22 Such states are called "exotic" because they cannot be formed from three quarks; see Section IV.

couples to $\pi N \to K\Sigma$ with a sign opposite to that of the **10**; a strongly-coupled exotic resonance would therefore be expected to spoil the observed homogeneity in sign. However, the Skyrme model provides a counterexample to this claim! For, as we shall see in the following Section, the model actually features an *overabundance* of resonances in the **27**. Nevertheless, in the isospin-$\frac{3}{2}$ channels of $\pi N \to K\Sigma$, these exotics are outweighed by the stronger resonances in the **10**, which are nearly degenerate with those in the **27**.[♮23] The net result is that the Skyrme-model amplitudes, too, favor the lower-half plane, as can be seen in Fig. 5.

The issue of exotic resonances in the Skyrme model is the topic of the following Section.

IV. KN Scattering

We turn, next, to the case of KN scattering. The isospin-0 and isospin-1 channels of KN correspond to pure $\overline{\textbf{10}}$'s and **27**'s of $SU(3)_{\text{flavor}}$. Consequently, a KN resonance, although not forbidden, cannot be composed of three quarks, but must consist instead of four quarks and an antiquark in the simplest case.

The existence of such resonances has been the subject of considerable controversy over the last two decades.[♮24] The most recent partial-wave analyses[33-35] tentatively favor such states in the P_{13} and D_{03} channels, and perhaps in the

---

♮23 This near-degeneracy is simply due to the fact that both sets of amplitudes are built from the *same* reduced amplitudes in the skyrmion formalism.

♮24 On opposite sides of the spectrum, Martin and Oades[31] claim that there are no *bona fide* poles on the second sheet for such processes, while Arndt, Roper and Steinberg[32] seem to find poles in almost every channel; however, in Arndt and Roper's later analysis[33] , most of these poles disappear thanks to a different choice of parametrization.
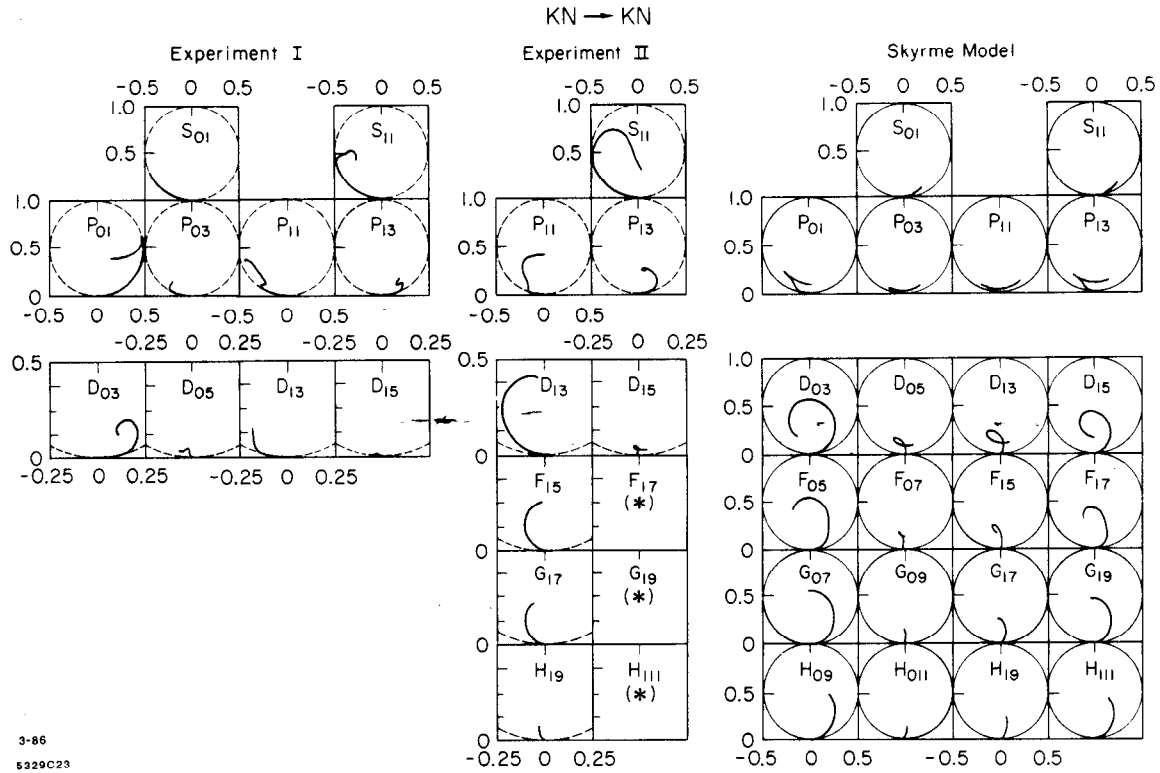
FIG. 6. $KN \to KN$: comparison between the Skyrme model and two experimental solutions: "Experiment I" from Ref. 34 (1.61 GeV $\leq E_{\mathrm{CM}} \leq$ 2.02 GeV), and "Experiment II" from Ref. 33 (1.43 GeV $\leq E_{\mathrm{CM}} \leq$ 2.61 GeV). Channels are labeled by $L_{I,2J}$. Note that experimental and Skyrme-model plots for $L \geq 2$ are shown on different scales.

P_{01}, P_{11}, D_{05} and D_{15} channels as well. It is interesting to see what the Skyrme model has to say on the matter.

Figure 6 illustrates elastic KN scattering in the Skyrme model juxtaposed with the results of the two latest partial-wave analyses.[33,34] The overall degree of agreement between the model and experiment is poor. This should not come as a surprise, for the following reason. It turns out that the 3-flavor Skyrme model with $N_c = 3$ contains as rotational excitations of the canonical "hedgehog" soliton (Eq. (15) below) an infinite tower of baryon multiplets *beyond* the usual spin-$\frac{1}{2}$ octet and spin-$\frac{3}{2}$ decuplet.[4] This tower includes, in particular, a spin-$\frac{1}{2}$ $\overline{10}$ and spin-$\frac{1}{2}$ and spin-$\frac{3}{2}$ 27's. Each of these multiplets would naturally be expected to have excitations of higher angular momentum, just as the usual octet and decuplet have; such states would manifest themselves as resonances in KN scattering. In short, there is nothing exotic about KN processes in the Skyrme model; this is confirmed by the multitude of obviously resonant Skyrme-model amplitudes in Fig. 6.

It is instructive to consider an analogous situation involving the 2-flavor Skyrme model. It is well known that this model contains states with $I = J = \frac{1}{2}, \frac{3}{2}, \frac{5}{2}, \frac{7}{2},...$ that emerge as rotational excitations of the hedgehog.[49] The two lowest-lying multiplets are naturally identified with the nucleons and Δ's, respectively, while the states with $I = J \geq \frac{5}{2}$ are traditionally labeled "artifacts of the model" and swept under the rug. Thankfully, isospin conservation forbids these states from appearing in the s-channel of πN scattering, so that they do not really cause a problem.[♮25] However, one can consider the *gedanken* ex-

---

♮25 Note that an isospin-$\frac{5}{2}$ baryon $B_{\frac{5}{2}}$ *can* be produced in the Skyrme model in the process $\pi N \rightarrow \pi B_{\frac{5}{2}}$ and is therefore required for unitarity.

periment of $\pi^+ \Delta^{++}$ scattering, which is pure isospin-$\frac{5}{2}$. From the quark point of view, this is an exotic process just like KN scattering, and we would expect to see a high proportion of repulsive amplitudes. In contrast, in the skyrmion approach, there is nothing exotic about this channel, since isospin-$\frac{5}{2}$ states exist; we have, in fact, explicitly verified that nearly all the Skyrme model graphs for $\pi^+ \Delta^{++} \to \pi^+ \Delta^{++}$ evince the usual resonant behavior.

The moral is that the skyrmion approach can hardly be expected to yield accurate information about KN scattering, as these processes directly probe those states that one would prefer to dismiss as unphysical artifacts of the model. This having been said, it is interesting to speculate about whether those exotic states that *do* seem to be present in Nature reflect in any way the "skyrminess" of the nucleon. We offer the following cautious observations:

1. Although the four P-wave Skyrme-model amplitudes appear to be repulsive, close inspection reveals that the P_{01} and P_{13} amplitudes actually curve anticlockwise before the cusps. Therefore, they might be interpreted as very weak resonances superimposed on a strongly repulsive background. It is interesting to note that these are the same two P-wave amplitudes that curve anticlockwise in Nature.

2. The D_{03} channel is the most prominent of the D-wave curves in the Skyrme model, and it is the most plausibly resonant D-wave channel in Nature as well.

3. Interestingly, there appears to be some unexpected resemblance in the P- and the D-wave sectors between the four $KN \to KN$ experimental amplitudes and their $\pi N \to \pi N$ counterparts (compare "Experiment I" in Fig. 6 to Fig. 1). In particular, in the P waves, the first and fourth amplitudes for both processes curve anticlockwise, while the second and third curve clockwise. Likewise, the D

waves are characterized by a pattern of "decreasingly resonant behavior" across the four graphs in each process. Consequently, it is conceivable that the same $1/N_c$ corrections that are expected to improve the agreement in these waves between the Skyrme model and experiment for $\pi N \to \pi N$ will do likewise for $KN \to KN$.

4. Finally, we have come to expect reasonable agreement between the Skyrme model and experiment in the F, G and H waves. It is unfortunate that the only such channels for which experimental $KN \to KN$ amplitudes have been presented, namely the F_{15}, G_{17} and H_{19}, are predicted by the Skyrme model to be small and rather featureless (Fig. 6). A much more critical test of whether the model has anything relevant to say about KN scattering would be the appearance of resonances in the F_{05}, G_{07} and H_{09} channels. An analysis of these channels can be expected in the not-too-distant future.[26]

The process $KN \to K\Delta$ is understood much less well than the elastic case. In fact, due to the dearth of data, the authors of the only existing partial-wave analysis[36] were unable to decide among three possible solutions, each of which gives a mediocre fit to the data ($\chi^2/\text{DOF} = 2.33, 2.33$, and 2.68, respectively, for Solutions A, B and C). We have depicted all three solutions in Fig. 7. Evidently the Skyrme-model graphs bear no resemblance to any of the three solutions, apart from a reasonable sign correlation with Solution B. Particularly disturbing is the fact that, while those channels in which the kaon jumps by two units of angular momentum contribute appreciably to the experimental T-matrix, they

---

[26] R. A. Arndt, private communication.
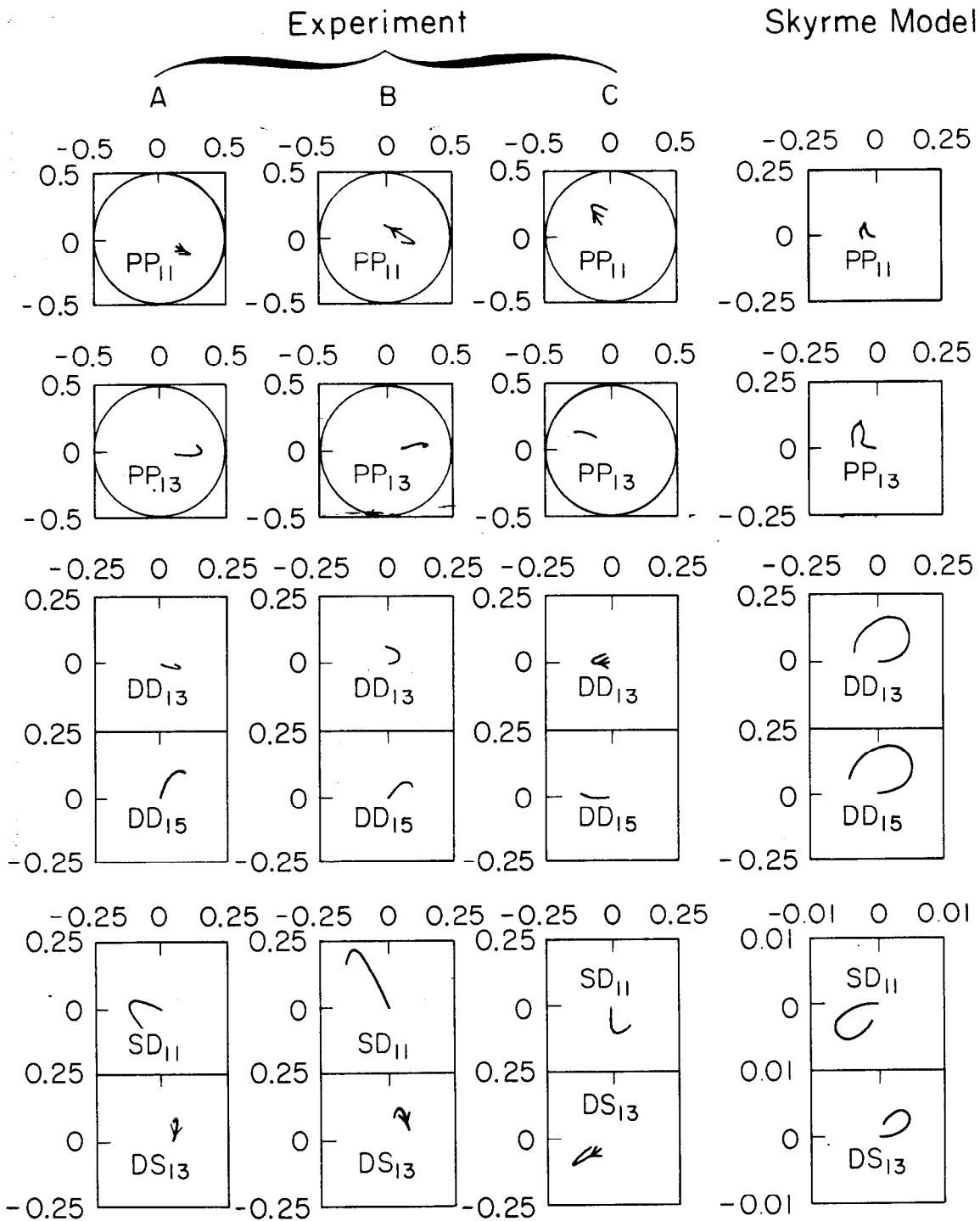
FIG. 7. $KN \to K\Delta$: comparison between the Skyrme model and the three experimental solutions given in Ref. 36 (1.75 GeV $\leq E_{\mathrm{CM}} \leq$ 2.02 GeV). Channels are labeled by $LL'_{I,2J}$. Note that experimental and Skyrme-model plots are shown on different scales.

are suppressed in the Skyrme model by roughly a factor of 25 compared with the channels in which L does not change.

All in all, it is unclear to what extent, if any, the Skyrme model has anything valid to contribute to our understanding of KN scattering.

V. $\overline{K}N$ Scattering

We turn, finally, to an examination of $\overline{K}N$ scattering. The elastic case $\overline{K}N \to \overline{K}N$ is considered very well established, with excellent agreement between the two most comprehensive partial-wave analyses (Refs. 37 and 38). Figure 8 presents the Skyrme model versus experiment[37] for this process. As in the case of πN scattering, there is poor agreement for the S and P waves, but reasonable agreement for the D waves and higher, with the F waves being the best. The most obvious feature of the Skyrme-model graphs is the "big-small-small-small" pattern characterizing the four independent amplitudes $\{L_{0,2L-1}, L_{0,2L+1}, L_{1,2L-1}, L_{1,2L+1}\}$ for each value of $L > 0$; for example, the F_{05} curve is larger than its F_{07}, F_{15} and F_{17} counterparts. In general, this pattern characterizes the experimental graphs as well. The P_{03} and D_{15} curves appear from Fig. 8 to be semi-exceptions to the rule; however, if one cuts off the energies at the "natural" resonance scale for each value of L (which we take to be the average value of the masses of the prominent resonances formed in these channels), then the big-small-small-small pattern shows up much more clearly.[♮27] This point is illustrated in Fig. 9 for the P and D waves.

♮27 As mentioned earlier, the same phenomenon occurs for elastic πN scattering, where the "big-small-small-big" pattern likewise emerges most clearly when the graphs are cut off at the natural resonance energies. In fact, if instead one goes out to ≈ 4 GeV uniformly, then the pattern disappears completely, and all four πN amplitudes for each value of L approach the same value.[8]
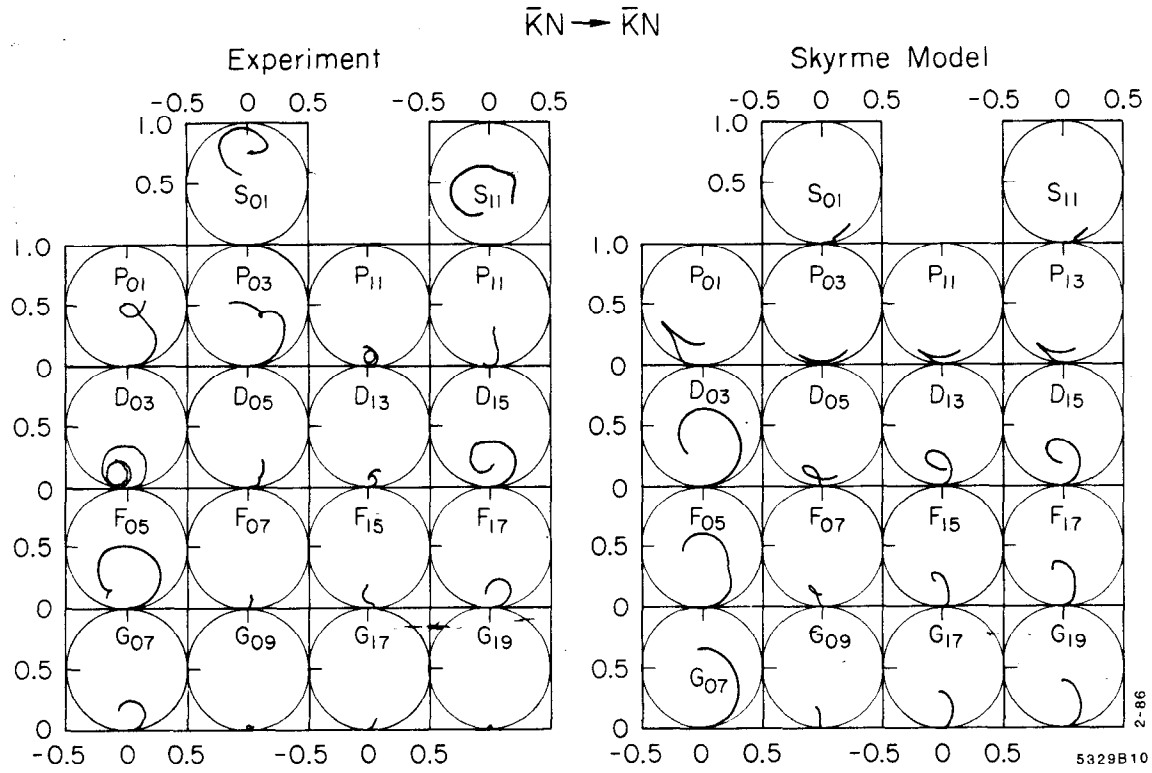
FIG. 8. $\overline{K}N \rightarrow \overline{K}N$: comparison between the Skyrme model and the experimental solution of Ref. 37 (1.48 GeV $\leq E_{\rm CM} \leq$ 2.17 GeV). Channels are labeled by $L_{I,2J}$.
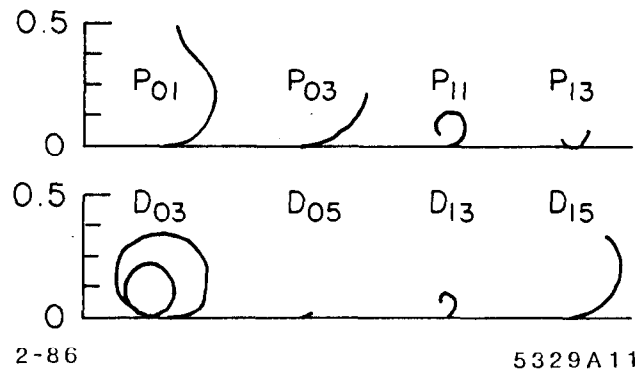

FIG. 9. Examples of the big-small-small-small pattern displayed by the experimental $\overline{K}N \rightarrow \overline{K}N$ amplitudes.[37] The energy was cut off at the average resonance scale for the P and D waves (taken to be 1.75 GeV in both cases).
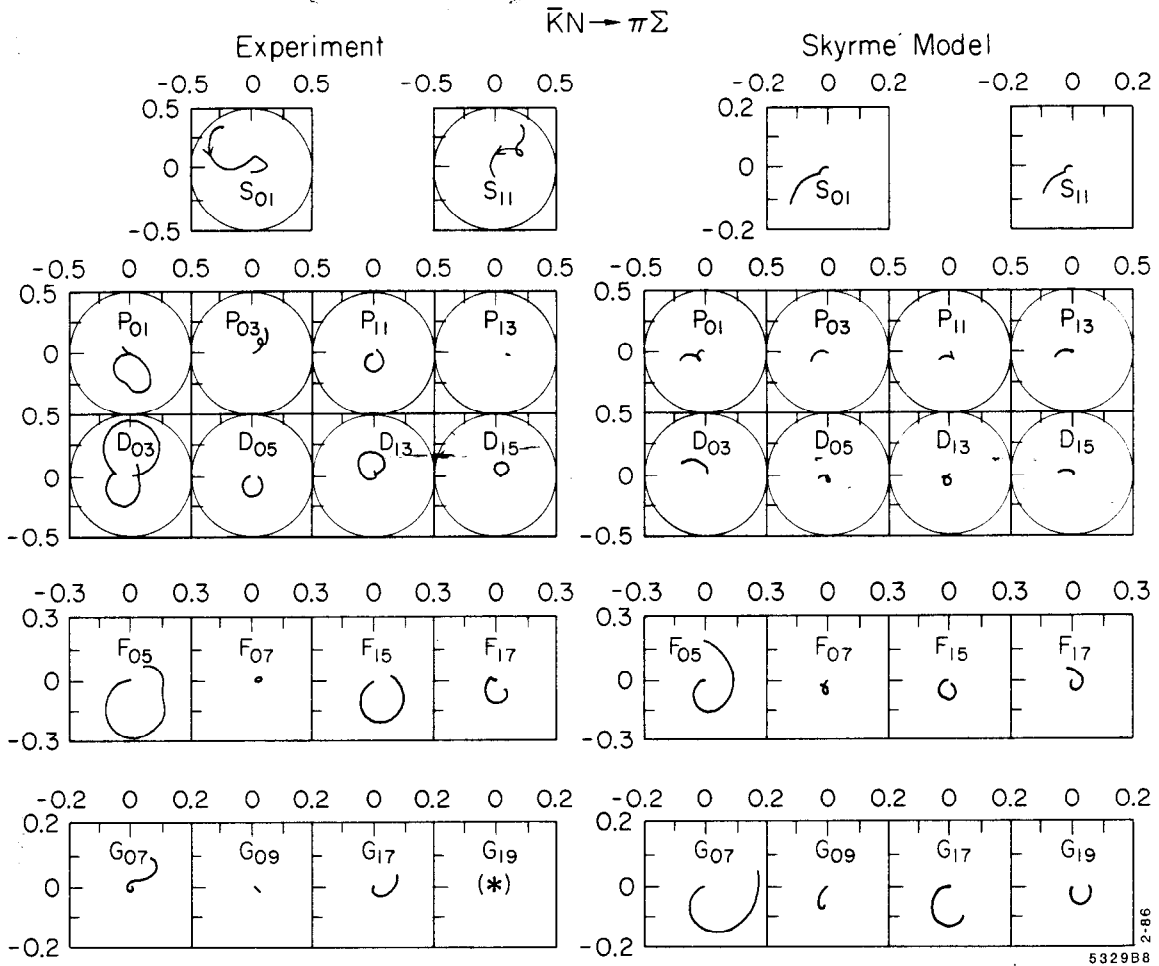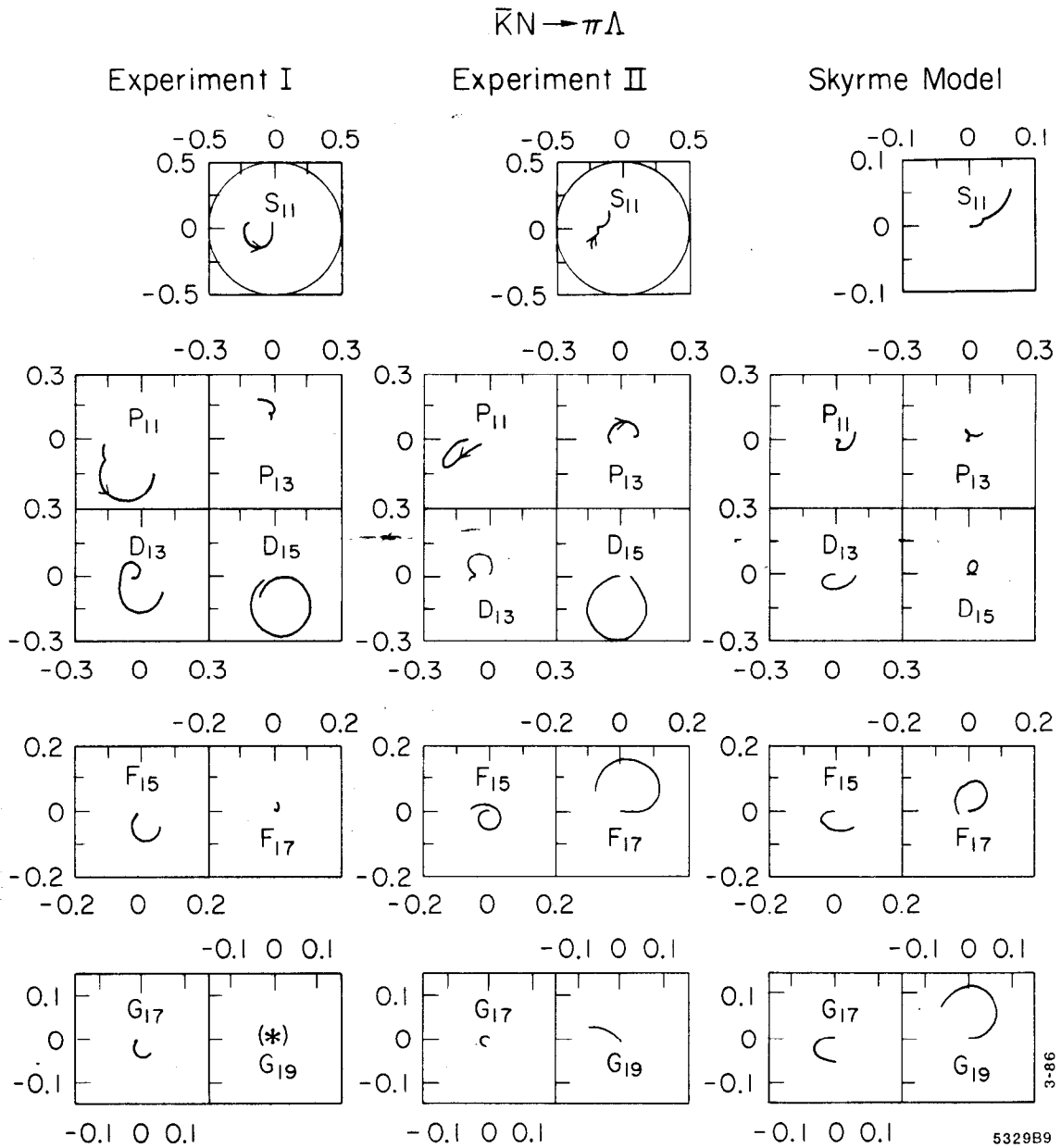
FIG. 10. $\overline{K}N \rightarrow \pi\Sigma$: comparison between the Skyrme model and the experimental solutions of Ref. 37 (1.48 GeV $\leq E_{\text{CM}} \leq$ 2.17 GeV). Channels are labeled by $L_{I,2J}$. Note that experimental and Skyrme-model plots for $L = 0$ are shown on different scales.

FIG. 11. $\overline{K}N \to \pi\Lambda$: comparison between the Skyrme model and two experimental solutions: "Experiment I" from Ref 39 (1.55 GeV $\leq E_{\mathrm{CM}} \leq$ 2.00 GeV), and "Experiment II" from Ref. 37 (1.47 GeV $\leq E_{\mathrm{CM}} \leq$ 2.17 GeV). Channels are labeled by $L_{I,2J}$. Note that experimental and Skyrme-model plots for $L = 0$ are shown on different scales.
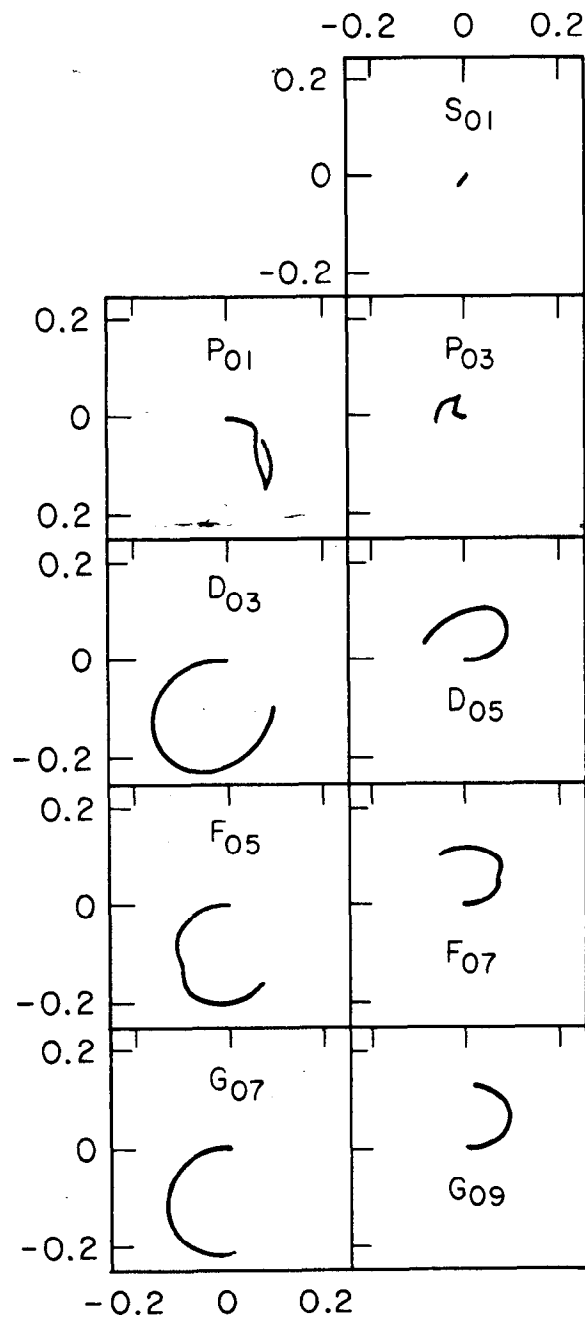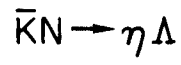
FIG. 12. Skyrme-model predictions for $\overline{K}N \to \eta\Lambda$.

A subsidiary pattern apparent from the Skyrme-model graphs of Fig. 8 is a relative size ordering among the three "small" amplitudes for each value of $L \geq 2$: for instance $D_{05} < D_{13} < D_{15}$, and likewise for the F and G waves. And indeed, with the glaring exception of the G_{19}, this ordering holds for the experimental curves as well (Figs. 8-9).

We turn next to the inelastic processes $\overline{K}N \to \pi\Sigma$ and $\overline{K}N \to \pi\Lambda$. Here there are areas of serious disaccord between competing partial-wave analyses.[37,39] As can be seen in Figs. 10 and 11, the agreement with the Skyrme model is likewise less good than for elastic scattering. Particularly disappointing in the case of $\overline{K}N \to \pi\Sigma$ (Fig. 10) is the discrepancy in the sign of the D_{13} channel. In contrast, the agreement in the F-wave sector is excellent. Moreover, the Skyrme model successfully predicts a big-small-small-small (or, perhaps more descriptively, a big-small-medium-small) pattern for $\overline{K}N \to \pi\Sigma$, just as for the elastic case.

In Fig. 11 we have juxtaposed the Skyrme-model graphs for $\overline{K}N \to \pi\Lambda$ with the results of two independent experimental analyses.[37,39] Clearly the model is in better agreement with Ref. 39 ("Experiment I") than with Ref. 37 ("Experiment II") in the P and D waves, although in either case the D_{15} amplitude is in complete disaccord. Conversely, the agreement is much better with Ref. 37 than with Ref. 39 in the S and F waves; however, for the F_{17} channel, this is simply due to the fact that the authors of Ref. 39 have cut off their analysis before the effect of the $\Sigma(2030)$ resonance could be felt. It is pleasing that the Skyrme model renders correctly the relative signs between the two graphs for each L for this process.

Figure 12 displays the Skyrme-model curves for $\overline{K}N \to \eta\Lambda$. Although an

experimental partial-wave analysis for this process has never been published in graphical form, Rader *et al.*quote couplings at resonance of approximately -.04, -.1, and -.05, respectively, for the D_{05}, F_{05}, and G_{07} amplitudes.[40] Note the sign disagreement with the Skyrme model in the first of these channels.

Finally, Figs. 13 and 14 present the graphs for the processes $\overline{K}N \to \pi\Sigma^*$ [41] and $\overline{K}N \to \overline{K}\Delta$.[42] Here the agreement with the Skyrme model is mediocre. In both cases the Skyrme model underestimates the importance of the amplitudes with $L' = L \pm 2$ compared to those with $L' = L$, as before. For $\overline{K}N \to \pi\Sigma^*$ the most serious discrepancies are the signs of the DD_{15} and PF_{03} channels; interestingly, the PF_{03} channel is also the site of greatest experimental disagreement with $SU(6)_W$.[41] There is also sign disagreement in the DG channels, but the authors of Ref. 41 consider these waves to be less well established. As for $\overline{K}N \to \overline{K}\Delta$, the comparison to the Skyrme model is hampered by the fact that the experimental solution finds only two clear resonances, the $D_{13}(1940)$ and the $F_{17}(2030)$, in the narrow energy-range probed. Disappointingly, the DD_{13} curve has the opposite sign of its Skyrme-model counterpart. It is noteworthy that a negative experimental amplitude in this channel disagrees, not just with the Skyrme model, but with the nonrelativistic quark model as well.[50]

In sum, although $\overline{K}N$ scattering in the Skyrme model works less well than πN, it is much more successful than KN. Many sign and size patterns are mimicked correctly. The agreement in the elastic case is particularly impressive, and on a par with $\pi N \to \pi N$ and $\pi N \to \pi\Delta$. It is an open question whether inclusion of $SU(3)$-breaking terms (*i.e.*, meson masses) into the effective Lagrangian would improve the agreement with experiment for the scattering data, as it does for the static properties of the model.[6]
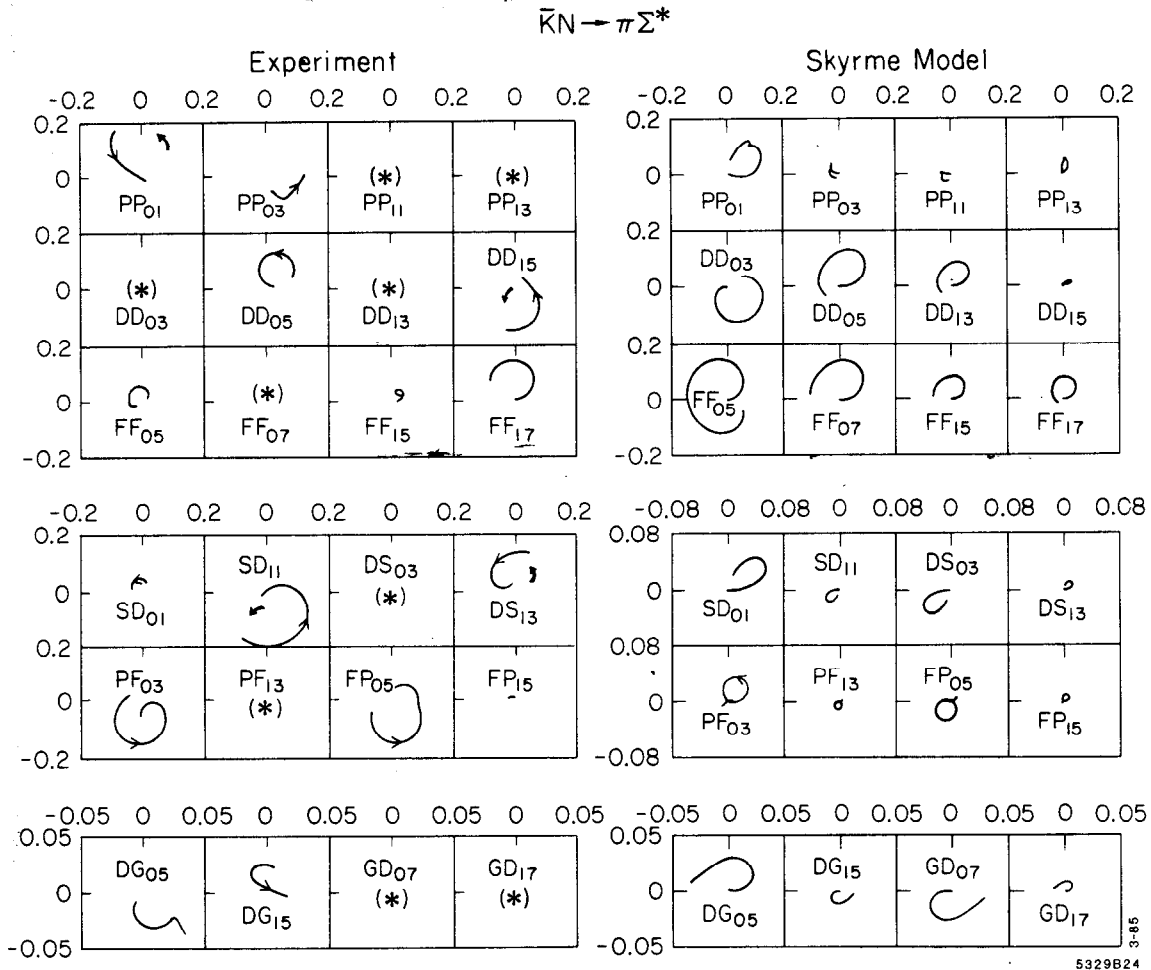
$\overline{K}N \rightarrow \pi\Sigma^*$

FIG. 13. $\overline{K}N \rightarrow \pi\Sigma^*$: comparison between the Skyrme model and the experimental solution of Ref. 41 (1.78 GeV $\leq E_{CM} \leq$ 2.17 GeV). Channels are labeled by $LL'_{I,2J}$. For a fairer comparison, we have added a detached arrow in the experimental PP_{01}, DD_{15}, SD_{11} and DS_{13} channels to indicate the expected behavior of these amplitudes if one were to extrapolate down to threshold. The experimental graphs have been multiplied by an overall minus-sign in order to conform to the "baryon-first" convention. Note that experimental and Skyrme-model plots for SD, DS, PF and FP channels are shown on different scales.
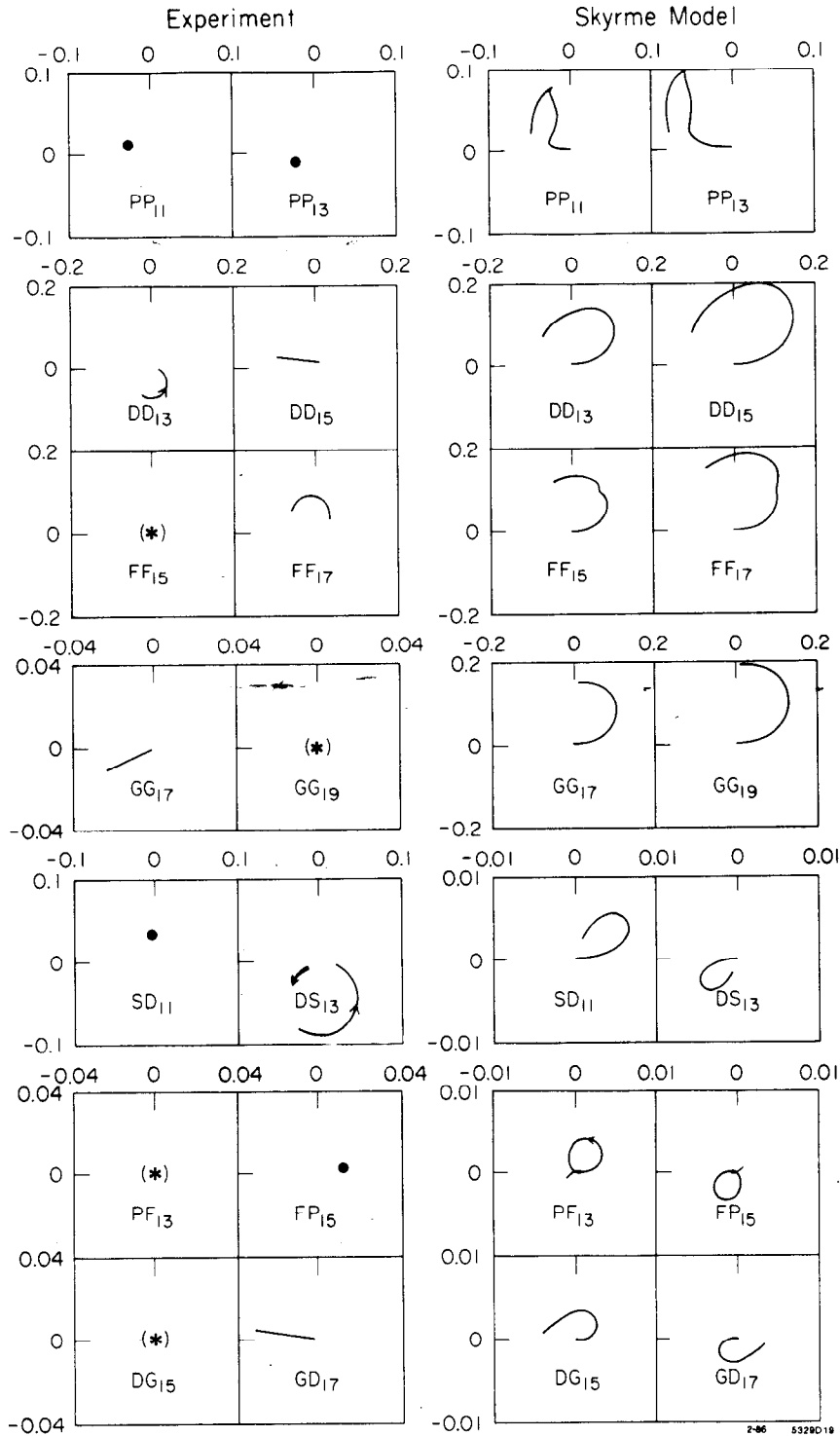
FIG. 14. $\overline{K}N \to \overline{K}\Delta$: comparison between the Skyrme model and the experimental solution of Ref. 42 (1.92 GeV $\leq E_{\text{CM}} \leq$ 2.17 GeV). The non-resonant experimental amplitudes have been parametrized either as constants or as linear functions of energy. Channels are labeled by $LL'_{I,2J}$. For a fairer comparison, we have added a detached arrow in the experimental DS_{13} channels to indicate the expected behavior of the amplitude if one were to extrapolate down to threshold. Note that experimental and Skyrme-model plots for $L = L' = 4$ and for $L' = L \pm 2$ are shown on different scales.

VI. How model-dependent are these results?

In the last three Sections, we have presented a detailed comparison of the Skyrme model with experiment covering 165 πN, KN and $\overline{K}N$ channels. Despite areas of deep disagreement, such as "exotic" KN scattering, and S and P waves in general, we consider the overall degree of accord obtained from such a simple model to be powerful evidence for the validity of the soliton approach to baryon physics.

In some people's view, the surprising successes of the Skyrme model indicate that the Skyrme Lagrangian, Eq. (1), must be extremely close to the optimal effective Lagrangian of Nature, $\mathcal{L}_{opt}$, which is derivable in principle from QCD:

$$\mathcal{L}_{opt} \cong \mathcal{L}_{skyrme}.$$

We do not share this opinion. In our view, the Skyrme Lagrangian is not much more than a convenient testing-ground for soliton dynamics; it is, in a sense, the "minimal" model. A more realistic starting point would necessarily involve many more low-lying mesons and higher-derivative interactions; there has already been progress toward extending the Skyrme model along both these lines.

In light of this, it is crucial to determine to what extent the Skyrme-model results presented here (both good and bad) can be expected to survive such modifications. This is the topic of the present Section. In the course of the discussion, we shall discover what we believe to be the key to the Skyrme model's success in describing meson-baryon scattering. This will enable us to define implicitly a large class of models which, we believe, would enjoy comparable overall success.

We shall focus at first on processes where the initial and final meson orbital angular momenta are equal. In our eyes, a particularly striking achievement of the Skyrme model in both its 2-flavor and 3-flavor incarnations is the big-small-small-big pattern characterizing the four elastic πN curves for each value of $L > 0$ (*cf*. Fig. 1). Let us start by reviewing the 2-flavor analysis of this pattern presented in Ref. 8. We will find it convenient to represent the $\pi N \to \pi N$ partial-wave amplitudes by the notation $\mathbf{T}^{\pi N \pi N}_{LIJ}$ with $I = \frac{1}{2}, \frac{3}{2}$ and $J = L \pm \frac{1}{2}$. From the formula for 2-flavor scattering, Eq. (2), we obtain:[28]

$$\mathbf{T}^{\pi N \pi N}_{L\frac{1}{2},L-\frac{1}{2}} = \frac{2L-1}{3L}\mathcal{T}_{L-1,LL} + \frac{L+1}{3L}\mathcal{T}_{LLL}, \tag{4a}$$

$$\mathbf{T}^{\pi N \pi N}_{L\frac{1}{2},L+\frac{1}{2}} = \frac{L}{3L+3}\mathcal{T}_{LLL} + \frac{2L+3}{3L+3}\mathcal{T}_{L+1,LL}, \tag{4b}$$

$$\mathbf{T}^{\pi N \pi N}_{L\frac{3}{2},L-\frac{1}{2}} = \frac{(2L-1)(L-1)}{6L(2L+1)}\mathcal{T}_{L-1,LL} + \frac{2L-1}{6L}\mathcal{T}_{LLL} + \frac{2L+3}{4L+2}\mathcal{T}_{L+1,LL}, \tag{4c}$$

$$\mathbf{T}^{\pi N \pi N}_{L\frac{3}{2},L+\frac{1}{2}} = \frac{2L-1}{4L+2}\mathcal{T}_{L-1,LL} + \frac{2L+3}{6L+6}\mathcal{T}_{LLL} + \frac{(L+2)(2L+3)}{(6L+6)(2L+1)}\mathcal{T}_{L+1,LL}. \tag{4d}$$

To make progress, let us make use of the fact that, in the Skyrme model, the variation of $\mathcal{T}_{L+1,LL}$ from the origin is essentially negligible compared with that of $\mathcal{T}_{L-1,LL}$ and $\mathcal{T}_{LLL}$ (*cf*. Appendix A). Accordingly, let us make the simplifying approximation

$$\mathcal{T}_{L+1,LL}(\omega) \approx 0$$

in Eq. (4). The big-small-small-big pattern then emerges as a natural consequence of the group-theory: it is simply due to the large group-theoretic coefficients multiplying $\mathcal{T}_{L-1,LL}$ and $\mathcal{T}_{LLL}$ in Eq. (4a) and (4d) compared with (4b)

---

[28] Although $\mathcal{T}_{KL'L}$ and $\mathcal{T}^{\{1,0\}}_{KL'L}$ refer to the same quantity, we shall employ the former notation when we are invoking the 2-flavor formalism.

and (4c). In this way, the pattern in the 2-flavor Skyrme model results from an elegant interplay between group-theory and dynamics.

How model-dependent *is* this argument? Recall that, as noted in Section II, the group-theoretic structure of Eq. (2), and hence of Eq. (4), is completely independent of the details of the meson Lagrangian that one starts with, but relies only on the "hedgehog" structure of the underlying skyrmion. The only specific dynamical input from the Skyrme model that we needed to formulate the argument was the presence of a two-tiered "hierarchy" among the reduced amplitudes. We can therefore assert that *the big-small-small-big pattern will characterize any 2-flavor skyrmion model for which the reduced amplitude $T_{L+1,LL}$ was negligible compared with $T_{L-1,LL}$ and T_{LLL}.* As such, the pattern can be considered a *quasi-model-independent* result. In particular, since the pattern characterizes the experimental amplitudes (apart from the D waves), it is a safe bet that the optimal effective Lagrangian of Nature, which we do not know, itself falls into this class of models. Further evidence for this claim will be put forth in the following Section.

There is a natural way to extend this line of reasoning to the 3-flavor formalism. Recall that, in the 3-flavor Skyrme model, the variation of the reduced amplitudes $T^{\{1,0\}}_{L+1,LL}$, $T^{\{0,0\}}_{LLL}$, $T^{+}_{L+\frac{1}{2},LL}$, $T^{-}_{L-\frac{1}{2},LL}$, and $T^{-}_{L+\frac{1}{2},LL}$ is small in comparison to $T^{\{1,0\}}_{L-1,LL}$, $T^{\{1,0\}}_{LLL}$, and $T^{+}_{L-\frac{1}{2},LL}$. If one neglects the former, Eq. (3) implies the following approximate expressions for the physical πN amplitudes:

$$\mathbf{T}^{\pi N \pi N}_{L\frac{1}{2},L-\frac{1}{2}} \cong \frac{(2L-1)(49L+24)}{135L(2L+1)} T^{\{1,0\}}_{L-1,LL} + \frac{25L+24}{135L} T^{\{1,0\}}_{LLL} + \frac{27L+10}{45(2L+1)} T^{+}_{L-\frac{1}{2},LL}, \quad (5a)$$

$$\mathbf{T}^{\pi N \pi N}_{L\frac{1}{2},L+\frac{1}{2}} \cong \frac{2L-1}{135(2L+1)} T^{\{1,0\}}_{L-1,LL} + \frac{25L+1}{135(L+1)} T^{\{1,0\}}_{LLL} + \frac{7L}{45(2L+1)} T^{+}_{L-\frac{1}{2},LL}, \quad (5b)$$

$$T^{\pi N\pi N}_{L\frac{3}{2},L-\frac{1}{2}} \cong \frac{(2L-1)(13L-12)}{135L(2L+1)}T^{\{1,0\}}_{L-1,LL} + \frac{25L-12}{135L}T^{\{1,0\}}_{LLL} + \frac{12L-5}{45(2L+1)}T^{+}_{L-\frac{1}{2},LL}, \quad (5c)$$

$$T^{\pi N\pi N}_{L\frac{3}{2},L+\frac{1}{2}} \cong \frac{37}{135}\frac{2L-1}{2L+1}T^{\{1,0\}}_{L-1,LL} + \frac{25L+37}{135(L+1)}T^{\{1,0\}}_{LLL} + \frac{22L}{45(2L+1)}T^{+}_{L-\frac{1}{2},LL}. \quad (5d)$$

Although these expressions are more complicated than their 2-flavor counterparts, the big-small-small-big pattern reveals itself, as before, in the relative sizes of the group-theoretic coefficients.

In addition, despite the different coefficients involved in Eqs. (4) and (5), the first of the "big" amplitudes in each instance is predicted to be "bigger" than the last:

$$\mathbf{T}^{\pi N\pi N}_{L\frac{1}{2},L-\frac{1}{2}} \quad > \quad \mathbf{T}^{\pi N\pi N}_{L\frac{3}{2},L+\frac{1}{2}}$$

This is manifestly the case in the 2- and 3-flavor Skyrme models; and indeed, with the exception of the P waves, it is true for the experimental amplitudes as well.

We can profitably apply this mode of analysis to a wide range of other processes. Most notably, for $\overline{K}N \to \overline{K}N$ we find:

$$\mathbf{T}^{\overline{K}N\overline{K}N}_{L0,L-\frac{1}{2}} \cong \frac{(2L-1)(20L+9)}{90L(2L+1)}T^{\{1,0\}}_{L-1,LL} + \frac{11L+9}{90L}T^{\{1,0\}}_{LLL} + \frac{14L+6}{15(2L+1)}T^{+}_{L-\frac{1}{2},LL}, \quad (6a)$$

$$\mathbf{T}^{\overline{K}N\overline{K}N}_{L0,L+\frac{1}{2}} \cong \frac{2L-1}{45(2L+1)}T^{\{1,0\}}_{L-1,LL} + \frac{11L+2}{90(L+1)}T^{\{1,0\}}_{LLL} + \frac{2L}{15(2L+1)}T^{+}_{L-\frac{1}{2},LL}, \quad (6b)$$

$$\mathbf{T}^{\overline{K}N\overline{K}N}_{L1,L-\frac{1}{2}} \cong \frac{(2L-1)(20L-3)}{270L(2L+1)}T^{\{1,0\}}_{L-1,LL} + \frac{23L-3}{270L}T^{\{1,0\}}_{LLL} + \frac{22L-4}{45(2L+1)}T^{+}_{L-\frac{1}{2},LL}, \quad (6c)$$

$$\mathbf{T}^{\overline{K}N\overline{K}N}_{L1,L+\frac{1}{2}} \cong \frac{13}{135}\frac{2L-1}{2L+1}T^{\{1,0\}}_{L-1,LL} + \frac{23L+26}{270(L+1)}T^{\{1,0\}}_{LLL} + \frac{2L}{3(2L+1)}T^{+}_{L-\frac{1}{2},LL}. \quad (6d)$$

Similarly, the T-matrix for $\overline{K}N \to \pi\Sigma$ is determined by

$$\mathbf{T}^{\overline{K}N\pi\Sigma}_{L0,L-\frac{1}{2}} \cong -\frac{(2L-1)(44L+21)\sqrt{6}}{540L(2L+1)}T^{\{1,0\}}_{L-1,LL} - \frac{(23L+21)\sqrt{6}}{540L}T^{\{1,0\}}_{LLL}$$

$$+ \frac{(9L+4)\sqrt{6}}{45(2L+1)} \mathcal{T}^{+}_{L-\frac{1}{2},LL}, \tag{7a}$$

$$\mathbf{T}^{\overline{K}N\pi\Sigma}_{L0,L+\frac{1}{2}} \cong -\frac{(2L-1)\sqrt{6}}{270(2L+1)} \mathcal{T}^{\{1,0\}}_{L-1,LL} - \frac{(23L+2)\sqrt{6}}{540(L+1)} \mathcal{T}^{\{1,0\}}_{LLL} + \frac{L\sqrt{6}}{45(2L+1)} \mathcal{T}^{+}_{L-\frac{1}{2},LL}, \tag{7b}$$

$$\mathbf{T}^{\overline{K}N\pi\Sigma}_{L1,L-\frac{1}{2}} \cong -\frac{(2L-1)(8L+1)}{90L(2L+1)} \mathcal{T}^{\{1,0\}}_{L-1,LL} - \frac{7L+1}{90L} \mathcal{T}^{\{1,0\}}_{LLL} + \frac{2L-3}{45(2L+1)} \mathcal{T}^{+}_{L-\frac{1}{2},LL}, \tag{7c}$$

$$\mathbf{T}^{\overline{K}N\pi\Sigma}_{L1,L+\frac{1}{2}} \cong -\frac{2L-1}{15(2L+1)} \mathcal{T}^{\{1,0\}}_{L-1,LL} - \frac{7L+6}{90(L+1)} \mathcal{T}^{\{1,0\}}_{LLL} + \frac{2L}{9(2L+1)} \mathcal{T}^{+}_{L-\frac{1}{2},LL}. \tag{7d}$$

For both these processes, as a moment's inspection of the coefficients confirms, we can expect to see a big-small-small-small pattern—which is precisely what we found in the previous Section for both the Skyrme model and experiment (Figs. 8-10). In addition, the group-theoretic coefficients appearing in Eq. (6) suggest a relative size ordering among the three "small" physical amplitudes,

$$\mathbf{T}^{\overline{K}N\overline{K}N}_{L0,L+\frac{1}{2}} < \mathbf{T}^{\overline{K}N\overline{K}N}_{L1,L-\frac{1}{2}} < \mathbf{T}^{\overline{K}N\overline{K}N}_{L1,L+\frac{1}{2}},$$

which we also noticed in Section V.

The same type of quasi-model-independent analysis successfully predicts the *signs* of many inelastic amplitudes, as well. As an example, consider the F_{15} and F_{17} channels for the process $\overline{K}N \to \pi\Lambda$ (Fig. 11). Eq. (3) tells us:

$$F_{15}: \quad \mathbf{T} = \left[-.03\,\mathcal{T}^{\{1,0\}}_{233} + .03\,\mathcal{T}^{\{1,0\}}_{333} - .08\,\mathcal{T}^{+}_{\frac{5}{2}33}\right]$$
$$+ .15\,\mathcal{T}^{\{1,0\}}_{433} - .04\,\mathcal{T}^{\{0,0\}}_{333} - .03\,\mathcal{T}^{+}_{\frac{7}{2}33} - .03\,\mathcal{T}^{-}_{\frac{5}{2}33} + .20\,\mathcal{T}^{-}_{\frac{7}{2}33} \tag{8a}$$

$$F_{17}: \quad \mathbf{T} = \left[.08\,\mathcal{T}^{\{1,0\}}_{233} + .07\,\mathcal{T}^{\{1,0\}}_{333} - .02\,\mathcal{T}^{+}_{\frac{5}{2}33}\right]$$
$$- .00\,\mathcal{T}^{\{1,0\}}_{433} - .04\,\mathcal{T}^{\{0,0\}}_{333} - .09\,\mathcal{T}^{+}_{\frac{7}{2}33} + .15\,\mathcal{T}^{-}_{\frac{5}{2}33} + .02\,\mathcal{T}^{-}_{\frac{7}{2}33}. \tag{8b}$$

If we assume that the reduced amplitudes enclosed in brackets dominate these channels in Nature as they do in the Skyrme model, we correctly predict the − and + signs for the F_{15} and F_{17}, respectively; nor are we surprised to find a 1:3 ratio in the magnitudes of the experimental curves (versus 1:2 in the Skyrme model).[29]

In sum, we have outlined a methodology that successfully explains many of the observed features of the experimental meson-baryon partial-wave T-matrix. Moreover, we have seen that the general success of the Skyrme model can be largely explained by the hypothesis that *the Skyrme Lagrangian shares with the (unknown) optimal effective Lagrangian $\mathcal{L}_{\mathrm{opt}}$: (i) the "K-symmetry" characteristic of hedgehog solitons, and (ii) a plausible two-tiered hierarchy among the reduced amplitudes.*

This hierarchy defines a large class of models which we expect to enjoy success comparable to that of the Skyrme model in explaining the experimental scattering data. It would, however, be a mistake to conclude that *all* predictions made by the Skyrme model are likewise quasi-model-independent. As a counterexample, consider once again the process $\overline{K}N \to \pi\Sigma$ (Fig. 10). The F_{05} and G_{07} channels are governed by Eq. (7a), with $L = 3$ and $L = 4$, respectively. Note that, taken together, the first two coefficients (which are negative) are comparable in size to the third (which is positive). Thus, the overall sign of the physical amplitudes will be determined by the detailed dynamical question of whether $T^{\{1,0\}}_{L-1,LL}$ and $T^{\{1,0\}}_{LLL}$ outweigh $T^{+}_{L-\frac{1}{2},LL}$ or *vice versa*. One would expect the answer to this question to depend crucially on our particular choice of Lagrangian. (The reader

---

[29] This analysis also works for the G_{17} and G_{19} channels but fails for the D_{13} and D_{15} channels. This suggests that, for the D waves, the two-tiered hierarchy that we have postulated for the reduced amplitudes runs into trouble; we shall return to this shortly.

should contrast this example with that of Eq. (8).) In light of this, it is not surprising to find disagreement between the Skyrme model and experiment in the G_{07} channel.

As a somewhat different example, consider the F_{07} and G_{09} amplitudes for the same process. Here, the coefficients given in Eq. (7b) are so small to begin with that it was probably an unjustified approximation to have dropped the contributions of the other reduced amplitudes. (Even a "small" amplitude, after all, can make a significant contribution if it is multiplied by a sufficiently large number.) In particular, the coefficients of $T_{L+1,LL}^{\{1,0\}}$ and $T_{L+\frac{1}{2},LL}^{+}$ for these channels turn out to be an order of magnitude bigger than those that appear in (7b), and of opposite sign from one another in addition. As a result, we can no longer with any degree of confidence make a quasi-model-independent sign prediction about the physical amplitudes, and should not be surprised to learn that the Skyrme model disagrees with experiment over the sign of the F_{07}.

We can summarize the discussion so far in this Section by the following statement: *Whenever a Skyrme-model prediction follows from (i) the two-tiered hierarchy among the reduced amplitudes and (ii) group theory, as illustrated in Eqs. (4)-(8), there is a high probability of agreement with experiment. Conversely, in all other cases the agreement is much less reliable.* In particular, we can certainly expect that specific details about the shapes of amplitudes will vary significantly from model to model, as will the precise values of masses and widths of resonances. In all of these areas, there is significant room for improvement over the Skyrme model.

One specific recipe for improvement is suggested by the observation that fully 35% of the channels with $L' = L$ for which the sign of the Skyrme-model

amplitude disagrees with experiment are D-wave processes. This leads one to suspect that the hierarchical hypothesis probably does not work very well in the D-wave sector of $\mathcal{L}_{opt}$—a conclusion bolstered by the violation of the big-small-small-big pattern in that sector (Fig. 1). (We will supply a further piece of evidence for this conclusion in the next Section.) Unfortunately, it is not clear how best to modify the hierarchical assumption for the D waves in order to predict the signs more accurately. However, an analysis similar to that used in Eq. (8) suggests that the reduced amplitudes $T_{322}^{\{1,0\}}$, $T_{222}^{\{0,0\}}$ and $T_{\frac{5}{2}22}^{+}$ probably cannot be neglected in Nature, as they can in the Skyrme model.

It is interesting to note that, in the Skyrme model, the two-tiered hierarchy (*i.e.*, the unexpectedly small size of five of the eight reduced amplitudes for each $L > 0$) actually comes about for three independent reasons:

(i) The reduced amplitudes $T_{L-\frac{1}{2},LL}^{-}$ and $T_{L+\frac{1}{2},LL}^{-}$ are small because they only receive contributions from the Wess-Zumino term.[13]

(ii) $T_{L+1,LL}^{\{1,0\}}$, $T_{L+\frac{1}{2},LL}^{-}$ and $T_{L+\frac{1}{2},LL}^{+}$ are small because the differential equations that determine the phase-shifts[7,13,14] contain attractive terms proportional to factors such as $[L(L+1) - K(K+1)]$; such terms therefore give a net *repulsive* contribution to these three reduced amplitudes, which have $K > L$. (Note that $T_{L+\frac{1}{2},LL}^{-}$ is thus "doubly small.")

(iii) $T_{LLL}^{\{0,0\}}$ vanishes identically in the Skyrme model because of the commutator in the middle term of Eq. (1).

In our opinion, conditions (i) and (ii) will almost surely survive the addition of extra terms into the Skyrme Lagrangian. In contrast, the size of $T_{LLL}^{\{0,0\}}$ can be expected to vary greatly from model to model. In fact, it is possible that this amplitude might not be completely negligible in the "optimal" 3-flavor ef-

fective Lagrangian of Nature, and that this might partially account for some of the disagreement with the Skyrme model.

Thus far in this Section, we have focused on processes in which the initial and final meson orbital angular momenta L and L' are equal. The analysis has involved an interplay between group theory and dynamics, the former providing the numerical coefficients, and the latter enabling us to focus on only three of the eight contributing reduced amplitudes. In contrast, processes with $L' = L \pm 2$ are much simpler to analyze, since, as discussed in Section II, the physical amplitudes are proportional to a single reduced amplitude $T_{KL'L}^{\{1,0\}} = T_{KLL'}^{\{1,0\}}$ with $K = (L + L')/2$. Thus *all PF* and *FP* πN, KN and $\overline{K}N$ amplitudes, for instance, are predicted to be proportional to one another in the skyrmion approach, regardless of the details of the effective Lagrangian that one starts with. Predictions of relative signs and sizes between such amplitudes thus reduce immediately to questions of pure group theory.

Tables XIV summarizes the situation for the 20 $\pi N \to \pi \Delta$, $KN \to K\Delta$, $\overline{K}N \to \overline{K}\Delta$ and $\overline{K}N \to \pi\Sigma^*$ channels with $L' = L \pm 2$ for which we presented experimental partial-wave data in Sections III-V. The column labeled "Coeff." gives the group-theoretic coefficients from Eq. (3) (rounded off) that multiply the reduced amplitude $T_{KL'L}^{\{1,0\}}$, $K = (L+L')/2$. (Since, in the Skyrme model, these reduced amplitudes lie in the lower half plane, the resulting physical Skyrme-model amplitudes will have *opposite* sign to the indicated coefficient.) The column labeled "size" gives our rough estimates of the global sizes of the experimental amplitudes (admittedly an ill-defined concept), together with the observed signs. The five channels in which the Skyrme-model graph disagrees in sign with the experimental analysis are marked by asterisks.

CHANNEL	COEFF.	SIZE	CHANNEL	COEFF.	SIZE
SD_{11} $(\pi N \to \pi\Delta)$	$-.44$	$.2$	FP_{15} $(\pi N \to \pi\Delta)$	$.33$	$-.3$
SD_{31} $(\pi N \to \pi\Delta)$	$.14$	$-.3$	FP_{35} $(\pi N \to \pi\Delta)$	$-.10$	$.15$
DS_{13} $(\pi N \to \pi\Delta)$	$.31$	$-.2$	PF_{03} $(\overline{K}N \to \pi\Sigma^*)$	$-.27$	$-.15^*$
DS_{33} $(\pi N \to \pi\Delta)$	$-.10$	$.2$	FP_{05} $(\overline{K}N \to \pi\Sigma^*)$	$.22$	$-.15$
SD_{11} $(KN \to K\Delta)$	$.04$	$.1?^*$	FP_{15} $(\overline{K}N \to \pi\Sigma^*)$	$-.08$	$.01$
DS_{13} $(KN \to K\Delta)$	$-.02$	$.1$	FP_{15} $(\overline{K}N \to \overline{K}\Delta)$	$.03$	$?$
SD_{01} $(\overline{K}N \to \pi\Sigma^*)$	$-.30$	$.05$			
SD_{11} $(\overline{K}N \to \pi\Sigma^*)$	$.11$	$-.2$	DG_{05} $(\overline{K}N \to \pi\Sigma^*)$	$-.27$	$-.03^*$
DS_{13} $(\overline{K}N \to \pi\Sigma^*)$	$=.07$	$.15$	DG_{15} $(\overline{K}N \to \pi\Sigma^*)$	$-.09$	$.03^*$
SD_{11} $(\overline{K}N \to \overline{K}\Delta)$	$-.04$	$.04$	GD_{17} $(\overline{K}N \to \overline{K}\Delta)$	$.03$	$.02^*$
DS_{13} $(\overline{K}N \to \overline{K}\Delta)$	$.02$	$-.1$			

Table XIV

The relative sign and size information contained in the "Coeff." column within each of the three categories SD/DS, PF/FP and DG/GD is completely *model-independent*. Unfortunately, the size predictions do not seem to correlate well with experiment, and no $SU(3)$-preserving modification of the Skyrme Lagrangian can improve matters. In particular, the $KN \to K\Delta$ and $\overline{K}N \to \overline{K}\Delta$ curves are predicted to be an order of magnitude smaller than the corresponding $\pi N \to \pi\Delta$ amplitudes, whereas if one trusts the experimental solutions they are almost as big. In contrast, the questions of the relative sizes *between* the three categories, as well as the relative sizes *vis-à-vis* the amplitudes with $L' = L$, are highly model-dependent; in both these areas, the latter especially, the Skyrme model can be improved upon greatly.

As for signs, there is of course no way to bring about agreement with the

experimental analyses regarding the sign of the $SD_{11}(KN \rightarrow K\Delta)$ and the $PF_{03}(\overline{K}N \rightarrow \pi\Sigma^*)$ graphs without destroying the agreement for the other SD/DS and PF/FP channels. On the other hand, one might imagine constructing a model in which the reduced amplitude $T_{324}^{\{1,0\}}$ lies in the upper half plane, as opposed to the lower half as in the Skyrme model; such a model would then agree with the experimental sign predictions for the three DG and GD channels listed in Table XIV. It is reassuring that the Skyrme-model sign predictions agree fully with the experimental solution for $\pi N \rightarrow \pi\Delta$, which we can trust much more than the other three processes.

VII. Linear Relations Between Experimental Amplitudes

In order to assess the validity of the 3-flavor scattering formalism that we have developed, it is crucial to verify that the successes of the 2-flavor approach are retained. In Section III and in Ref. 13, we showed that, in fact, including a third flavor *improves* the agreement between the Skyrme model and experiment for the process $\pi N \rightarrow \pi N$. In this Section we consider the effect of incorporating strangeness on the *model-independent* linear relations between *experimental* πN amplitudes that were analyzed in Ref. 8. In addition, we shall supply evidence for the "hierarchical hypothesis" put forth in Section VI.

Our analysis in this Section is predicated on the assumption that Eqs. (2) and (3) are applicable, not only to the specific case of the Skyrme model, but also to the optimal effective Lagrangian $\mathcal{L}_{\text{opt}}$, to which the Skyrme model is at best a crude approximation. (Of course, the reduced amplitudes will differ.) With this in mind, we now leave the Skyrme model behind, and apply Eqs. (2)-(3) directly to the study of the real-world πN amplitudes. In short, we are assuming that a

skyrmion interpretation of the baryon is legitimate, and that the simultaneous approximations of large-N_c and exact $SU(3)_{\text{flavor}}$ (both of which enter crucially in the derivation of (3)) are physically relevant.

If we represent the physical amplitudes for $\pi N \to \pi N$ by $\mathbf{T}_{LIJ}^{\pi N \pi N}$ as before, then Eq. (3) can be shown to imply:

$$(4L+2)\mathbf{T}_{L\frac{3}{2},L-\frac{1}{2}}^{\pi N \pi N} \quad - (L-1)\mathbf{T}_{L\frac{1}{2},L-\frac{1}{2}}^{\pi N \pi N} \quad - (3L+3)\mathbf{T}_{L\frac{1}{2},L+\frac{1}{2}}^{\pi N \pi N}$$

$$= \quad \frac{13L-5}{45}\mathcal{T}_{L-\frac{1}{2},LL}^{-} \quad + \quad \frac{23(L+1)}{45}\mathcal{T}_{L+\frac{1}{2},LL}^{-} \tag{9a}$$

and

$$(4L+2)\mathbf{T}_{L\frac{3}{2},L+\frac{1}{2}}^{\pi N \pi N} \quad - \quad 3L\mathbf{T}_{L\frac{1}{2},L-\frac{1}{2}}^{\pi N \pi N} \quad - \quad (L+2)\mathbf{T}_{L\frac{1}{2},L+\frac{1}{2}}^{\pi N \pi N}$$

$$= \quad \frac{23L}{45}\mathcal{T}_{L-\frac{1}{2},LL}^{-} \quad + \quad \frac{13L+18}{45}\mathcal{T}_{L+\frac{1}{2},LL}^{-} \, . \tag{9b}$$

These equations relate the experimental πN amplitudes to reduced amplitudes which can presumably be extracted from a phase-shift analysis of $\mathcal{L}_{\text{opt}}$. Unfortunately, $\mathcal{L}_{\text{opt}}$, obtainable in principle from QCD, is unknown. Thus, without some further approximation, Eq. (9) is entirely without predictive power.

However, using the 3-flavor Skyrme model as a *guide* (*cf.* Appendix A), one can expect the right-hand sides of (9) to be extremely small (note that they would vanish identically were it not for the Wess-Zumino term). Accordingly, let us examine the linear relations between *experimental* amplitudes that result from setting the right-hand sides of (9) to zero. Here we find a surprise: these are precisely the same relations that follow, without any such dynamical approximation,[30]

---

[30] Recall that the Wess-Zumino term vanishes in the 2-flavor case.

from the 2-flavor formalism![8,15] In general, these relations work quite well, with the exception of severe problems in some of the lower partial waves, for which a leading-order $1/N_c$ analysis is inadequate; the reader is directed to Ref. 8 for full details. The logical conclusion is that the Wess-Zumino term must make only a small numerical contribution to the real-world meson-baryon T-matrix.[31]

It should be emphasized that, *a priori*, we had no right to expect *any* relations, approximate or not, between physical $\pi N \to \pi N$ amplitudes to emerge from the 3-flavor formalism. The reason is the following. In the 2-flavor approach, the four physical πN amplitudes for each $L > 0$ (*i.e.*, $J = L \pm \frac{1}{2}$ and $I = \frac{1}{2}, \frac{3}{2}$) are expressed through Eq. (2) as superpositions of only three reduced amplitudes. Consequently, at least one nontrivial relation between physical amplitudes is guaranteed for each value of L (in fact, there are two). In contrast, in the 3-flavor approach, these same four amplitudes are linear combinations of *eight* reduced amplitudes. That the relations turn out to be the *same* in both formalisms is cause for further surprise, since the group-theoretic factors multiplying the $T_{KLL}^{\{1,0\}}$'s are completely different in the two approaches.[32]

We can also extract from (3) information about $\pi N \to \pi \Delta$. Let us represent the physical amplitudes for this process by $\mathbf{T}_{LL'IJ}^{\pi N \pi \Delta}$ with L' the exiting pion angular momentum (which can differ from L by two). For the case $L = L'$, Eq. (3) implies:

$$\mathbf{T}_{LL\frac{3}{2},L-\frac{1}{2}}^{\pi N \pi \Delta} - \frac{4(L-1)}{\sqrt{10}(2L+1)} \cdot \mathbf{T}_{LL\frac{1}{2},L-\frac{1}{2}}^{\pi N \pi \Delta} - \frac{3}{2L+1}\sqrt{\frac{(L+1)(2L+3)(2L-1)}{10L}} \cdot \mathbf{T}_{LL\frac{1}{2},L+\frac{1}{2}}^{\pi N \pi \Delta}$$

$$= \frac{\sqrt{(2L-1)(L+1)}}{9(2L+1)}\left(T_{L-\frac{1}{2},LL}^{-} - T_{L+\frac{1}{2},LL}^{-}\right) \tag{10a}$$

---

[31] This conclusion differs from that of Ref. 16.
[32] Compare Table XVI of Appendix C to Appendix B of Ref. 8.

and likewise

$$\mathbf{T}^{\pi N \pi \Delta}_{LL\frac{3}{2},L+\frac{1}{2}} - \frac{3}{2L+1}\sqrt{\frac{L(2L+3)(2L-1)}{10(L+1)}} \cdot \mathbf{T}^{\pi N \pi \Delta}_{LL\frac{1}{2},L-\frac{1}{2}} - \frac{4(L+2)}{\sqrt{10}(2L+1)} \cdot \mathbf{T}^{\pi N \pi \Delta}_{LL\frac{1}{2},L+\frac{1}{2}}$$

$$\tag{10b}$$

$$= \frac{1}{9(2L+1)}\sqrt{\frac{L(2L+3)(2L+1)}{L+1}}(\mathcal{T}^{-}_{L-\frac{1}{2},LL} - \mathcal{T}^{-}_{L+\frac{1}{2},LL}) \, .$$

Setting the right-hand sides to zero as before, we again recover precisely the 2-flavor predictions of Ref. 8. Similarly, for the case $L' = L \pm 2$, Eq. (3) can be shown to imply the simple proportionality relations

$$\sqrt{L+1} \cdot \mathbf{T}^{\pi N \pi \Delta}_{L,L+2,\frac{1}{2},L+\frac{1}{2}} = -\sqrt{10(L+1)} \cdot \mathbf{T}^{\pi N \pi \Delta}_{L,L+2,\frac{3}{2},L+\frac{1}{2}}$$

$$\tag{11}$$

$$= -\sqrt{L+2} \cdot \mathbf{T}^{\pi N \pi \Delta}_{L+2,L\frac{1}{2},L+\frac{3}{2}} = \sqrt{10(L+2)} \cdot \mathbf{T}^{\pi N \pi \Delta}_{L+2,L\frac{3}{2},L+\frac{3}{2}}$$

which are identical to the 2-flavor results, with no "Wess-Zumino corrections."

In the 2-flavor case, there was, for each L, one further (fairly successful) model-independent prediction relating the processes $\pi N \to \pi N$ to $\pi N \to \pi \Delta$:[8]

$$\mathbf{T}^{\pi N \pi N}_{L\frac{1}{2},L-\frac{1}{2}} - \mathbf{T}^{\pi N \pi N}_{L\frac{1}{2},L+\frac{1}{2}}$$

$$\tag{12}$$

$$= \sqrt{\frac{2L-1}{L+1}} \cdot \mathbf{T}^{\pi N \pi \Delta}_{LL\frac{1}{2},L-\frac{1}{2}} + \sqrt{\frac{2L+3}{L}} \cdot \mathbf{T}^{\pi N \pi \Delta}_{LL\frac{1}{2},L+\frac{1}{2}},$$

but this is completely lost in the 3-flavor approach.

In sum, we have shown that, with the dynamical assumption

$$\mathcal{T}^{-}_{L\pm\frac{1}{2},LL}(\omega) \approx 0$$

suggested by the 3-flavor Skyrme model, the 3-flavor formalism yields almost all the model-independent linear relations between experimental πN scattering

amplitudes that emerged from the 2-flavor approach. It is natural to explore the consequences of making additional dynamical assumptions about the optimal 2- and 3-flavor effective Lagrangians of Nature.
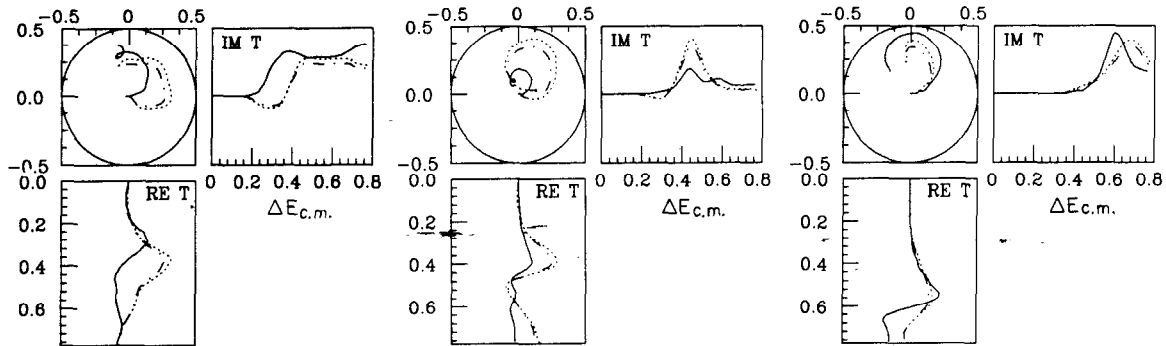
A natural set of such assumptions is suggested by the "big-small-small-big" and "big-small-small-small" patterns exhibited by the experimental πN and $\overline{K}N$ amplitudes, respectively. As reviewed in detail in the previous Section, we can expect the big-small-small-big pattern to occur *automatically* for a broad class of 2-flavor models for which the reduced amplitude $T_{L+1,LL}^{\{1,0\}}$ are negligible compared with $T_{L-1,LL}^{\{1,0\}}$ and $T_{LLL}^{\{1,0\}}$. Similarly, we saw that the same pattern would characterize 3-flavor models if, out of the eight reduced amplitudes for each $L > 0$, the amplitudes $T_{L+1,LL}^{\{1,0\}}$, $T_{LLL}^{\{0,0\}}$, $T_{L\pm\frac{1}{2},LL}^{-}$, and $T_{L+\frac{1}{2},LL}^{+}$ are small compared to the others. We have seen that these conditions are met in the 2- and 3-flavor Skyrme models. Fortunately, we have the means of testing whether these dynamical assumptions are valid approximations for the optimal 2- and 3-flavor effective Lagrangians of Nature as well. For, with these additional approximations, the 2-flavor formalism (Eq. (2)) and the 3-flavor formalism (Eq. (3)) can be shown to imply the extra relations:

$$
\begin{aligned}
&3L\mathbf{T}_{L\frac{1}{2},L-\frac{1}{2}}^{\pi N \pi N} + (L+2)\mathbf{T}_{L\frac{1}{2},L+\frac{1}{2}}^{\pi N \pi N} \\
&\cong 3L\sqrt{\frac{2L-1}{L+1}}\mathbf{T}_{LL\frac{1}{2},L-\frac{1}{2}}^{\pi N \pi \Delta} + (10L+11)\sqrt{\frac{L}{2L+3}}\mathbf{T}_{LL\frac{1}{2},L+\frac{1}{2}}^{\pi N \pi \Delta}
\end{aligned}
\tag{13}
$$

and

$$
\begin{aligned}
&3L\mathbf{T}_{L\frac{1}{2},L-\frac{1}{2}}^{\pi N \pi N} + (L+2)\mathbf{T}_{L\frac{1}{2},L+\frac{1}{2}}^{\pi N \pi N} \\
&\cong 32L\sqrt{\frac{2L-1}{90(L+1)}}\mathbf{T}_{LL\frac{1}{2},L-\frac{1}{2}}^{\pi N \pi \Delta} + 8(14L+15)\sqrt{\frac{L}{90(2L+3)}}\mathbf{T}_{LL\frac{1}{2},L+\frac{1}{2}}^{\pi N \pi \Delta},
\end{aligned}
\tag{14}
$$

respectively, which relate the processes $\pi N \to \pi N$ and $\pi N \to \pi \Delta$.

$$\frac{1}{2}(P_{11} + P_{13}) \cong \begin{cases} \dfrac{7\sqrt{2}}{8} PP_{33} - \dfrac{3}{8\sqrt{2}} PP_{11} \\[2mm] \dfrac{29}{9\sqrt{5}} PP_{33} - \dfrac{13}{18\sqrt{5}} PP_{11} \end{cases} \qquad \frac{1}{10}(3D_{13} + 2D_{15}) \cong \begin{cases} \dfrac{3}{10} DD_{13} + \dfrac{31}{20}\sqrt{\dfrac{2}{7}} DD_{15} \\[2mm] \dfrac{16}{15\sqrt{10}} DD_{13} + \dfrac{86}{15\sqrt{35}} DD_{15} \end{cases} \qquad \frac{1}{14}(9F_{15} + 5F_{17}) \cong \begin{cases} \dfrac{27}{14\sqrt{2}} FF_{35} + \dfrac{11}{42}\sqrt{\dfrac{6}{5}} FF_{37} \\[2mm] \dfrac{26}{7\sqrt{5}} FF_{35} + \dfrac{16\sqrt{3}}{105} FF_{37} \end{cases}$$

3-86

5329A28

FIG. 15. Test of Eqs. (13) and (14). The upper and lower expressions in braces, which refer to the process $\pi N \rightarrow \pi\Delta$, are the 2-flavor and 3-flavor predictions, depicted by dot-dash and dotted lines, respectively. The expressions to the left of the equalities, which refer to $\pi N \rightarrow \pi N$, are depicted by solid lines.

Figure 15 tests these relations as applied to the experimental $\pi N \to \pi N$ [17] and $\pi N \to \pi \Delta$ [20] P-, D- and F-wave amplitudes.[#33] Clearly, there is no substantial difference between the 2- and 3-flavor predictions in the degree of agreement. It should be noted that the agreement in the *signs* of the amplitudes is in itself a nontrivial result. For the P and F waves, the relations appear rather well satisfied. In particular, Eqs. (13) and (14) work roughly as well as Eq. (12), which likewise relates $\pi N \to \pi N$ and $\pi N \to \pi \Delta$. Equation (12), however, was derived from the 2-flavor approach *without* additional dynamical approximations (*cf.* Ref. 8 and Fig. 7 therein). In other words, incorporating these extra approximations does not noticeably worsen the agreement for the P and F waves. Unlike Eq. (12), however, there is poor agreement evident in Fig. 15 in the D waves—which is *consistent* with the fact that the big-small-small-big pattern itself does not work well for the D waves (*cf.* Fig. 1.)

Our conclusion, suggested by the big-small-small-big and big-small-small-small patterns and reinforced by Fig. 15, is that the dynamical assumptions stated above are (with the probable exception of the D waves) good descriptions of the effective Lagrangian derivable, in principle, from QCD. We hope that, as such, they will prove to be useful constraints on the current model-building efforts in skyrmion physics.

[#33] In order to make use of the available curves for $\pi N \to \pi \Delta$,[20] we have combined Eqs. (13) and (14) with Eq. (10) for the P and F waves. As discussed in Ref. 8, it is not obvious how best to relate energies when comparing processes such as $\pi N \to \pi N$ and $\pi N \to \pi \Delta$ with different thresholds; following the practice adopted there, we have parametrized the amplitudes in Fig. 15 by "excitation energy" ΔE_{CM}, measured from the *average* of the πN and $\pi \Delta$ thresholds.

Acknowledgments

APPENDIX A. Reduced Amplitudes of the Skyrme Model

This Appendix depicts the reduced amplitudes of the 3-flavor Skyrme model. The amplitudes $T_{KL'L}^{\{1,0\}}$ are identical to their 2-flavor counterparts, and were presented previously in a less transparent form.[7,14] It is convenient to present the results for the linear combinations

$$T_{KLL}^{\pm} = \frac{1}{2}(T_{KLL}^{\{\frac{1}{2},1\}} \pm T_{KLL}^{\{\frac{1}{2},-1\}}).$$

The differential equations from which the $T_{KL'L}^{\{1,0\}}$'s and $T_{KLL}^{\{\frac{1}{2},\pm 1\}}$'s are extracted are given in Refs. 7 and 14 and in Ref. 13, respectively.[‡34]

It is clear from Fig. 16 that, with some exceptions in the lower partial waves, the reduced amplitudes $\{T_{L-1,LL}^{\{1,0\}}, T_{LLL}^{\{1,0\}}, T_{L-\frac{1}{2},LL}^{+}\}$ vary much more dramatically as functions of energy than do the other five amplitudes $\{T_{L+1,LL}^{\{1,0\}}, T_{LLL}^{\{0,0\}}, T_{L+\frac{1}{2},LL}^{+}, T_{L-\frac{1}{2},LL}^{-}, T_{L+\frac{1}{2},LL}^{-}\}$.

---

‡34 *N.B.* The reader should exercise caution in applying the formalism presented in Section II of Ref. 7 to processes with $L' = L \pm 2$: On the one hand, there ought to have been a minus-sign in the off-diagonal elements of S_K defined in Eq. (16) of Ref. 7 due to our Bessel-function conventions. On the other hand, Fig. 6 of Ref. 7 is in error and should be disregarded.
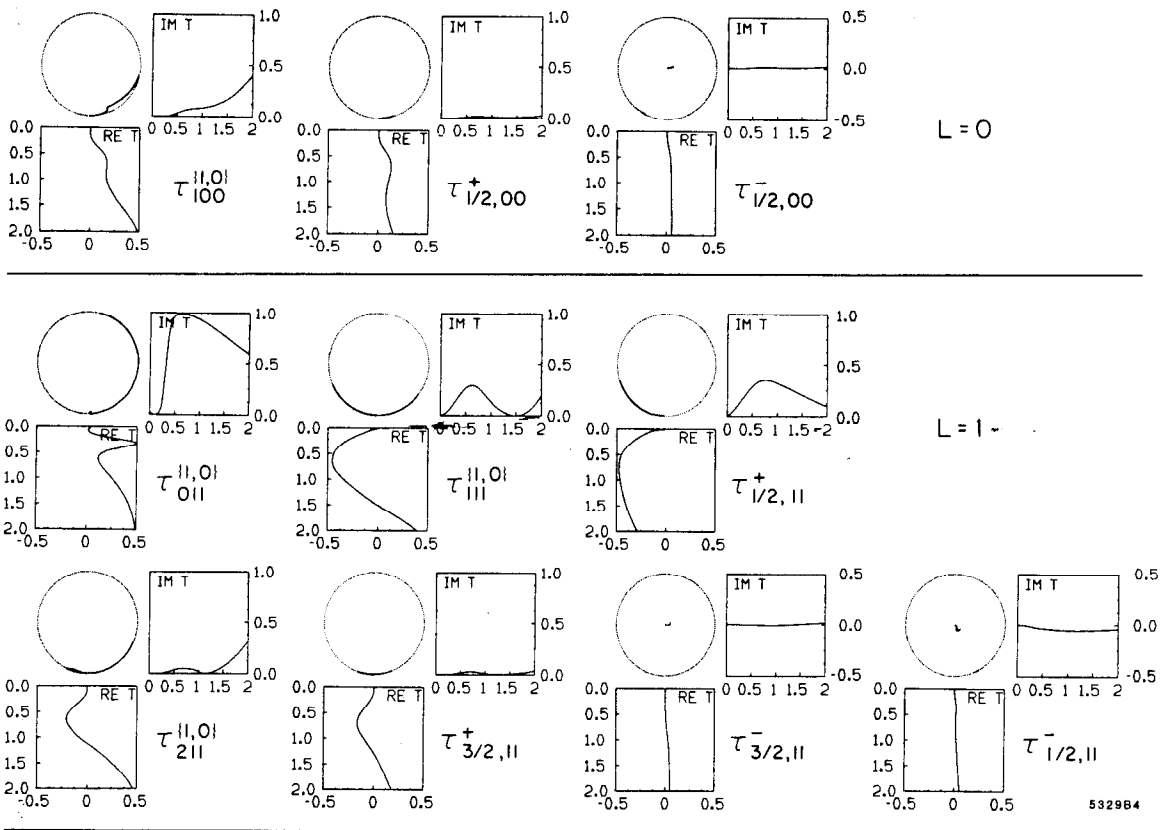
FIG. 16. The reduced amplitudes of the Skyrme model for the case $L = L'$. See text of Appendix A for details.
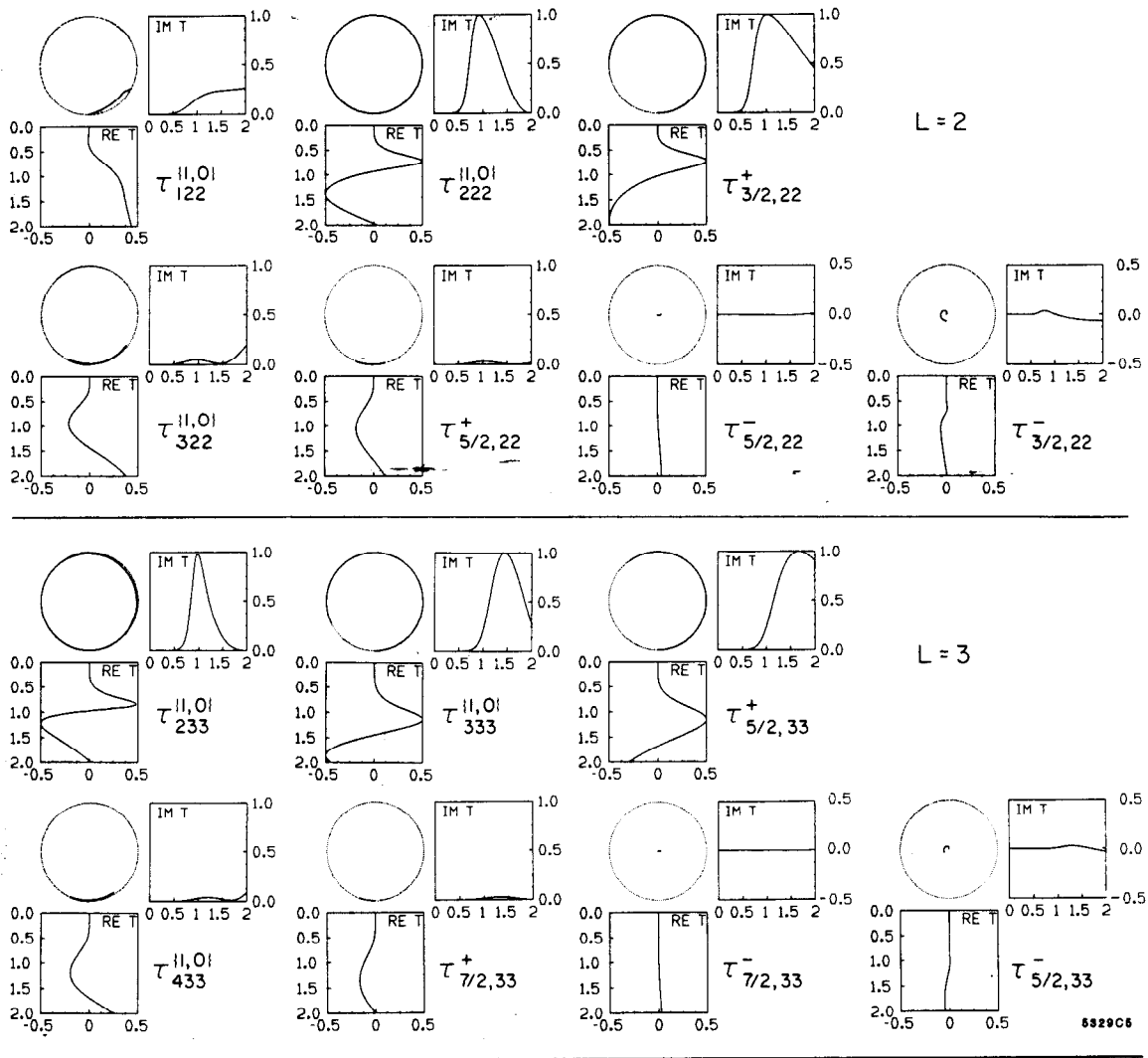
IM T 1.0 0.5 0.0
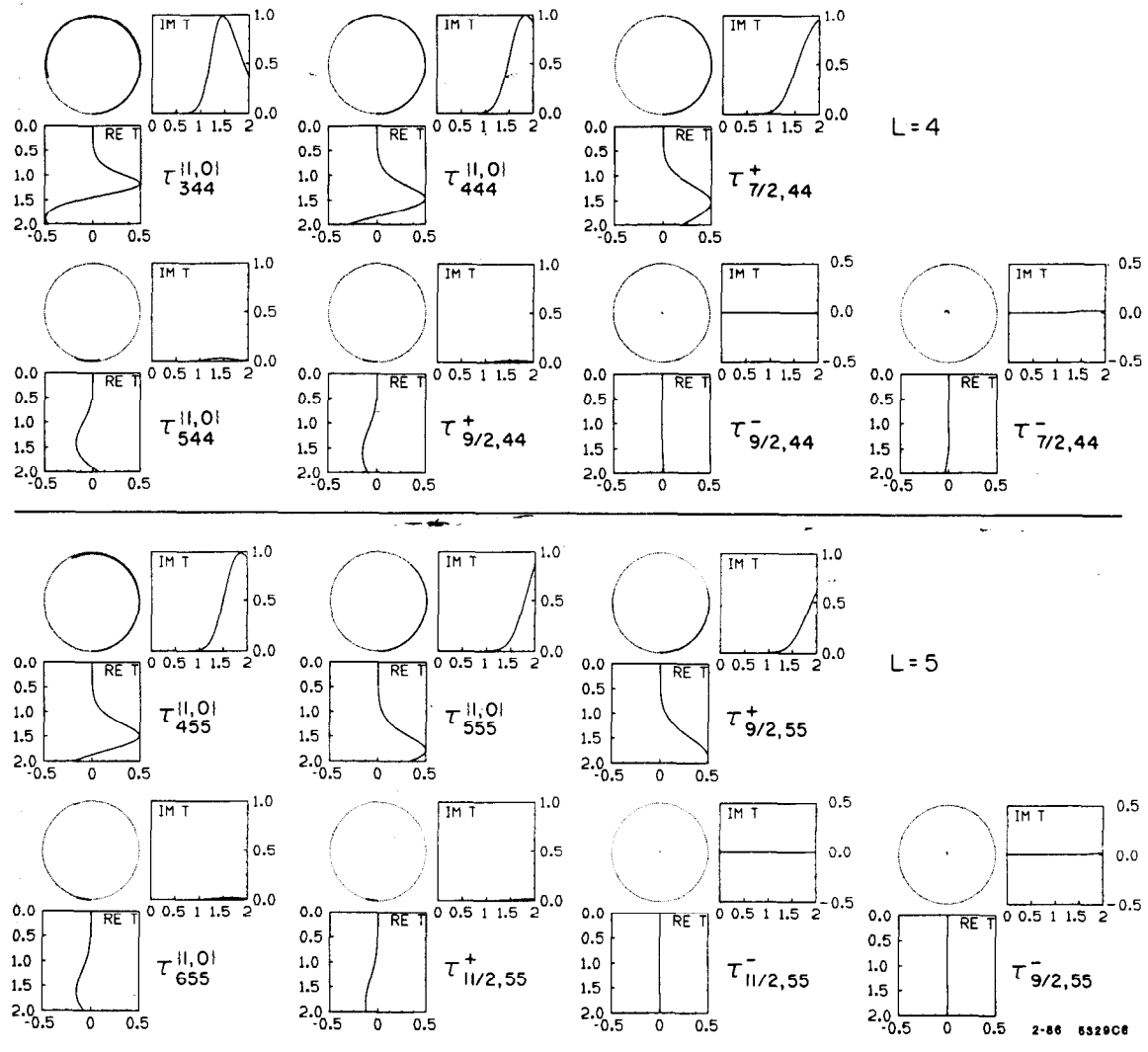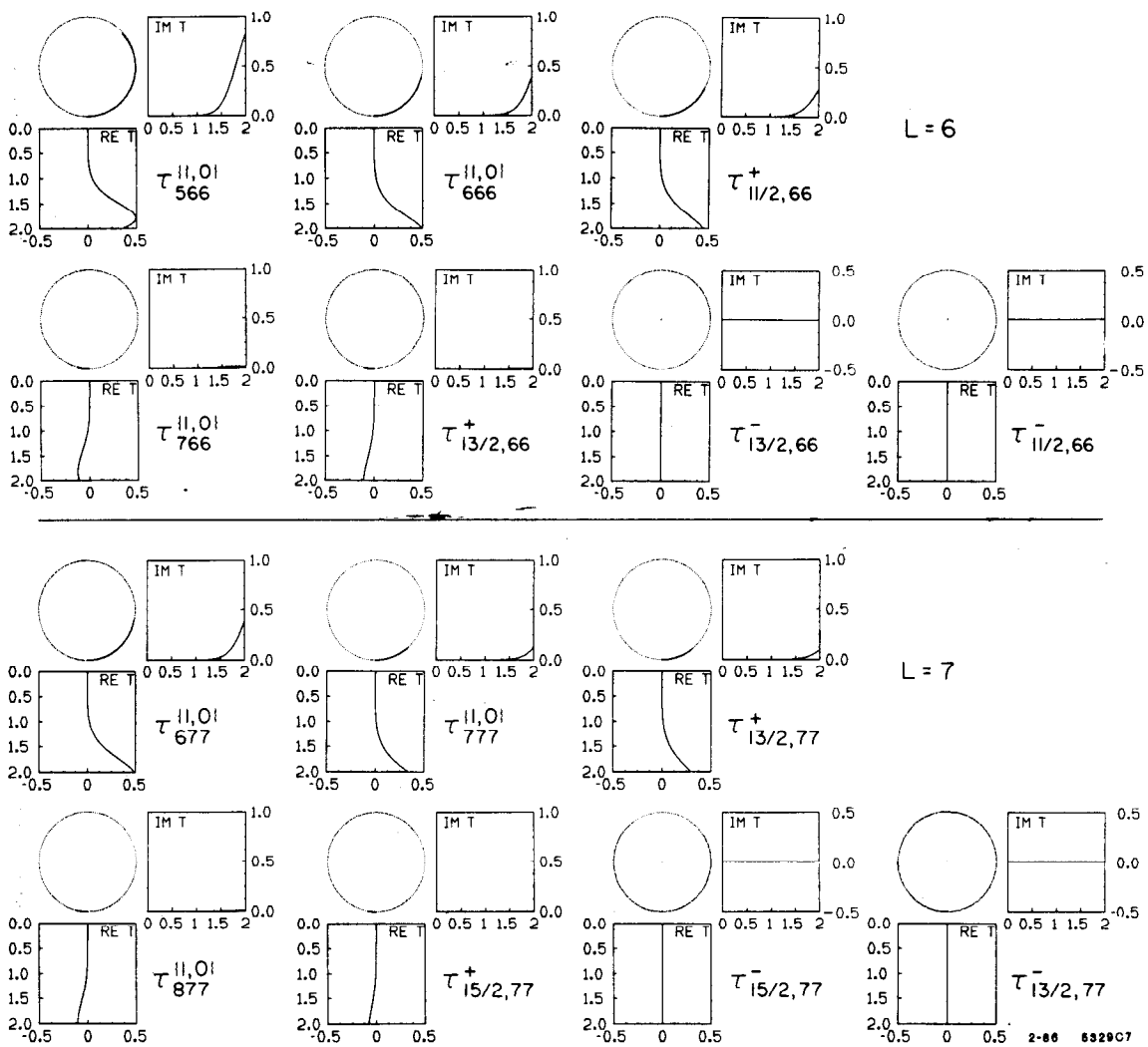0 0.5 1 1.5 2
0.0 0.5 1.0 1.5 2.0
-0.5 0 0.5
RE T
$\tau_{122}^{|1,0|}$

IM T 1.0 0.5 0.0
0 0.5 1 1.5 2
0.0 0.5 1.0 1.5 2.0
-0.5 0 0.5
RE T
$\tau_{222}^{|1,0|}$

IM T 1.0 0.5 0.0
0 0.5 1 1.5 2
0.0 0.5 1.0 1.5 2.0
-0.5 0 0.5
RE T
$\tau_{3/2,22}^{+}$

L = 2

IM T 1.0 0.5 0.0
0 0.5 1 1.5 2
0.0 0.5 1.0 1.5 2.0
-0.5 0 0.5
RE T
$\tau_{322}^{|1,0|}$

IM T 1.0 0.5 0.0
0 0.5 1 1.5 2
0.0 0.5 1.0 1.5 2.0
-0.5 0 0.5
RE T
$\tau_{5/2,22}^{+}$

IM T 0.5 0.0 -0.5
0 0.5 1 1.5 2
0.0 0.5 1.0 1.5 2.0
-0.5 0 0.5
RE T
$\tau_{5/2,22}^{-}$

IM T 0.5 0.0 -0.5
0 0.5 1 1.5 2
0.0 0.5 1.0 1.5 2.0
-0.5 0 0.5
RE T
$\tau_{3/2,22}^{-}$

IM T 1.0 0.5 0.0
0 0.5 1 1.5 2
0.0 0.5 1.0 1.5 2.0
-0.5 0 0.5
RE T
$\tau_{233}^{|1,0|}$

IM T 1.0 0.5 0.0
0 0.5 1 1.5 2
0.0 0.5 1.0 1.5 2.0
-0.5 0 0.5
RE T
$\tau_{333}^{|1,0|}$

IM T 1.0 0.5 0.0
0 0.5 1 1.5 2
0.0 0.5 1.0 1.5 2.0
-0.5 0 0.5
RE T
$\tau_{5/2,33}^{+}$

L = 3

IM T 1.0 0.5 0.0
0 0.5 1 1.5 2
0.0 0.5 1.0 1.5 2.0
-0.5 0 0.5
RE T
$\tau_{433}^{|1,0|}$

IM T 1.0 0.5 0.0
0 0.5 1 1.5 2
0.0 0.5 1.0 1.5 2.0
-0.5 0 0.5
RE T
$\tau_{7/2,33}^{+}$

IM T 0.5 0.0 -0.5
0 0.5 1 1.5 2
0.0 0.5 1.0 1.5 2.0
-0.5 0 0.5
RE T
$\tau_{7/2,33}^{-}$

IM T 0.5 0.0 -0.5
0 0.5 1 1.5 2
0.0 0.5 1.0 1.5 2.0
-0.5 0 0.5
RE T
$\tau_{5/2,33}^{-}$

5329C5

FIG. 16. Continued

68

FIG. 16. Continued

$\tau^{|1,0|}_{566}$ $\tau^{|1,0|}_{666}$ $\tau^{+}_{11/2,66}$ L = 6

$\tau^{|1,0|}_{766}$ $\tau^{+}_{13/2,66}$ $\tau^{-}_{13/2,66}$ $\tau^{-}_{11/2,66}$

$\tau^{|1,0|}_{677}$ $\tau^{|1,0|}_{777}$ $\tau^{+}_{13/2,77}$ L = 7

$\tau^{|1,0|}_{877}$ $\tau^{+}_{15/2,77}$ $\tau^{-}_{15/2,77}$ $\tau^{-}_{13/2,77}$

2-86 6329C7

FIG. 16. Continued

IM T 0.5

0.0

RE T 0 0.5 1 1.5 2 -0.5

0.0
0.5
1.0
1.5
2.0
-0.5 0 0.5

$\tau^{\{1,0\}}_{102}$

IM T 0.5

0.0

RE T 0 0.5 1 1.5 2 -0.5

0.0
0.5
1.0
1.5
2.0
-0.5 0 0.5

$\tau^{\{1,0\}}_{213}$

IM T 0.5

0.0

RE T 0 0.5 1 1.5 2 -0.5

0.0
0.5
1.0
1.5
2.0
-0.5 0 0.5

$\tau^{\{1,0\}}_{324}$

IM T 0.5

0.0

RE T 0 0.5 1 1.5 2 -0.5

0.0
0.5
1.0
1.5
2.0
-0.5 0 0.5

$\tau^{\{1,0\}}_{435}$

IM T 0.5

0.0

RE T 0 0.5 1 1.5 2 -0.5

0.0
0.5
1.0
1.5
2.0
-0.5 0 0.5

$\tau^{\{1,0\}}_{546}$

IM T 0.5

0.0

RE T 0 0.5 1 1.5 2 -0.5

0.0
0.5
1.0
1.5
2.0
-0.5 0 0.5

$\tau^{\{1,0\}}_{657}$

2-86
5329B12

FIG. 17. The reduced amplitudes of the Skyrme model for the case $L' = L \pm 2$. See text of Appendix A for details.

71

APPENDIX B. Formalism for 3-Flavor Scattering

In this Appendix we review the derivation of the 3-flavor scattering formula, Eq. (3), given in Ref. 12. We shall be focusing on Lagrangians such as Eq. (1) where $U \in SU(3)$. The key assumption is that the Lagrangian admits a "hedgehog" soliton solution U_0 that lives in the conventional isospin subgroup of $SU(3)$, *viz* :

$$U_0 = \exp\{iF(r) \sum_{i=1}^{3} \hat{r}^i \lambda^i\}, \tag{15}$$

with λ^a, $a = 1, ..., 8$, the Gell-Mann matrices. We shall refer to U_0 as a skyrmion in its *canonical* orientation.[35]

Of course, other orientations of the skyrmion are possible. In fact, by virtue of the assumed $SU(3)_{flavor}$ invariance of the Lagrangian, one can construct a family of degenerate solitons simply by taking

$$U_A = AU_0A^{-1}, \quad A \in SU(3). \tag{16}$$

However, let us forget for the moment about the existence of these degenerate configurations, and concentrate on the simplified problem of mesons scattering from U_0. This entails letting[36]

$$U_0 \longrightarrow \exp\{iF(r) \sum_{i=1}^{3} \hat{r}^i \lambda^i + \frac{2i}{f_\pi} \sum_{a=1}^{8} \phi^a \lambda^a\} \tag{17}$$

and expanding the Lagrangian to quadratic order in the ϕ's. Higher-order terms

---

[35] The results of this Section would be unaffected if the η field had a radially-dependent expectation-value as well, although this is not the case for the particular example of Skyrme's Lagrangian.

[36] For calculating on-shell amplitudes, this parametrization of the meson fields is equivalent to the one advocated by Schnitzer.[48]

are suppressed by powers of $1/f_\pi \sim 1/\sqrt{N_c}$, and are therefore ignored in our lowest-order treatment.

What will the resulting quadratic Lagrangian look like? Thanks to the hedgehog structure of the skyrmion, it will consist of a sum of terms in which all isospin and spatial indices have been contracted together in all possible ways to form singlets under the "hybrid" angular momentum $\mathbf{K}$, which is the vectorial sum of isospin and angular momentum. Also, since the skyrmion commutes with λ^8, the Lagrangian will embody hypercharge conservation. Consequently, kaons will be coupled only to kaons, and antikaons to antikaons. There will be $\pi\pi$ and $\eta\eta$ couplings as well, but $\pi\eta$ terms are forbidden by G-parity. In other words, the T-matrix $\mathbf{T}^{ba}$ characterizing the process

$$\phi^a + \text{canonical skyrmion} \longrightarrow \phi^b + \text{canonical skyrmion},$$

which is *a priori* an 8×8 matrix in the flavor-space of pseudoscalar-octet mesons, actually block-diagonalizes into a 3×3, a 1×1, and two 2×2 pieces, corresponding to π, η, K and $\overline{K}$ scattering, respectively.

We have not yet made full use of the $\mathbf{K}$ symmetry of the canonical skyrmion. To do so, we first expand ϕ^a and ϕ^b in spherical harmonics Y_{LM} and $Y_{L'M'}$, with primes henceforth denoting final-state quantities. These orbital angular momenta are, in turn, added to the mesons' isospin $\mathbf{I}^a$ and $\mathbf{I}^b$ by familiar Clebsch-Gordanry to form states $|\mathbf{K}^2 K_z L I^a >$ and $|\mathbf{K}'^2 K'_z L' I^b >$. The $\mathbf{K}$ symmetry of the canonically-oriented skyrmion then implies $K = K'$ and $K_z = K'_z$; likewise, thanks to the block-diagonal nature of $\mathbf{T}^{ba}$, we must have $I^a = I^b$. In contrast, L and L' will not necessarily be equal, but can differ by two. Scattering in these $\mathbf{K}$-channels will then be described by the reduced amplitudes $T_{KL'L}^{\{1,0\}}$, $T_{KL'L}^{\{0,0\}}$ and

$T_{KL'L}^{\{\frac{1}{2};\pm1\}}$ defined in Section II (just as scattering from a spherical potential can be characterized by reduced amplitudes T_L). In equations, the T-matrix will thus be given by:

$$
\begin{aligned}
\mathbf{T}^{ba} = {} & \delta_{I^a I^b} \delta_{Y^a Y^b} \sum_{LML'M'} < \phi^b(x')|L'M' > < LM|\phi^a(x) > \\
& \times \sum_{KK_z} < L'I^b M' I_z^b | KK_z > < KK_z | LI^a M I_z^a > T_{KL'L}^{\{I^a Y^a\}}
\end{aligned}
\tag{18}
$$

where $\{I^a, I_z^a, Y^a\}$ and $\{I^b, I_z^b, Y^b\}$ are the $SU(3)$ quantum numbers of the incoming and outgoing meson, respectively.

This formula is easily generalized to account for the scattering of a meson, not from a canonically-oriented skyrmion U_0, but rather from a rotated skyrmion U_A as defined by Eq. (16). The prescription is simply

$$
\mathbf{T}^{ba} \longrightarrow \sum_{cd} \mathcal{D}^{(8)}(A)_{bd} \, \mathbf{T}^{dc} \, \mathcal{D}^{(8)}(A)_{ca}^{\dagger}
\tag{19}
$$

with $\mathcal{D}^{(8)}(A)$ the adjoint representation of A. Armed with Eqs. (18) and (19), we are finally prepared to tackle the scattering of a meson off a physical baryon, which, in the soliton approach, is characterized by a *superposition* of U_A's for all values of $A \in SU(3)$, weighted by appropriately-constructed wavefunctions $\chi(A)$. The physical T-matrix is then given by:

$$
\int_{SU(3)} dA \, \chi_{\text{final}}^{\dagger}(A) \sum_{cd} \mathcal{D}^{(8)}(A)_{bd} \, \mathbf{T}^{dc} \, \mathcal{D}^{(8)}(A)_{ca}^{\dagger} \chi_{\text{initial}}(A)
\tag{20}
$$

The final ingredient that we need is an explicit expression for the baryon wavefunctions $\chi(A)$ describing a baryon with spin, isospin and hypercharge quantum numbers $\{s, s_z, i, i_z, Y\}$. Unfortunately, the 3-flavor wavefunctions given by

74

Guadagnini,[4] which are often used in the literature, are characterized by non-standard transformation properties under isospin and angular momentum. The correct wavefunctions are, instead,

$$\chi(A) = \frac{i}{\pi}\sqrt{\frac{\dim R}{2}}[\mathcal{D}^R(A)^\dagger]_{\alpha,\beta} \cdot (-1)^{s-s_z} \tag{21}$$

where $\alpha = \{s, -s_z, 1\}$, $\beta = \{i, i_z, Y\}$, R denotes the $SU(3)_{\text{flavor}}$ representation of the baryon, and $\dim R$ is its dimension[♮37]

As in the 2-flavor case,[8] the integration over A can be carried out in closed form, thanks to some standard identities. The resulting expression simplifies greatly if, as indicated in Section II, we project the initial and final meson-baryon systems onto states of definite total angular momentum and $SU(3)_{\text{flavor}}$. (The latter projection is accomplished with the help of an $SU(3)$ Clebsch-Gordan coefficient

$$\langle R_1 i_1 i_{z1} Y_1; R_2 i_2 i_{z2} Y_2 | R_{\text{tot}}\gamma I_{\text{tot}} I_{z\text{tot}} Y_{\text{tot}}\rangle$$

which can be factored conveniently into the product

$$\langle i_1 i_2 i_{z1} i_{z2} | I_{\text{tot}} I_{z\text{tot}}\rangle \cdot \begin{pmatrix} R_1 & R_2 & R_{\text{tot}}\gamma \\ i_1 Y_1 & i_2 Y_2 & I_{\text{tot}} Y_{\text{tot}} \end{pmatrix}$$

of an $SU(2)$ Clebsch-Gordan coefficient with a so-called isoscalar factor.[44]) With

---

♮37 See, for example, Manohar.[51] The fact that the "left-handed hypercharge" is unity is a nontrivial quantization condition arising from consideration of the Wess-Zumino term.[4] Our normalization in (21) is such that $\int_{SU(3)} dA = 2\pi^2$.

quantum numbers defined as in Section II, we find, after some manipulation:

$$\mathbf{T}(\{LsRR_{\text{tot}}\gamma I_{\text{tot}}I_{z\text{tot}}Y_{\text{tot}}\mathbf{J}\} \rightarrow \{L's'R'R'_{\text{tot}}\gamma'I'_{\text{tot}}I'_{z\text{tot}}Y'_{\text{tot}}\mathbf{J}'\}) \quad =$$

$$\delta_{R_{\text{tot}}R'_{\text{tot}}} \, \delta_{I_{\text{tot}}I'_{\text{tot}}} \, \delta_{I_{z\text{tot}}I'_{z\text{tot}}} \, \delta_{Y_{\text{tot}}Y'_{\text{tot}}} \, \delta_{JJ'} \, \delta_{J_z J'_z} \quad \times$$

$$(-1)^{s'-s}\frac{\sqrt{\dim R \cdot \dim R'}}{\dim R_{\text{tot}}} \sum_{\{IY\}} \sum_{i} \sum_{K} (2i+1)(2K+1) \left\{ \begin{matrix} KiJ \\ s'L'I \end{matrix} \right\} \left\{ \begin{matrix} KiJ \\ sLI \end{matrix} \right\} \qquad (22)$$

$$\times \quad \left(\begin{matrix} R_{\text{tot}}\gamma' \\ i, 1+Y \end{matrix} \,\middle|\, \begin{matrix} R' & \mathbf{8} \\ s'1 & IY \end{matrix} \right) \left(\begin{matrix} R & \mathbf{8} \\ s1 & IY \end{matrix} \,\middle|\, \begin{matrix} R_{\text{tot}}\gamma \\ i, 1+Y \end{matrix} \right) \tau_{KL'L}^{\{IY\}} \, .$$

The long string of Kronecker δ's expresses the reassuring fact that total angular momentum and $SU(3)_{\text{flavor}}$ are conserved in the scattering process. This is Eq. (3).

Note that the derivation of this formula is independent of the particular Lagrangian that we started from, apart from the requirement that it admit a hedgehog soliton as in Eq. (15).

APPENDIX C: Explicit Formulae
for $SU(3)$ Scattering Coefficients

In this Appendix we present explicit formulae for the group-theoretic coefficients multiplying the reduced amplitudes in the $SU(3)$ scattering formula, Eq. (3). For fixed initial and final baryon representations, these depend only on the total meson-baryon representation R_{tot} and the total angular momentum J. We will restrict ourselves to the physically relevant cases when the initial baryon is in the spin-$\frac{1}{2}$ octet, and the final baryon is in either the octet or the spin-$\frac{3}{2}$ decuplet.

Table XV presents the coefficients of the reduced amplitudes for the case when the initial and final baryon are both in the octet. The decomposition for both the initial and final meson-baryon states is given by:

$$8 \times 8 = 27 + \overline{10} + 10 + 8_1 + 8_2 + 1$$

where (following DeSwart[44]) the 8_1 and 8_2 are synonymous with 8_{sym} and 8_{antisym}, respectively. Note that, from Eq. (3),

$$< 8_1 | 8_2 > = < 8_2 | 8_1 > \ .$$

Of course, for most physical processes, one is interested in a *superposition* of pure $SU(3)_{\text{flavor}}$ representations. Consider, for instance, the case $\overline{K}N \to \pi\Sigma$ in the isospin-1 channel. With the help of the table of isoscalar factors given in Ref. 44, the initial and final states can be written as

$$|\Psi>_{\text{in}} = \frac{1}{\sqrt{5}}|27> + \frac{1}{\sqrt{6}}|\overline{10}> - \frac{1}{\sqrt{6}}|10> - \frac{\sqrt{30}}{10}|8_1> + \frac{1}{\sqrt{6}}|8_2>$$

$$8 \times 8 \longrightarrow 8 \times 8$$

$$J = L - \tfrac{1}{2}$$

R_{tot}	$T_{L-1,LL}^{\{1,0\}}$	$T_{LLL}^{\{1,0\}}$	$T_{L+1,LL}^{\{1,0\}}$	$T_{LLL}^{\{0,0\}}$	$T_{L-\frac{1}{2},LL}^{\{\frac{1}{2},1\}}$	$T_{L+\frac{1}{2},LL}^{\{\frac{1}{2},1\}}$	$T_{L-\frac{1}{2},LL}^{\{\frac{1}{2},-1\}}$	$T_{L+\frac{1}{2},LL}^{\{\frac{1}{2},-1\}}$
$\langle 27\|27\rangle$	$\frac{2}{135}\frac{(2L-1)(4L-3)}{L(2L+1)}$	$\frac{2}{135}\frac{7L-3}{L}$	$\frac{4}{27}\frac{2L+3}{2L+1}$	$\frac{2}{15}$	$\frac{4}{27}\frac{2L-1}{2L+1}$	$\frac{16}{27}\frac{L+1}{2L+1}$	$\frac{1}{135}\frac{14L-1}{2L+1}$	$\frac{16}{135}\frac{L+1}{2L+1}$
$\langle \overline{10}\|\overline{10}\rangle$	$\frac{1}{15}\frac{2L-1}{L}$	$\frac{1}{15}\frac{L+1}{L}$	0	$\frac{1}{5}$	$\frac{2}{5}$	0	$\frac{1}{15}\frac{2L-1}{2L+1}$	$\frac{4}{15}\frac{L+1}{2L+1}$
$\langle 10\|10\rangle$	$\frac{2}{15}\frac{(2L-1)(L-1)}{L(2L+1)}$	$\frac{2}{15}\frac{2L-1}{L}$	$\frac{2}{5}\frac{2L+3}{2L+1}$	0	0	0	$\frac{1}{15}\frac{2L-1}{2L+1}$	$\frac{4}{15}\frac{L+1}{2L+1}$
$\langle 8_1\|8_1\rangle$	$\frac{3}{20}\frac{2L-1}{L}$	$\frac{3}{20}\frac{L+1}{L}$	0	$\frac{1}{20}$	0	0	$\frac{1}{10}\frac{4L-1}{2L+1}$	$\frac{3}{5}\frac{L+1}{2L+1}$
$\langle 8_2\|8_2\rangle$	$\frac{2L-1}{12L}$	$\frac{L+1}{12L}$	0	$\frac{1}{4}$	0	0	$\frac{1}{6}\frac{4L+1}{2L+1}$	$\frac{1}{3}\frac{L+1}{2L+1}$
$\langle 8_1\|8_2\rangle$	$\frac{2L-1}{L\sqrt{80}}$	$\frac{L+1}{L\sqrt{80}}$	0	$\frac{-1}{\sqrt{80}}$	0	0	$\frac{1}{2\sqrt{5}(2L+1)}$	$\frac{-(L+1)}{\sqrt{5}(2L+1)}$
$\langle 1\|1\rangle$	0	0	0	0	0	0	1	0

$$J = L + \tfrac{1}{2}$$

R_{tot}	$T_{L-1,LL}^{\{1,0\}}$	$T_{LLL}^{\{1,0\}}$	$T_{L+1,LL}^{\{1,0\}}$	$T_{LLL}^{\{0,0\}}$	$T_{L-\frac{1}{2},LL}^{\{\frac{1}{2},1\}}$	$T_{L+\frac{1}{2},LL}^{\{\frac{1}{2},1\}}$	$T_{L-\frac{1}{2},LL}^{\{\frac{1}{2},-1\}}$	$T_{L+\frac{1}{2},LL}^{\{\frac{1}{2},-1\}}$
$\langle 27\|27\rangle$	$\frac{4}{27}\frac{2L-1}{2L+1}$	$\frac{2}{135}\frac{7L+10}{L+1}$	$\frac{2}{135}\frac{(2L+3)(4L+7)}{(L+1)(2L+1)}$	$\frac{2}{15}$	$\frac{16}{27}\frac{L}{2L+1}$	$\frac{4}{27}\frac{2L+3}{2L+1}$	$\frac{16}{135}\frac{L}{2L+1}$	$\frac{1}{135}\frac{14L+15}{2L+1}$
$\langle \overline{10}\|\overline{10}\rangle$	0	$\frac{1}{15}\frac{L}{L+1}$	$\frac{1}{15}\frac{2L+3}{L+1}$	$\frac{1}{5}$	0	$\frac{2}{5}$	$\frac{4}{15}\frac{L}{2L+1}$	$\frac{1}{15}\frac{2L+3}{2L+1}$
$\langle 10\|10\rangle$	$\frac{2}{5}\frac{2L-1}{2L+1}$	$\frac{2}{15}\frac{2L+3}{L+1}$	$\frac{2}{15}\frac{(L+2)(2L+3)}{(L+1)(2L+1)}$	0	0	0	$\frac{4}{15}\frac{L}{2L+1}$	$\frac{1}{15}\frac{2L+3}{2L+1}$
$\langle 8_1\|8_1\rangle$	0	$\frac{3}{20}\frac{L}{L+1}$	$\frac{3}{20}\frac{2L+3}{L+1}$	$\frac{1}{20}$	0	0	$\frac{3}{5}\frac{L}{2L+1}$	$\frac{1}{10}\frac{4L+5}{2L+1}$
$\langle 8_2\|8_2\rangle$	0	$\frac{L}{12(L+1)}$	$\frac{2L+3}{12(L+1)}$	$\frac{1}{4}$	0	0	$\frac{1}{3}\frac{L}{2L+1}$	$\frac{1}{6}\frac{4L+3}{2L+1}$
$\langle 8_1\|8_2\rangle$	0	$\frac{L}{(L+1)\sqrt{80}}$	$\frac{2L+3}{(L+1)\sqrt{80}}$	$\frac{-1}{\sqrt{80}}$	0	0	$\frac{-L}{\sqrt{5}(2L+1)}$	$\frac{-1}{2\sqrt{5}(2L+1)}$
$\langle 1\|1\rangle$	0	0	0	0	0	0	0	1

Table XV

$$\pi N \longrightarrow \pi N$$

$\tau_{L-1,LL}^{\{1,0\}}$	$\tau_{LLL}^{\{1,0\}}$	$\tau_{L+1,LL}^{\{1,0\}}$	$\tau_{LLL}^{\{0,0\}}$	$\tau_{L-\frac{1}{2},LL}^{\{\frac{1}{2},1\}}$	$\tau_{L+\frac{1}{2},LL}^{\{\frac{1}{2},1\}}$	$\tau_{L-\frac{1}{2},LL}^{\{\frac{1}{2},-1\}}$	$\tau_{L+\frac{1}{2},LL}^{\{\frac{1}{2},-1\}}$	J	I
$\frac{98L^2-L-24}{135L(2L+1)}$	$\frac{25L+24}{135L}$	$\frac{2L+3}{135(2L+1)}$	$\frac{1}{15}$	$\frac{58L+25}{270(2L+1)}$	$\frac{4(L+1)}{135(2L+1)}$	$\frac{104L+35}{270(2L+1)}$	$\frac{17(L+1)}{135(2L+1)}$	$L-\frac{1}{2}$	$\frac{1}{2}$
$\frac{2L-1}{135(2L+1)}$	$\frac{25L+1}{135(L+1)}$	$\frac{98L^2+197L+75}{135(2L^2+3L+1)}$	$\frac{1}{15}$	$\frac{4L}{135(2L+1)}$	$\frac{58L+33}{270(2L+1)}$	$\frac{17L}{135(2L+1)}$	$\frac{104L+69}{270(2L+1)}$	$L+\frac{1}{2}$	$\frac{1}{2}$
$\frac{(26L^2-37L+12)}{135L(2L+1)}$	$\frac{25L-12}{135L}$	$\frac{37}{135}\frac{2L+3}{2L+1}$	$\frac{1}{15}$	$\frac{2(2L-1)}{27(2L+1)}$	$\frac{8(L+1)}{27(2L+1)}$	$\frac{16L-5}{135(2L+1)}$	$\frac{26(L+1)}{135(2L+1)}$	$L-\frac{1}{2}$	$\frac{3}{2}$
$\frac{37}{135}\frac{2L-1}{2L+1}$	$\frac{25L+37}{135(L+1)}$	$\frac{26L^2+89L+75}{135(2L^2+3L+1)}$	$\frac{1}{15}$	$\frac{8L}{27(2L+1)}$	$\frac{2(2L+3)}{27(2L+1)}$	$\frac{26L}{135(2L+1)}$	$\frac{16L+21}{135(2L+1)}$	$L+\frac{1}{2}$	$\frac{3}{2}$

Table XVI

$$8 \times 8 \longrightarrow 10 \times 8; \quad \mathbf{L' = L}$$

$$J = L - \tfrac{1}{2}$$

R_{tot}	$\mathcal{T}^{\{1,0\}}_{L-1,LL}$	$\mathcal{T}^{\{1,0\}}_{LLL}$	$\mathcal{T}^{\{1,0\}}_{L+1,LL}$	$\mathcal{T}^{\{0,0\}}_{LLL}$	$\mathcal{T}^{\{\frac{1}{2},1\}}_{L-\frac{1}{2},LL}$	$\mathcal{T}^{\{\frac{1}{2},1\}}_{L+\frac{1}{2},LL}$	$\mathcal{T}^{\{\frac{1}{2},-1\}}_{L-\frac{1}{2},LL}$
$\langle 27|\,27\rangle$	$\dfrac{(3-4L)\sqrt{10(L+1)(2L-1)}}{135L(2L+1)}$	$\dfrac{-(L+6)}{135L}\sqrt{\dfrac{5(2L-1)}{2(L+1)}}$	$\dfrac{2L+3}{27(2L+1)}\sqrt{\dfrac{5(2L-1)}{2(L+1)}}$	0	$\dfrac{-2\sqrt{10(2L-1)(L+1)}}{27(2L+1)}$	$\dfrac{2\sqrt{10(2L-1)(L+1)}}{27(2L+1)}$	$\dfrac{2\sqrt{(2L-1)(L+}}{27(2L+1)}$
$\langle 10|\,10\rangle$	$\dfrac{2(1-L)\sqrt{(2L-1)(L+1)/5}}{3L(2L+1)}$	$\dfrac{-(L+4)}{6L}\sqrt{\dfrac{2L-1}{5(L+1)}}$	$\dfrac{2L+3}{2(2L+1)}\sqrt{\dfrac{2L-1}{5(L+1)}}$	0	0	0	$\dfrac{-\sqrt{(2L-1)(L-}}{3(2L+1)}$
$\langle 8|\,8_1\rangle$	$\dfrac{-\sqrt{(L+1)(2L-1)/10}}{2L}$	$\dfrac{\sqrt{(L+1)(2L-1)/10}}{2L}$	0	0	0	0	$\dfrac{-\sqrt{(L+1)(2L-}}{2L+1}$
$\langle 8|\,8_2\rangle$	$\dfrac{-\sqrt{2(L+1)(2L-1)}}{12L}$	$\dfrac{\sqrt{2(L+1)(2L-1)}}{12L}$	0	0	0	0	$\dfrac{\sqrt{2(L+1)(2L}}{6(2L+1)}$

$$J = L + \tfrac{1}{2}$$

R_{tot}	$\mathcal{T}^{\{1,0\}}_{L-1,LL}$	$\mathcal{T}^{\{1,0\}}_{LLL}$	$\mathcal{T}^{\{1,0\}}_{L+1,LL}$	$\mathcal{T}^{\{0,0\}}_{LLL}$	$\mathcal{T}^{\{\frac{1}{2},1\}}_{L-\frac{1}{2},LL}$	$\mathcal{T}^{\{\frac{1}{2},1\}}_{L+\frac{1}{2},LL}$	$\mathcal{T}^{\{\frac{1}{2},-1\}}_{L-\frac{1}{2},LL}$
$\langle 27|\,27\rangle$	$\dfrac{1-2L}{27(2L+1)}\sqrt{\dfrac{5(2L+3)}{2L}}$	$\dfrac{L-5}{135(L+1)}\sqrt{\dfrac{5(2L+3)}{2L}}$	$\dfrac{2(4L+7)\sqrt{5L(2L+3)/2}}{135(L+1)(2L+1)}$	0	$\dfrac{-2\sqrt{10L(2L+3)}}{27(2L+1)}$	$\dfrac{2\sqrt{10L(2L+3)}}{27(2L+1)}$	$\dfrac{2\sqrt{L(2L+3)/1}}{27(2L+1)}$
$\langle 10|\,10\rangle$	$\dfrac{1-2L}{2(2L+1)}\sqrt{\dfrac{2L+3}{5L}}$	$\dfrac{L-3}{6(L+1)}\sqrt{\dfrac{2L+3}{5L}}$	$\dfrac{2(L+2)\sqrt{L(2L+3)/5}}{3(L+1)(2L+1)}$	0	0	0	$\dfrac{-\sqrt{L(2L+3)/5}}{3(2L+1)}$
$\langle 8|\,8_1\rangle$	0	$\dfrac{-\sqrt{L(2L+3)/10}}{2(L+1)}$	$\dfrac{\sqrt{L(2L+3)/10}}{2(L+1)}$	0	0	0	$\dfrac{-\sqrt{L(2L+3)/1}}{2L+1}$
$\langle 8|\,8_2\rangle$	0	$\dfrac{-\sqrt{2L(2L+3)}}{12(L+1)}$	$\dfrac{\sqrt{2L(2L+3)}}{12(L+1)}$	0	0	0	$\dfrac{\sqrt{2L(2L+3)}}{6(2L+1)}$

Table XVII

$$8 \times 8 \longrightarrow 10 \times 8; \quad L' = L \pm 2$$

R_{tot}	$(L, L') = (K - 1, K + 1)$	$(L, L') = (K + 1, K - 1)$
$\langle 27\|27 \rangle$	$\frac{1}{9}\sqrt{\frac{2K+1}{30K}}$	$\frac{1}{9}\sqrt{\frac{2K+1}{30(K+1)}}$
$\langle 10\|10 \rangle$	$\frac{-\sqrt{2K+1}}{60K}$	$\frac{\sqrt{2K+1}}{60(K+1)}$
$\langle 8\|8_1 \rangle$	$\frac{3}{2}\sqrt{\frac{2K+1}{30K}}$	$\frac{-3}{2}\sqrt{\frac{2K+1}{30(K+1)}}$
$\langle 8\|8_2 \rangle$	$\frac{1}{4}\sqrt{\frac{2(2K+1)}{3K}}$	$\frac{-1}{4}\sqrt{\frac{2(2K+1)}{3(K+1)}}$

Table XVIII

81

and

$$_{\text{out}} < \Psi| = -\frac{1}{\sqrt{6}} < \overline{10}| + \frac{1}{\sqrt{6}} < 10| + \frac{\sqrt{6}}{3} < 8_2|.$$

The amplitude for this process is thus given by

$$_{\text{out}} < \Psi|\Psi >_{\text{in}} = -\frac{1}{6} < \overline{10}|\overline{10} > -\frac{1}{6} < 10|10 > -\frac{1}{\sqrt{5}} < 8_2|8_1 > +\frac{1}{3} < 8_2|8_2 > .$$

Each term in this expression can, in turn, be expressed in terms of reduced amplitudes using Table XV.

As an important example of this procedure, Table XVI gives the coefficients for the case of πN elastic scattering in the 3-flavor formalism. These coefficients can be directly compared to their 2-flavor counterparts presented in Appendix B of Ref. 8.

Table XVII presents the relevant coefficients when the initial and final baryons are in the octet and decuplet, respectively, and when the initial and final meson angular momenta are the same $(L = L')$. The relevant decomposition of the final state is now:

$$10 \times 8 = 35 + 27 + 10 + 8.$$

Table XVIII lists the coefficients for the analogous $8 \times 8 \longrightarrow 10 \times 8$ processes when $|L - L'| = 2$. Note that these coefficients all multiply the *single* contributing reduced amplitude $T_{KL'L}^{\{1,0\}} \equiv T_{KLL'}^{\{1,0\}}$, where $K = (L + L')/2$.

APPENDIX D: Skyrme-model predictions for additional processes

In this Appendix we display the Skyrme-model amplitudes for the six $\phi_{\rm PS} N \to \phi_{\rm PS} B$ processes for which we were unable to find experimental partial-wave analyses in the literature, namely: $\pi N \to \eta \Delta$, $\pi N \to K\Sigma^*$, $\overline{K}N \to \eta\Sigma$, $\overline{K}N \to \eta\Sigma^*$, $\overline{K}N \to K\Xi$ and $\overline{K}N \to K\Xi^*$. As always, the plots are from threshold to an excitation energy of $2ef_\pi$. On the basis of the results of Sections III and V, we would expect good agreement for the F and G waves, mixed agreement in the D waves, and poor agreement in the S and P waves.

$$\pi N \rightarrow \eta \Delta$$
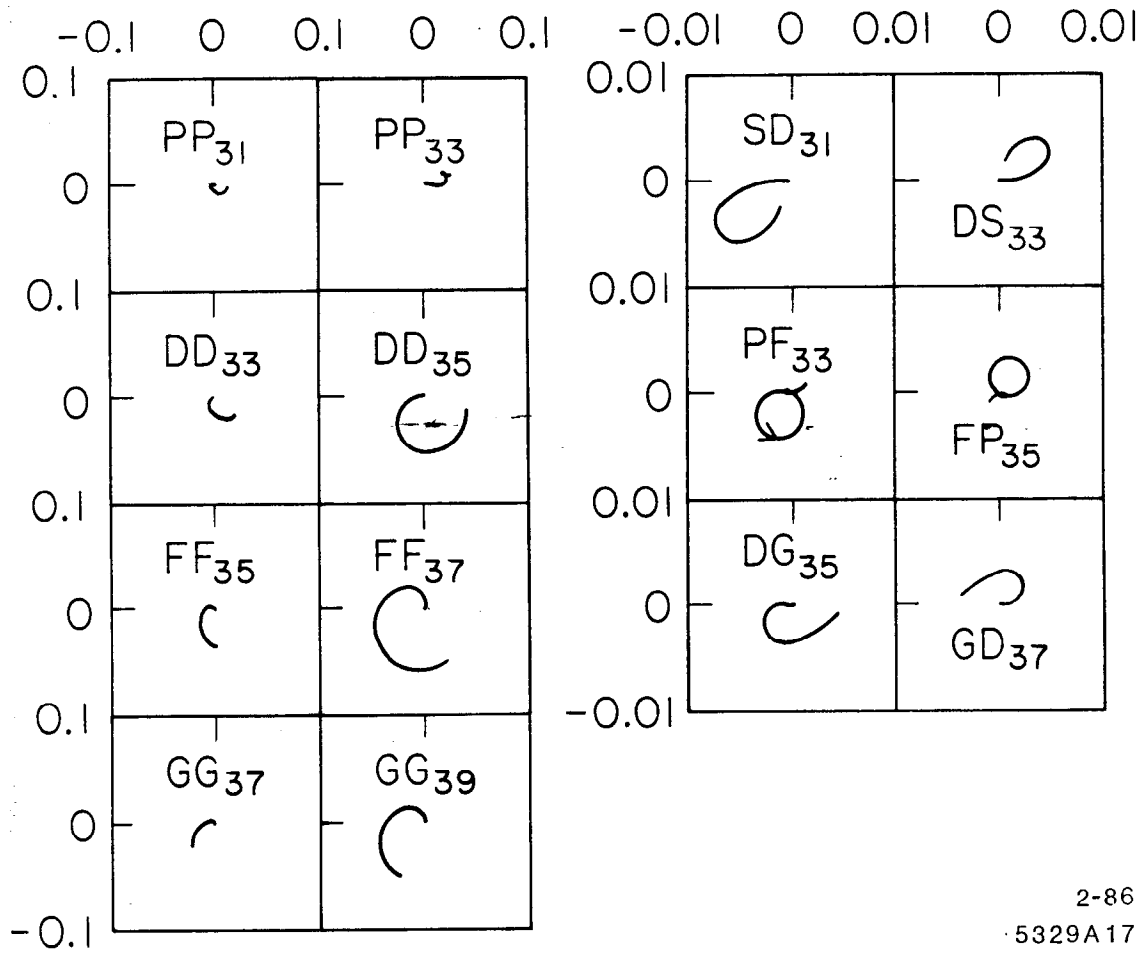
FIG. 18. Skyrme-model predictions for $\pi N \rightarrow \eta \Delta$

2-86
5329A17
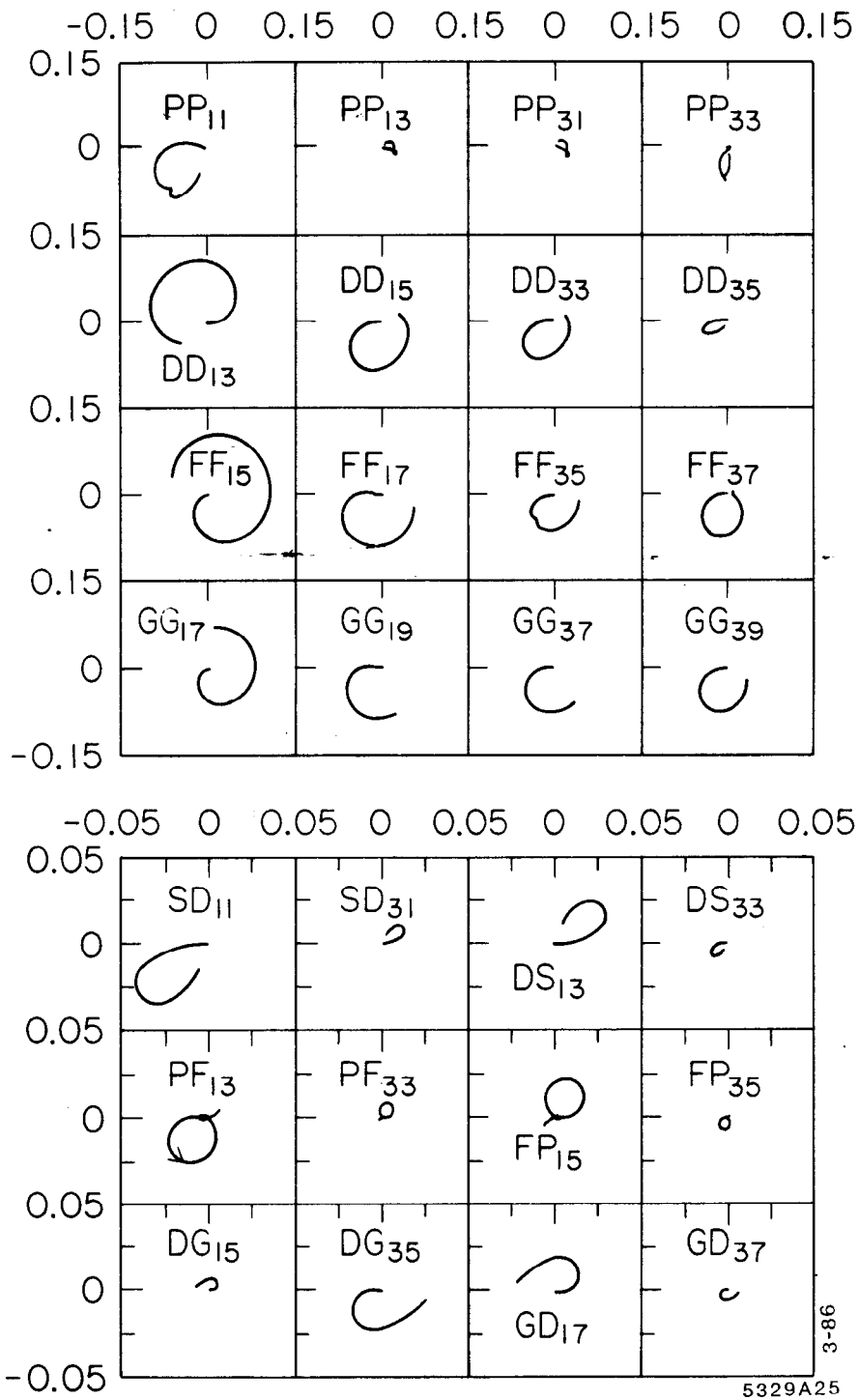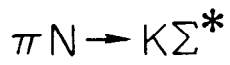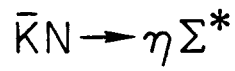
FIG. 19. Skyrme-model predictions for $\pi N \to K\Sigma^*$.
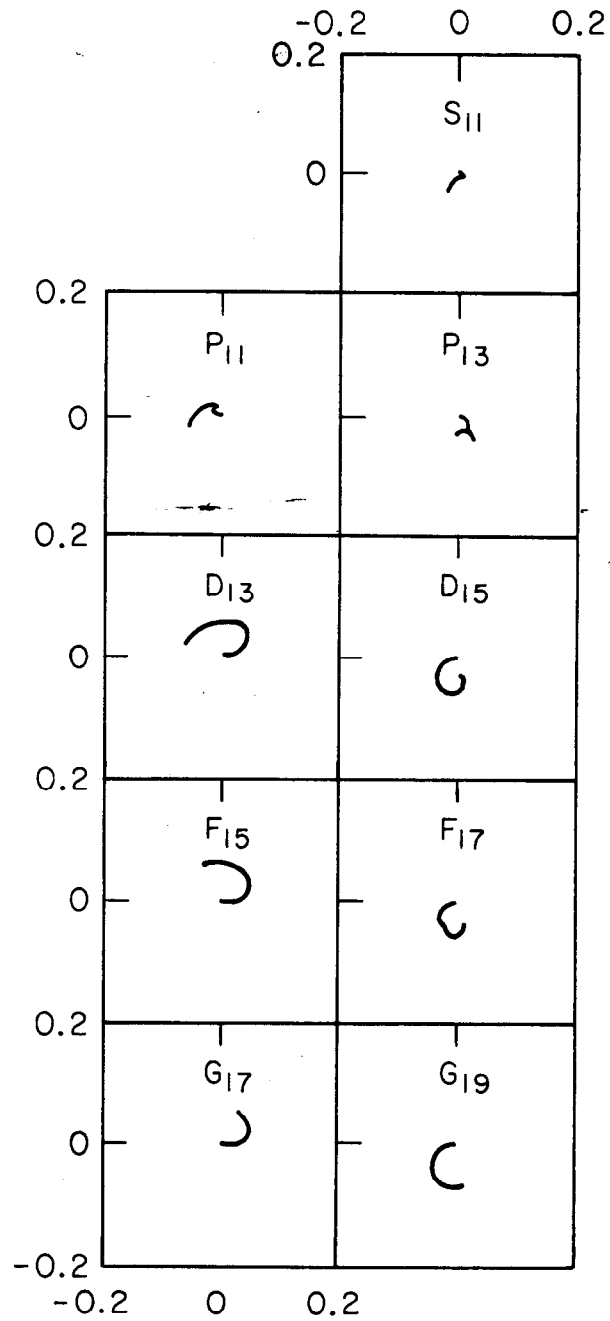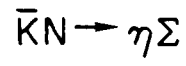
FIG. 20. Skyrme-model predictions for $\overline{K}N \to \eta\Sigma$.

2-86

5329A15

86
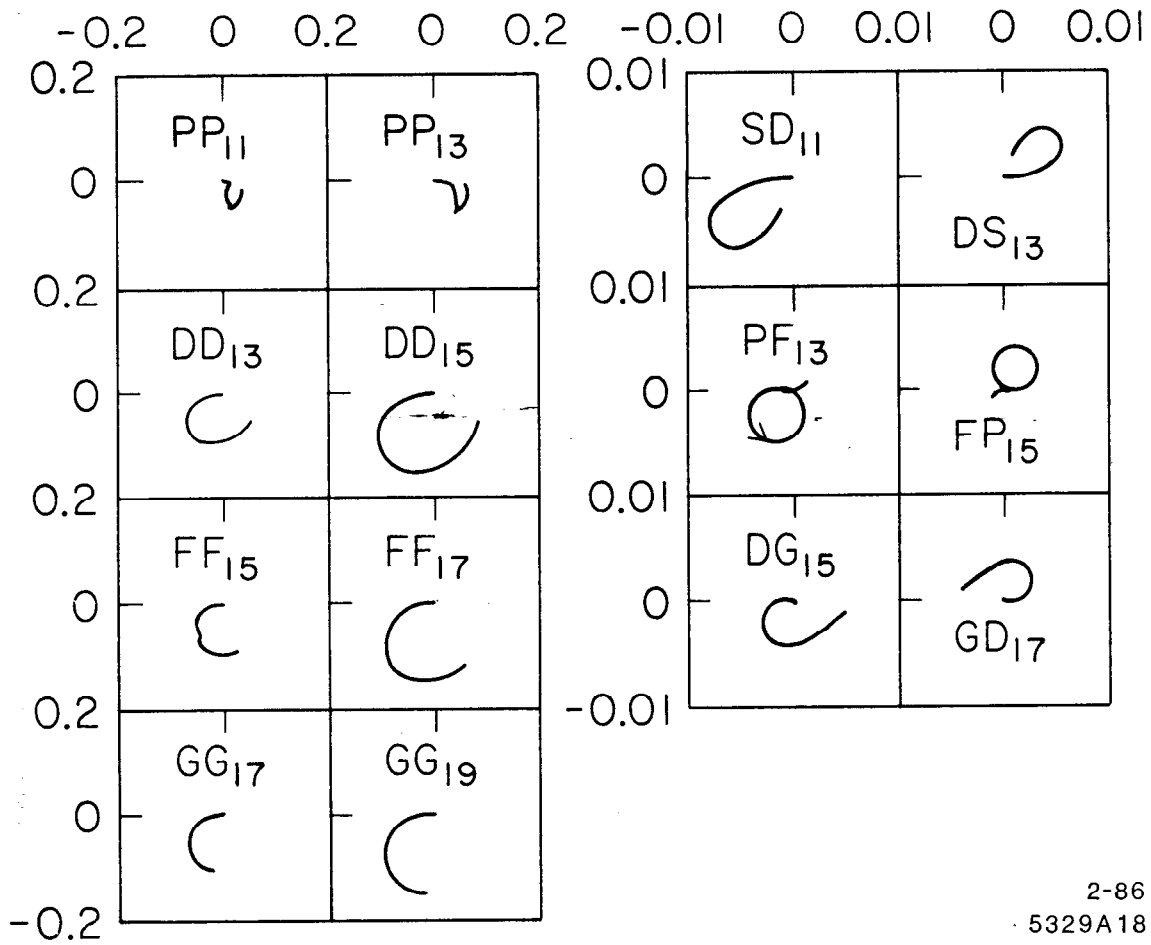
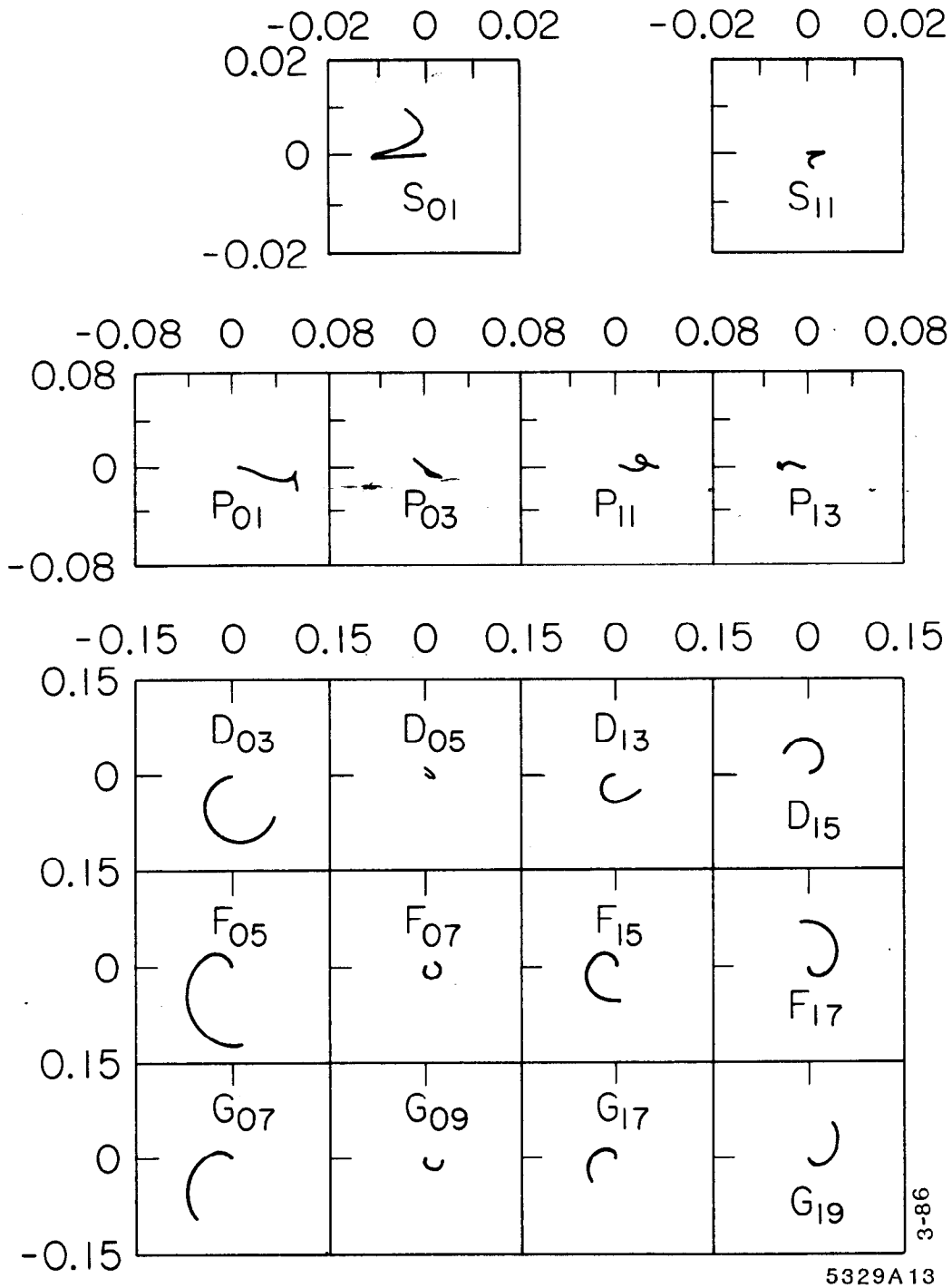FIG. 21. Skyrme model predictions for $\overline{K}N \to \eta\Sigma^*$.

$\overline{K}N \rightarrow K\Xi$

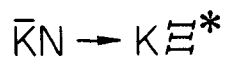FIG. 22. Skyrme-model predictions for $\overline{K}N \rightarrow K\Xi$.

5329A13
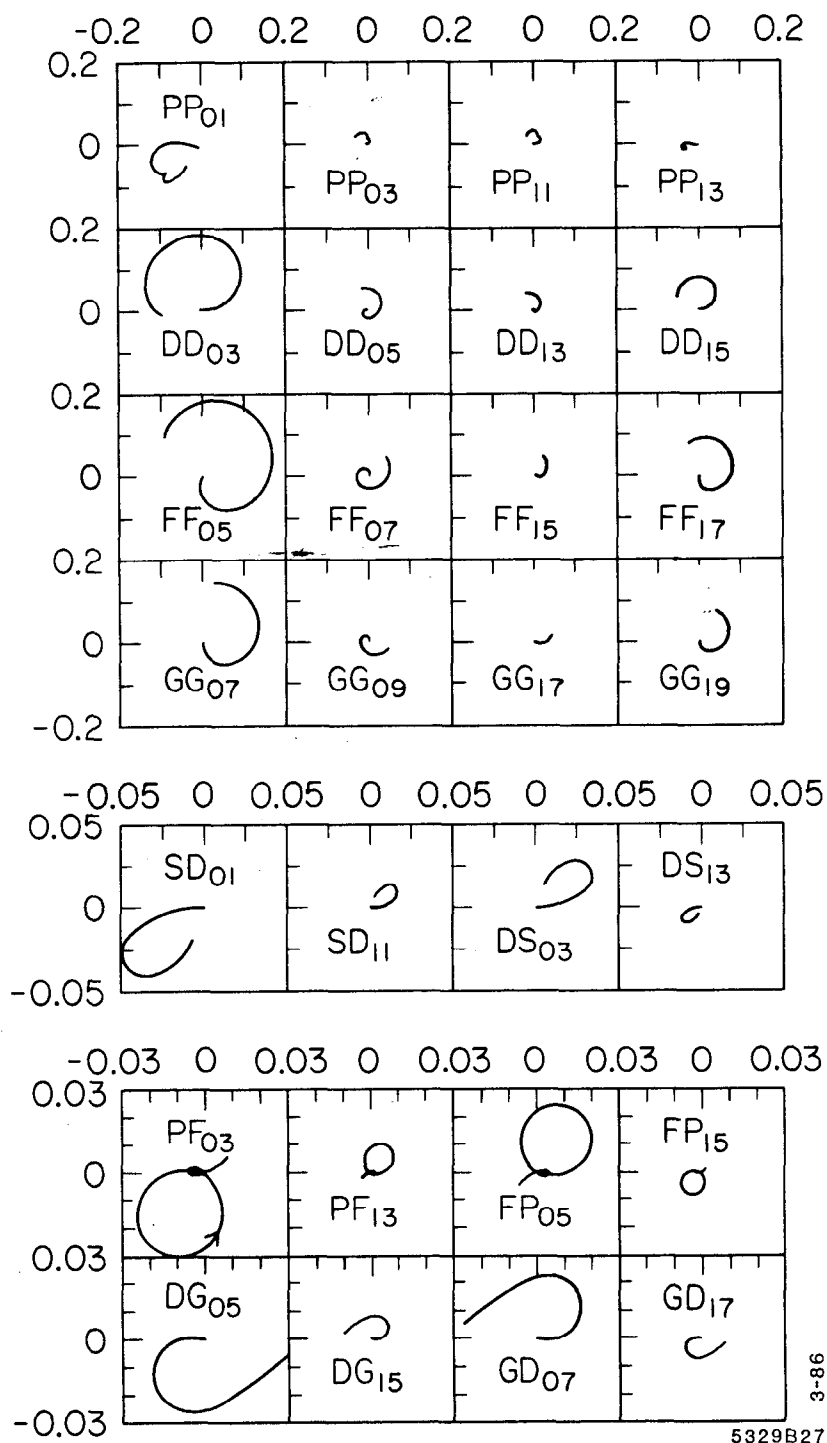
FIG. 23. Skyrme-model predictions for $\overline{K}N \to K\Xi^*$.

REFERENCES

1. T. H. R. Skyrme *Proc. Roy. Soc.* **A260** (1961) 127.

2. T. H. R. Skyrme *Nucl. Phys.* **31** (1962) 556.

3. E. Witten, *Nucl. Phys.* **B223** (1983) 422; *ibid.* 433.

4. E. Guadagnini, *Nucl. Phys.* **B236** (1984) 35.

5. For recent reviews of the Skyrme model see: I. Zahed, G.E. Brown, *The Skyrme Model*, SUNY preprint Print-86-0160, Jan. 1986, to appear in *Physics Reports*; U.G. Meissner and I. Zahed, *Skyrmions in nuclear physics*, SUNY preprint Print-86-0162, Dec. 1985., to appear in Adv. Nucl. Phys.

6. Some aspects of the static phenomenology of the 3-flavor Skyrme model are reviewed in: C. Nappi, *Topics in skyrmion physics*, included in S. Brodsky and E. Moniz, eds., Proceedings of the 1985 ITP Workshop on Nuclear Chromodynamics, World Scientific Press.

7. M. P. Mattis and M. Karliner, *Phys. Rev.* **D31** (1985) 2833.

8. M. P. Mattis and M. Peskin, *Phys. Rev.* **D32** (1985) 58.

9. M. Peskin, *Pion-skyrmion scattering: collective coordinates at work*, SLAC-PUB 3703, published in *Recent Developments in Quantum Field Theory*, J. Ambjørn, B.J. Durhuus and J.L. Petersen, *eds.*, Elsevier Science Publishers B.V., 1985.

10. M. P. Mattis, *Phys. Rev. Lett.* **56** (1986) 1103.

11. M. P. Mattis, *Phenomenology of the meson-skyrmion system*, to be included in *Chiral Solitons*, ed. K. Liu, World Scientific, Singapore 1986 (in press).

12. M. P. Mattis, *Aspects of Meson-Skyrmion Scattering*, SLAC-PUB. 3795, September 1985, in S. Brodsky and E. Moniz, *op. cit.*

13. M. Karliner and M. P. Mattis, *Phys. Rev. Lett.* **56** (1986) 428.

14. H. Walliser and G. Eckart, *Nucl. Phys.* **A429**, 514 (1984).

15. A. Hayashi, G. Eckart, G. Holzwarth, and H. Walliser, *Phys. Lett.* **147B**, 5 (1984).

16. C. G. Callan and I. Klebanov, *Nucl. Phys.* **B262** (1985) 365.

17. G. Höhler, F. Kaiser, R. Koch, and E. Pietarinen, *Handbook of Pion-Nucleon Scattering* (Fachinformationszentrum, Karlsruhe, 1979), Physik Daten No. 12-7. Reproduced in Review of Particle Properties, *Rev. Mod. Phys.* **56**, part II (1984). ($\pi N \rightarrow \pi N$)

18. R. E. Cutkosky *et al.*, in *Baryon* 1980 (conference proceedings), ed. N. Isgur; reproduced in Review of Particle Properties, *op. cit.* ($\pi N \rightarrow \pi N$)

19. R. A. Arndt, J. M. Ford and L. D. Roper, *Phys. Rev.* **D32** (1985) 1085. ($\pi N \rightarrow \pi N$)

20. D. M. Manley, R. A. Arndt, Y. Goradia, and V. L. Teplitz, *Phys. Rev.* **D30**, 904 (1984). ($\pi N \rightarrow \pi \Delta$)

21. D. J. Herndon *et al.*, *Phys. Rev.* **D11** (1975) 3183. ($\pi N \rightarrow \pi \Delta$)

22. J. Dolbeau *et al.*, *Nucl. Phys.* **B108** (1976) 365. ($\pi N \rightarrow \pi \Delta$)

23. K. W. J. Barnham *et al.*, *Nucl. Phys.* **B168** (1980) 243. ($\pi N \rightarrow \pi \Delta$)

24. R. D. Baker *et al.*, *Nucl. Phys.* **B156** (1979) 93. ($\pi N \rightarrow \eta N$)

25. J. Feltesse *et al.*, *Nucl. Phys.* **B93** (1975) 242. ($\pi N \rightarrow \eta N$)

26. K. W. Bell *et al.*, *Nucl. Phys.* **B222** (1983) 389. ($\pi N \rightarrow K \Lambda$)

27. D. J. Candlin *et al.*, *Nucl. Phys.* **B238** (1984) 477. ($\pi N \rightarrow K \Sigma$)

28. P. Livanos *et al.*, in *Baryon* 1980 (conference proceedings), ed. N. Isgur. ($\pi N \rightarrow K \Sigma$)

29. S. R. Deans et al., Nucl. Phys. **B96** (1975) 90. ($\pi N \to K\Sigma$)

30. W. Langbein and F. Wagner, Nucl. Phys. **B53** (1973) 251. ($\pi N \to K\Sigma$)

31. B. R. Martin and G. C. Oades, *KN phase shift analysis including constraints from fixed t analyticity*, University College report, Print-80-0806, July 1980. ($KN \to KN$)

32. R. A. Arndt, L. D. Roper and P. H. Steinberg, Phys. Rev. **D18** (1978) 3278. ($KN \to KN$)

33. R. A. Arndt and L. D. Roper, Phys. Rev. **D31** (1985) 2230. ($KN \to KN$)

34. K. Hashimoto, Phys. Rev. **C29** (1984) 1377. ($KN \to KN$).

35. K. Nakajima et al., Phys. Lett. **112B**, 80 (1982).

36. G. Giacomelli et al., Nucl. Phys. **B110** (1976) 67. ($KN \to K\Delta$)

37. G. P. Gopal et al., Nucl. Phys. **B119** (1977) 362. Reproduced in Review of Particle Properties, *op. cit.* ($\overline{K}N \to \overline{K}N$, $\overline{K}N \to \pi\Sigma$, $\overline{K}N \to \pi\Lambda$)

38. M. Alston-Garnjost et al., Phys. Rev. **D18** (1978) 182; reproduced with many more partial waves in Review of Particle Properties, *op. cit.* ($\overline{K}N \to \overline{K}N$)

39. B. R. Martin and M. K. Pidcock, Nucl. Phys. **B126** (1977) 285; reproduced in Review of Particle Properties, *op. cit.* ($\overline{K}N \to \pi\Lambda$ and $\overline{K}N \to \pi\Sigma$)

40. R. Rader et al., Nuov. Cim. **16A** (1973) 178. ($\overline{K}N \to \eta\Lambda$)

41. W. Cameron et al., Nucl. Phys. **B143** (1978) 189. ($\overline{K}N \to \pi\Sigma^*$)

42. P. J. Litchfield et al., Nucl. Phys. **B74** (1974) 39. ($\overline{K}N \to \overline{K}\Delta$)

43. J. Wess and B. Zumino, Phys. Lett. **37B** (1971) 95.

44. J. J. deSwart, Rev. Mod. Phys. **35** (1963) 916; reprinted in M. Gell-Mann and Y. Ne'eman, *The Eightfold Way*, New York 1964, p. 120.

45. This point is discussed in R. L. Jaffe, in *Baryon Resonances* (conference proceedings), R. T. Ross and D. H. Saxon, eds., Rutherford Lab., 1976.

46. S. Weinberg, *Phys. Rev. Lett.* **17,** 616 (1966); Y. Tomozawa, *Nuovo Cim.* **46A** (1966) 707.

47. M. Uehara and H. Kondo, *πN Scattering lengths in the skyrmion model*, Saga Univ. preprint, SAGA-HE-19, Dec. 1985.

48. H. Schnitzer, *Phys. Lett.* **139B**, 217 (1984); *Nucl. Phys.* **B261** (1985) 546.

49. G. Adkins, C. Nappi, and E. Witten, *Nucl. Phys.* **B228**, 552 (1983).

50. R. Koniuk and N. Isgur, *Phys. Rev.* **D21** (1980) 1868.

51. A. Manohar, *Nucl. Phys.* **B248** 19 (1984).